Doctoral Dissertations

Student Scholarship

Spring 1985

HYDRODYNAMIC CHARACTERISTICS AND COAL COMBUSTION MODELING OF A HIGH VELOCITY FLUIDIZED BED (SOLIDS FRICTION FACTOR, TWO PHASE FLOW, PRESSURE PROFILE, FAST)

RONALD WAYNE BREAULT
University of New Hampshire, Durham

Follow this and additional works at: https://scholars.unh.edu/dissertation

INFORMATION TO USERS

This reproduction was made from a copy of a document sent to us for microfilming. While the most advanced technology has been used to photograph and reproduce this document, the quality of the reproduction is heavily dependent upon the quality of the material submitted.

The following explanation of techniques is provided to help clarify markings or notations which may appear on this reproduction.

1. The sign or "target" for pages apparently lacking from the document photographed is "Missing Page(s)". If it was possible to obtain the missing page(s) or section, they are spliced into the film along with adjacent pages. This may have necessitated cutting through an image and duplicating adjacent pages to assure complete continuity.

2. When an image on the film is obliterated with a round black mark, it is an indication of either blurred copy because of movement during exposure, duplicate copy, or copyrighted materials that should not have been filmed. For blurred pages, a good image of the page can be found in the adjacent frame. If copyrighted materials were deleted, a target note will appear listing the pages in the adjacent frame.

3. When a map, drawing or chart, etc., is part of the material being photographed, a definite method of "sectioning" the material has been followed. It is customary to begin filming at the upper left hand corner of a large sheet and to continue from left to right in equal sections with small overlaps. If necessary, sectioning is continued again—beginning below the first row and continuing on until complete.

4. For illustrations that cannot be satisfactorily reproduced by xerographic means, photographic prints can be purchased at additional cost and inserted into your xerographic copy. These prints are available upon request from the Dissertations Customer Services Department.

5. Some pages in any document may have indistinct print. In all cases the best available copy has been filmed.

8521491

Breault, Ronald Wayne

HYDRODYNAMIC CHARACTERISTICS AND COAL COMBUSTION MODELING
OF A HIGH VELOCITY FLUIDIZED BED

University of New Hampshire   Ph.D.   1985

University
  Microfilms
International 300 N. Zeeb Road, Ann Arbor, MI 48106

HYDRODYNAMIC CHARACTERISTICS
AND COAL COMBUSTION MODELING
OF A HIGH VELOCITY
FLUIDIZED BED

By

Ronald W. Breault

B.S., Clarkson College of Technology, 1979
M.S., University of New Hampshire, 1982

A DISSERTATION

Submitted to the University of New Hampshire
in Partial Fulfillment of the
Requirements of the Degree of

Doctor of Philosophy
in
Chemical Engineering

May, 1985

This dissertation has been reviewed and approved.

Vireudra K. Mathur
Dissertation Director, Dr. V. K. Mathur
Professor Chemical Engineering

Stephen S.T. Fan
Dr. S. S. T. Fan, Chairman Department of Chemical Engineering
Professor Chemical Engineering

Ihab Farag
Dr. I. H. Farag, Associate Professor of Chemical Engineering

L. D. Meeker
Dr. L. D. Meeker, Professor of Mathematics

M. R. Swift
Dr. M. R. Swift, Associate Professor of Mechanical Engineering

P. S. Mei
Dr. P. S. Mei, Mechanical Engineer,
Morgantown Energy Technology Center
United States Department of Energy

May 6, 1985
Date

DEDICATION

TO MARY BETH

iv

ACKNOWLEDGEMENTS

The successful accomplishments of a graduate student are, to a large extent, attributed to the guidance of the research committee. I am very fortunate to have a strong and dedicated committee. I extend special thanks to Dr. V. K. Mathur, my dissertation director, for his advice and encouragement. His supervision has been both spontaneous and stimulating. I also extend thanks to Dr. S. S. T. Fan and Dr. I. H. Farag of the Chemical Engineering Department, for their tutelage, patience, and inspiration. I thank Dr. L. D. Meeker of the Mathematics Department and Dr. M. R. Swift of the Mechanical Engineering Department for their special interest in my development, shown by their membership in this committee. I thank Dr. J. S. Mei of Morgantown Energy Technology, U. S. DOE for providing me with the opportunity to pursue this topic of research and his special efforts in the early stages of this work and at its completion.

A special tribute is due to the Department of Chemical Engineering, University of New Hampshire, for providing me with the facilities to conduct the experimental investigation.

I acknowledge the funding by Morgantown Energy Technology Center for the initial monies, that supported this work during the first year.

Finally, I acknowledge the ever present love and encouragement by my wife, Mary Beth.

v

TABLE OF CONTENTS

vii

LIST OF TABLES

LIST OF FIGURES

xiii

xv

ABSTRACT

HYDRODYNAMIC CHARACTERISTICS
AND COAL COMBUSTION MODELING
OF A HIGH VELOCITY
FLUIDIZED BED

by

Ronald W. Breault

University of New Hampshire, May, 1985

A Loop Fluidized Bed (LFB) based on the fast fluidization
concept is a novel method for effective solid-gas contact and can
play an important role in coal combustion. It can be operated under
pressure making it eminently suited for the production of high
temperature gas from coal for operating gas turbines for power
generation. The LFB can operate over a wide range of gas flow rates
and coal can be introduced at various points without excessive
pressure drops. Further, it is possible to capture higher amounts of
sulfur dioxide due to the use of fine dolomite or limestone
particles. This process can also be used for the smelting of mineral
ores. However, the LFB concept is relatively new and data in the
literature are scarce.

The LFB process is best described by considering the process to consist of four sections. These are: 1) riser, 2) disengaging zone, 3) standpipe, and 4) eductor zone. The riser section is the core of the LFB combustor. This is the zone where the majority of coal combustion and sulfur adsorption occurs. Operating in the fast fluidization regime, the LFB can utilize gas velocities several times the entrainment velocity with the solids exhibiting a high degree of backmixing. The backmixing increases the solids residence time, which allows for the utilization of larger coal particles in the LFB than in entrained combustors. The disengaging zone operates under principles similar to a cyclone, only that separation must occur in less than one complete pass of the gas. The fine particles follow the gas stream lines as the gas exits the loop into the primary cyclone. The larger particles are thrown to the outside of the loop and into the standpipe by centrifugal force. The standpipe has two regions of gas-solids flow: aerated and moving bed. The height of the moving bed plays an important role in creating a solid plug to prevent the gas from short circuiting up the standpipe. At the bottom of the standpipe is the eductor zone. Solids are entrained and conveyed through the loop by the gas entering the LFB.

In this study a bench scale loop fluidized bed has been designed, fabricated and installed. The unit has been operated using sand, limestone, and gypsum particles. The latter two solids are chosen because of their presence in the coal combustion process for

xvii

sulfur removal.   Data have been collected to study the effect of particle size, particle density, air flux, and solid flux on fluidizing characteristics of the three solids.

The experimental set up is assembled in a pyrex brand glass pipe.   The unit is provided with four steel nozzles for supplying air.   The solid particles are fed manually to the LFB at the top of the standpipe.   The particles traverse the standpipe in the packaged bed flow, entering the eductor zone.   The particles are entrained in the high velocity gas stream at this zone.   The flow rate is measured with four rotameters.   The particles conveyed upwards travel through an Auburn solids fraction monitor.   This monitor continuously determines the percent solids of the two-phase stream as it flows past.   The pressure drop across the monitor is continuously monitored with a differential pressure transducer - indicator system.   These instruments give analog outputs proportional to the corresponding variables.   The analog outputs are recorded on a strip chart recorder.   The solids and gas travel through the remainder of the riser and loop around the top via a bend.   The gas exits while the solid particles are returned to the standpipe.   The gas containing a small amount of solid particles flows through a cyclone and a bag filter; solids leave the loop through the cylone bottom.   Pressure ports are provided approximately every 1/3 of a meter around the loop for pressure monitoring with water manometers.

Extensive data have been obtained to study the effect of particle size, particle density, air flux, and solids flux on fluidizing characteristics of sand, limestone, and gypsum.   It is

xviii

found that solids flow behavior was sensitive to nozzle positions and air flow rates. Three dimensional plots have been prepared for predicting good operating regions for the LFB with respect to nozzle combination, air flow rate and riser solids fraction. Pressure drop data have been correlated with solids velocity and solids fraction to obtain a better solids friction factor equation than available in the literature. A computer program has been developed to predict the static pressure of every point in the LFB. The computer program predictions and the static pressure data show good agreement. Coal combustion and sulfur removal models for the LFB coal combustor have been developed. The predictions from these models agree with commercial data. A conceptual LFB coal combustor has been designed and the results have been compared with commercial coal combustion data. The LFB coal combustion process is found to provide better coal combustion and sulfur removal effectiveness than bubbling bed coal combustion and pulverized coal combustion with limestone injection processes.

1. INTRODUCTION

The U. S. has about one-third of the world's known coal reserves. The reserves which are mineable under present mining and economic conditions are estimated to be about 437 billion tons of which about 265 billion tons can be recovered. But coal is difficult to mine, expensive to transport and heavily polluting. The pollution is mainly due to the presence of mineral matter (ash) and sulfur which give rise to the formation of fly ash and sulfur dioxide. It is estimated that about 55 percent of our demonstrated coal reserves have more than one percent sulfur and cannot be used without the use of special equipment to reduce sulfur dioxide emissions.

Fossil energy research, development, and demonstration strategy is to develop a wide variety of coal utilization techniques that are clean, efficient, and conserve resources. Industry can then choose promising processes which will eventually be commercialized providing the energy needed for our continued economic growth and well being. The many processes and techniques of coal conversion have as a basic concept the transmutation of coal into forms acceptable to our transportation and heating equipment.

For nearly fifteen years considerable efforts have been made on the development of fluidized bed combustion of coal. This process holds a number of attractions, all stemming from the concept of maintaining low temperatures in the range of $1100°-1200°K$ in the combustion chamber. However, it is reported that one of the main

1

disadvantages of a fluidized bed combustion system is that turndown of combustion rate is difficult. Fluidized beds are not operable over wide ranges of loads.

A high velocity fluidized bed (HVFB) can operate over a wide range of gas throughputs. The gas rate may be reduced to such a degree that the bed becomes turbulent, or even enters the bubbling regime without losing uniformity of bed temperature. It is also claimed that in a HVFB coal might be introduced at fewer points without excessive pressure drop. Furthermore, it may be possible to capture higher amounts of sulfur dioxide due to the use of fine dolomite or limestone particles in a HVFB. A special case of the high velocity fluidized bed concept, recently developed at the Morgantown Energy Technology Center (METC), is the Loop Fluidized Bed (LFB).

All HVFB processes including the LFB are best described by considering the process to consist of four sections. These are: 1) the riser, 2) the disengaging zone, 3) the standpipe, and 4) the eductor zone.

The riser, as shown in Figure 1, is the core of the LFB combustor. This is the zone where the majority of coal combustion and sulfur adsorption occurs. Operating in the "fast fluidization" regime, the LFB can utilize gas velocities several times the entrainment (terminal) velocity with the solids exhibiting a high degree of backmixing. The backmixing increases the solids residence time, which allows for the high coal combustion efficiencies at the
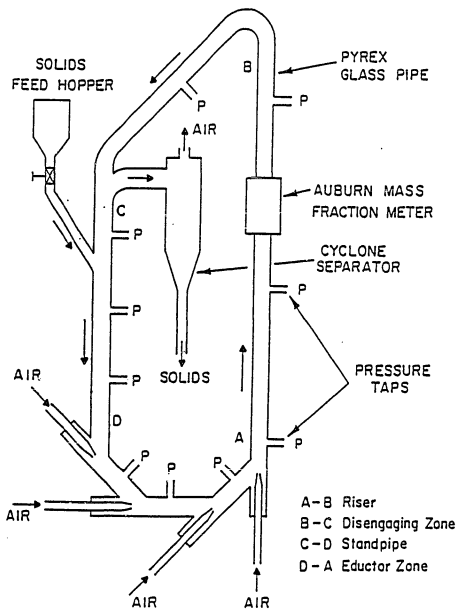
FIG I LOOP FLUIDIZED BED

lower temperatures in the LFB than in entrained bed combustors. Also, the backmixing gives rise to the uniformity of bed temperature.

The disengaging zone operates under principles similar to a cyclone which it replaces. The fine particles follow the gas stream and exit the loop into the primary cyclone. The large particles are thrown to the outside of the loop and return into the standpipe by the centrifugal force.

The standpipe has two regions of gas-solids flow: lean (aerated) and dense (moving) zones. The height of the moving bed plays an important role in creating a solids plug which prevents the gas from short circuiting up the standpipe.

At the bottom of the standpipe is the eductor zone. Solids are entrained and conveyed through the loop by the gas entering the LFB.

Circulating fluidized bed processes have been proposed recently to eliminate some of the problems encountered in conventional fluidized beds. The circulating fluidized bed is a transport reactor system in which the solid and gas go through many different flow regimes. The loop fluidized bed is one such circulating fluidized bed which is being considered for pressurized combustion of coal in the presence of a sulfur sorbent such as dolomite. No available model incorporates the flow phenomena with the kinetic operations of coal combustion and sulfur removal.

This study has been conducted to provide fundamental knowledge of the hydrodynamics in the LFB with special reference to the riser section which operates in the high velocity fluidization regime. Experimental data have been used for the development of mathematical

models to predict the pressure profile in the LFB. Combustion and desulfurization mathematical models have been developed for the LFB combustor by modifying existing models currently available in the literature for conventional combustion systems. Finally, a conceptual design for the combustion of 1000 kg/hr of coal is provided to demonstrate the use of these models and to compare the results with the commercial data.

2. OBJECTIVE

The overall objective of this thesis is two fold. First to experimentally study the hydrodynamics of solid-air systems in a Loop Fluidized Bed (LFB) and to develop a model to predict the pressure profile in the equipment. Second, to develop a model for the coal combustion and sulfur removal taking place in a LFB. In order to achieve these objectives, the following tasks were established and completed.

(1) Review the literature on all aspects of gas-solid two phase flow, coal combustion, and desulfurization.

(2) Install a bench scale cold flow loop fluidized bed experimental unit with the necessary instrumentation.

(3) Conduct experimental studies of the flow characteristics of sand, limestone, and gypsum particles in the LFB with respect to the particle size, particle density, gas flux, solids flux, solids fraction and standpipe depth.

(4) Develop a mathematical model to predict the pressure profile in the LFB.

(5) Develop coal combustion and sulfur removal models in an LFB system.

(6) Provide a conceptual design of a loop fluidized bed combustor utilizing experimentally generated information and the developed models.

6

This chapter is divided into three major Sections A, B, and C that discuss the hydrodynamics of gas-solid flow in circular conduits, coal combustion, and coal desulfurization, respectively. Each section is further divided into sub-sections labeled as A.1, A.2, etc. These sub-sections present the details of these operations and processes.

A. Hydrodynamics of Gas-Solid Flow in Circular Conduits

The literature surveyed covered all aspects of gas-solid flow phenomena including all the flow regimes present in a HVFB and specifically the LFB. The literature reviewed is divided in several categories for reading convenience.

A.1 Riser

The rise section (Figure 1) of the LFB operates in the fast fluidization regime. The term "fast fluidization" was first used by Yerushalmi et al. [1] This fast fluidization term is used to describe the phenomena of dense strands and clusters moving to and fro, rising and falling, and forming and breaking apart, as the solid particles are conveyed through the riser. This mode of gas-solid contact has been primarily investigated at the City College,

7

Manhattan, New York, by J. Yerushalmi and co-workers [1, 2, 3, 4, 5, 6, 7, 8]. Theoretical studies have also been conducted by Matsen [9], and Gidaspow and co-workers [10, 11, 12].

Yerushalmi and co-workers [1, 2, 3, 4, 5, 6, 7] conducted investigations in three experimental set-ups: (1) a rectangular (two dimensional bed, (2) a three inch diameter bed, and (3) a six inch diameter bed. They developed a pressure drop correlation [7] based on the following assumptions:

(1) all solid particles are densely packed clusters.

(2) clusters are spherical.

(3) there are no wall or acceleration effects.

(4) clusters have a voidage equal to that at minimum fluidization.

(5) clusters are discreetly distributed in the bed.

Based on these assumptions, the pressure drop per unit length can be described by the following equations:

$$\frac{\Delta P}{\Delta L} = (1 - \varepsilon_c) \ (1 - \varepsilon_{mf}) \ \rho_s g \qquad (1)$$

$$\frac{\Delta P}{\Delta L} = \frac{N}{A} \frac{1}{2} \rho_g \ U_{c,sl}^2 \ Cd_{sl} \ \varepsilon_c^{-2n} \ \frac{\pi}{4} \ d_c^2 \qquad (2)$$

where:

$$Cd_{sl} = f \ (Re_{sl}) = f \ (\rho_g d_c U_{c,sl}/\mu) \qquad (3)$$

$$U_{c,sl} = \frac{G_g}{\rho_g \varepsilon_c} - \frac{G_s}{\rho_s} \qquad (4)$$

The index n in Equation (2) is called the Richard and Zaki index and describes the voidage in a fluidized bed. The index is developed for solid-liquid particulate fluidization and its value ranges from 4.65 to 2.4 for terminal Reynold's number less than or equal to 0.2 to greater than or equal to 500. The pressure drop obtained from these equations agrees with experimental data. The cluster voidage is essentially an adjustable parameter allowing the model to fit the data. Yerushalmi et al. [7] calculated the cluster diameter as a function of the solids concentration. The data fall about a single curve, obtained from the equations, showing good agreement between the experiment and the model.

Matsen [9] proposed a theory to describe: (1) bubbling fluidization, (2) pneumatic transport (3) choking, and (4) fast fluidization in a two phase solid-gas vertical up-flow system. The theory is based on the following assumptions:

   (1) slip velocity is independent of the solids and
       gas flow rates.

   (2) wall and accaleration effects are negligible.

   (3) all the particles are spherical and uniform in size.

   (4) slip velocity in the dense region can be expressed
       by the Equation (5).

The slip velocity between the solid and gas is an important parameter and is given by the relation

$$U_{sl} = \frac{G_g}{\epsilon \rho_g} - \frac{G_s}{\rho_s} \frac{1}{(1-\epsilon)} \qquad (5)$$

for dilute suspensions, $\varepsilon > 0.9$. Equation (5) can be rearranged to obtain

$$\frac{G_s}{\rho_s} = \frac{1-\varepsilon}{\varepsilon} \left(\frac{G_g}{\rho_g} - \varepsilon U_{s1}\right) \tag{6}$$

For dense phase, the solids velocity, G_s/ρ_s, can be estimated by the correlation presented by Matsen [13].

$$\frac{G_s}{\rho_s} = \frac{1-\varepsilon}{\varepsilon} \left(\frac{G_g}{\rho_g} - U_{mf} - \frac{\varepsilon-\varepsilon_{mf}}{1-\varepsilon} U_B\right) \tag{7}$$

The bubble velocity, U_B in the case of small diameter vessels can be expresed as $U_B = 0.35 \sqrt{gD}$ [=] m/s. To estimate the solids velocity in the dilute region, Matsen proposed the following emperical equation to correlate the slip velocity with the voidage and terminal velocity (bubble velocity in this case),

$$\frac{U_{s1}}{U_B} = 10.8 \ (1-\varepsilon)^{0.293} \tag{8}$$

for voidages, $\varepsilon < 0.9997$.

Substitution of Equation (8) into (6) gives

$$\frac{G_s}{\rho_s} = \frac{1-\varepsilon}{\varepsilon} \left(\frac{G_g}{\rho_g} - 10.8 \ (1-\varepsilon)^{0.293} \ \varepsilon U_B\right) \tag{9}$$

Dividing both sides of Equations (7) and (9) by the bubble velocity gives the dimensionless equations given below.

For the dilute region:

$$\frac{G_s}{\rho_s U_B} = \frac{1-\epsilon}{\epsilon} \left(\frac{G_g}{\rho_g U_B} - 10.8 \, (1-\epsilon)^{0.293} \, \epsilon \right) \tag{10}$$

For the dense region:

$$\frac{G_s}{\rho_s U_B} = \frac{1-\epsilon}{\epsilon} \left(\frac{G_g}{\rho_g U_B} - \frac{U_{mf}}{U_B} - \frac{\epsilon - \epsilon_{mf}}{1-\epsilon} \right) \tag{11}$$

Plotting $\frac{G_s}{\rho_s U_B}$ Vs. $\frac{G_g}{\rho_g U_B}$ in Equations (10) and (11) for constant values of voidage, Matsen obtained a series of curves representing two-phase vertical-up flow. The locus of intersection of the two equations for values of constant voidage is called the choking curve. If this series of curves is cross plotted, $\frac{G_s}{\rho_g U_B}$ Vs (1-ϵ) , with the solids velocity as a parameter, another series of curves resembling a single component vapor/liquid equilibrium diagram is obtained. Only one phase is present outside the envelope. Matsen suggested that this was the region of fast fluidization. Within the phase envelope, two phases can exist simultaneously; a dilute phase and a relatively more dense phase.

Gidaspow [10, 12] developed a one dimensional two-phase model based on an entropy production principle from non-equilibrium thermodynamics. He postulated that the internal energy of the system was a function of the usual single phase thermodynamic variables such as entropy, volume, mass and external potential. In addition,

Gidaspow postulated that the internal energy was also a function of the relative velocity (slip velocity) of the two phases. Gidaspow and Arastoopour [14] applied Gidaspow's model to the vertical pneumatic conveying situation with the following assumptions:

(1) flow is one dimensional.

(2) flow is isothermal.

(3) flow is in steady state.

(4) there is no phase change.

The gas continuity equation can be written as:

$$\frac{d}{dx} \left(\epsilon \, \rho_g \, U_g \right) = 0 \tag{12}$$

The solid continuity equation can be presented as:

$$\frac{d}{dx} \left((1 - \epsilon) \, \rho_s \, U_s \right) = 0 \tag{13}$$

The momentum equations are combined to give the following gas-solid mixture momentum equation:

$$(1-\epsilon) \, \rho_s \, U_s \, \frac{d}{dx} (U_s) + \epsilon \rho_g \, U_g \, \frac{d}{dx} (U_g)$$

$$+g \, [\rho_s \, (1-\epsilon) + \rho_g \epsilon] = \frac{dP}{dx} - fw \tag{14}$$

The equation which fully describes the slip velocity is given by:

$$\frac{1}{2} \frac{d}{dx} (U_{sl})^2 + \frac{3}{4} C_d \, \frac{\rho_g}{\rho_s} \, \frac{(U_{sl})^2}{d_p \, (\epsilon)^{2.65}} = g \tag{15}$$

The voidage exponent is obtained from the familiar Richards and Zaki work. The drag coefficient, C_d, is stated to obey the relations:

$$C_d = \frac{24}{Re_{sl}} (1 + 0.15 \ Re_{sl}^{0.687}); \ Re_{sl} < 1000 \qquad (16)$$

$$C_d = 0.44; \quad Re_{sl} > 1000$$

$$\text{where } Re_{sl} = \rho_g \ d_p \ U_{sl}/\mu$$

This model was applied to the data obtained by Yerushemi et al. for an assumed voidage. The model estimated $\frac{\Delta P}{\Delta L}$ to be in the range of 400 to 2000 kg/m^{2}s^2 for values of solid mass flow between 40 and 200 kg/m^{2}s. These estimates agree well with experimental data at low solids flow rates. The disagreement at high solids flux values is attributed to: (1) the error in the assumed void fraction value, (2) wall effects, (3) variance in cluster size, and (4) radial and tangential effects.

A.2 Standpipe

The experimental work conducted at the Morgantown Energy Technology Center [24] has shown that the quantity of solid particles in the standpipe affects the operation of the riser in the LFB. A considerable amount of research has been conducted on various regimes of standpipe flow [15, 16, 17, 18, 19, 20, 21, 22, 23].

The standpipe has both dilute phase as well as dense phase flow regions. The solid particles in the standpipe act as a solid plug - keeping the gas from short circuiting up the standpipe. Since most of the mass is contained in the dense phase region, this section of the literature review has been confined to this flow regime.

Leung et al. [18] have analyzed the flow of solids down a standpipe with a restriction (slide valve) at the bottom. Leung et al. [18] state that for packed moving bed flow, the slip velocity must be less than the minimum fluidized velocity.

$$U_{sl} < \frac{G_s}{\rho_s (1-\epsilon_{mf})} - \frac{G_g}{\rho_g \epsilon_{mf}} = U_{mf} \qquad (17)$$

Yoon and Kunii [19] developed the following pressure drop correlation for flow through a standpipe by modifying the Ergun Equation.

$$\frac{\Delta P}{\Delta L} = \frac{150 \mu (1-\epsilon)^2 U_{sl}}{(\phi d_p)^2 \epsilon^3} - \frac{1.75 \rho_g (1-\epsilon) U_{sl}^2}{\phi d_p \epsilon^3} \qquad (18)$$

A.3 Particle-Gas Disengaging Zone

Published information related to the performance of the solid-gas disengaging section of the LFB is limited. According to experimental studies conducted by Breault [24] at METC, using two different particle sizes ($\bar{d}_p$ = 265 μm and $\bar{d}_p$ = 170 μm) the solid particles remaining in the LFB had a larger particle size of approximately 320 μm. For the larger particles, the mass throughput

(system elutriation rate) increased linearly from 1.8 to 2.2 x 10^{-4} kg/s with an increase in the gas velocity from 7.5 to 9.6 m/s. The smaller particles had a mass throughput equal to 3.1 x 10^{-4} kg/s at a gas velocity of 7.1 m/s.

A.4   Solids Eductor Zone

Published literature on the entrainment rate of solids is rather limited. In most studies solid particles are fed to solid-gas systems with mechanical devices. There is some similarity between the J-valve and the eductor zone in the LFB. The J-valves have been investigated by Knowlton and Hirsan [25] and Knowlton, Hirsan, and Leung [26]. These valves control the solid particle flow from a standpipe to a vertical pneumatic conveyor line. The performance of the J-valve is found to be dependent on the amount and position of injected aeration fluid [25, 26]. It is reported by Knowlton et al. [25, 26] and Singh [48] that the maximum solids flux was obtained when the solids in the standpipe were just at the fluidizing point.

A.5   Choking

The solid particle movement in the riser section of the LFB is termed "Fast Fluidization" by Yerushalmi et al. [1] or "non-slugging dense phase flow" by Leung [15, 18]. Leung defines choking as the point at which dilute phase flow in the riser section undergoes a sharp transition to a slugging dense phase flow. The gas velocity

under this condition is called the "choking" velocity. However, Matsen [9] defines choking as an abrupt transition from dilute phase flow to dense phase flow regardless of the nature of the dense phase.

It is important to know the conditions under which choking occurs so that a LFB can be designed to operate smoothly. Choking is found to be a function of gas properties, the solid properties, and the diameter of the riser [27]. Several investigators have developed mathematical correlations to predict the choking velocity [9, 27, 28, 29, 30, 31, 32, 33].

Matsen [9] presented a mechanism to describe the choking phenomena. He defined choking mathematically as the intersection of the dilute and dense phase solids mass flow relations given earlier, Equations (10) and (11). Choking is likely to occur when the design parameters place the operation of the riser within the phase envelope.

Leung et al. [28] developed a correlation to estimate the choking flow rate assuming that choking occurred over a narrow range of voidage and that the slip velocity was equal to the terminal velocity. They obtained:

$$U_c = 32.3 \frac{G_s}{\rho_p} (1-\varepsilon) + 0.97 U_t \qquad (19)$$

Yousfi and Gau [29, 30] reported that choking would occur when the Froude number based on particle diameter exceeded 140.

$$Fr = \frac{U_t^2}{g \, d_p} > 140 \qquad (20)$$

Yang [31, 32] reported that choking would occur when the Froude number based on tube diameter was greater than 0.12.

$$Fr = \frac{U_t^2}{gd_t} > .12 \qquad\qquad (21)$$

Smith [33] investigated choking and found it to occur when the Froude number based on tube diameter obeyed the following relation.

$$Fr = (\epsilon^{n-1} n (1-\epsilon))^2 > .17 \qquad\qquad (22)$$

A.6 Solids Mass Fraction Measurement

One of the problems of studying any two-phase flow process is the inherent difficulties associated with measuring G_s, G_g, U_s and ϵ that are needed to fully understand the system. After investigating the different techniques used to obtain these quantities, the Auburn Monitor (used to measure the solids volume fraction) was chosen as the best available instrument for the purposes of this study. The monitor operates such that the flow is not obstructed during the measuring process. A rapidly rotating electric field establishes a uniform measuring system within the sensing volume. These advantages allow one to make sensitive and accurate measurements. Other techniques for measuring solids fraction are as follows:

(1) Determining the void fraction by weighing particles
collected in the sampling pipe.

This technique requires that the flow be obstructed by some
catch pot in the line, and that the process be stopped
frequently in order to remove the sample.

(2) Measuring the void fraction using a laser beam. Several
techniques using lasers have been tried. Essentially, the
laser establishes a control area, and the number of
particles crossing the boundary is recorded as a function of
time. It is reported that optical or acoustical devices did
not generally give accurate estimates of the mean value in
any cross-section [34].

(3) Determining the particle concentration using radioisotopes,
and beta beams.

A counter is used to measure the time it takes a particle to
travel a distance L. Problems with mixing and particle
acceleration have been found. Problems also arise in
storing these radiochemical tracers. Strict disposal
techniques must be observed [35].

(4) Measuring the gas and solids velocities using a Laser
Doppler Velocimeter (LDV).

The degree of attenuation is measured while particles cross
a control volume, the source of light being a helium-neon
laser. Though the LDV does not obstruct the flow, it is not
considered suitable for turbulent flow measurements. The
LDV set up is considerable expensive as well [36].

(5) Determining the mass flow rate using a Micro-Motion (M/M) flow meter.

The M/M uses the coriolis force exerted by the two-phase flow moving through a U-tube. Because there is a sharp bend resulting from the U-tube, a large pressure drop is observed, and thus flow is obstructed [37]. The solids fraction is calculated from the equation of continuity.

The techniques described above have been used by various workers [34, 35, 36, 37, 38, 39] for estimating solids mass fraction and they have encountered some of the problems discussed earlier. The Auburn Monitor appears to eliminate these shortcomings. The monitor uses the capacitance of the system, which is found to be proportional to the volume fraction occupied by the solids. It measures the average dielectric constant of any two-phase nonconductive flow. The average dielectric constant, E_{avg}, is related to the voidage, ε, by the following equation:

$$E_{avg} = \varepsilon E_g + (1-\varepsilon) E_s \qquad (23)$$

which can be used for calculating the void fraction [38]. This quantity is read directly off the instrument. The accuracy of the monitor can be attributed to the fact that it finds the average value, E_{avg}, for a control volume. Since flow fluctuations are always present in a pneumatic transport system, the meter provides only an average value for the volume under study.

A.7 Pressure Drop in High Velocity Fluidized Bed Systems

The HVFB system which includes the solids circulation as well as the entrained flow section consists of several gas-solid flow regimes. These are aerated gas-solid down flow, aerated solids down flow and gas up flow, horizontal pneumatic transport, vertical pneumatic transport and standpipe flow. Research workers have modeled the pressure drop in each of these regimes as the sum of individual contributions due to the effects of acceleration, kinetic energy, potential energy and friction [40, 41, 42, 43, 44, 45, 46, 47, 48, 49]. These flow regimes are discussed as per Fig. 2.

A.7.1 Aerated Solids Flow.

This is the region (section H-A) of aerated gas-solid down flow which exists in the LFB. The pressure drop for this regime of gas-solid flow can be represented by the sum of the potential energy and a frictional term.

$$\Delta P_{A-B} = \Delta P_{SPE} - \Delta P_f \qquad (24)$$

where

$$\Delta P_{SPE} = \rho_s (1-\epsilon) \, g \Delta L \sin\theta \qquad (25)$$

and

$$\Delta P_f = \frac{32\bar{\mu} U_s \Delta L}{d_t^2} \qquad (26)$$
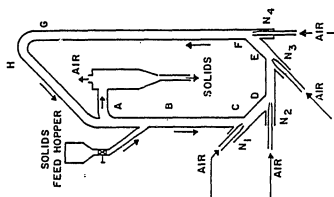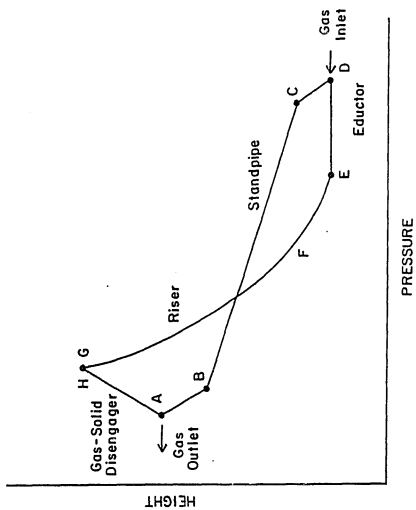
FIG. 2 PRESSURE PROFILE IN HIGH VELOCITY FLUIDIZED BED SYSTEM

for

$$Re = \frac{d_t \bar{\rho} U_s}{\mu} < 1300$$

The sections A-B and C-D are regimes of aerated solid down flow and gas up flow. The pressure drop across these sections can also be represented by the sum of the potential energy and a frictional term.

$$\Delta P_{A-B} = \Delta P_{SPE} + \Delta P_f \qquad (27)$$
or C-D

where ΔP_{SPE} and ΔP_f can be obtained from Equation (25) and (26), respectively.

A.7.2   Standpipe Flow.   Standpipe flow (section B-C) has been extensively studied by various workers as discussed earlier in this report. The pressure drop through this section of the LFB can be modeled by:

$$\Delta P_{B-C} = (\frac{150\mu(1-\epsilon)^2 U_{s1}}{(\phi d_p)^2 \epsilon^3} + \frac{1.75\rho_g(1-\epsilon)U_{s1}^2}{(\phi d_p)\epsilon^3}) \Delta L \qquad (28)$$

where the slip velocity is given by:

$$U_{s1} = \frac{G_s}{\rho_s(1-\epsilon)} - \frac{G}{\rho_g \epsilon} < U_{mf} \qquad (29)$$

A.7.3. Pneumatic Transport. The eductor is a region of horizontal pneumatic transport, section D-E. The pressure drop is modeled by summing contributions due to kinetic energy requirements and frictional resistance.

$$\Delta P_{E-F} = \Delta P_{SKE} + \Delta P_f \tag{30}$$

The pressure drop due to the particles kinetic energy is

$$\Delta P_{SKE} = U_s G_s \tag{31}$$

where

$$U_s = U_g - U_t$$

The pressure drop due to the frictional resistances is due to the gas and solids.

$$\Delta P_f = \Delta P_{GWF} + \Delta P_{SWF} \tag{32}$$

The pressure drop due to the gas frictional resistance can be expressed by the Fanning Equation:

$$\Delta P_{GWF} = \frac{2 \ f_g \rho_g U_g^2 \Delta L}{d_t} \tag{33}$$

where the friction factor can be estimated from the following equations:

$$f_g = \frac{16}{Re} \qquad Re = \frac{\rho_g U_o d_t}{\mu} < 3 \times 10^3 \qquad (34A)$$

$$f_g' = 0.791/Re^{0.25} \qquad 3 \times 10^3 < Re < 10^5 \qquad (34B)$$

$$f_g = 0.008 + 0.0552/Re^{0.237} \qquad 10^5 < Re < 10^8 \qquad (34C)$$

The pressure drop due to the solids frictional resistance has been studied by a number of investigators. Two approaches are generally taken to express this effect. Rose et al. [42] obtained the solids frictional resistance term by modifying the gas frictional resistance:

$$\Delta P_{SWF} = \frac{\pi}{8} (\frac{f_p}{f_g}) (\frac{\rho_s}{\rho_g})^{1/2} (\frac{G_s}{G_g}) \Delta P_{GWF} \qquad (35)$$

The particle friction factor, f_p, is presented in a graphic form [42]. An alternative approach has been to use a modified Fanning Equation

$$\Delta P_{SWF} = \frac{2f_s \rho_s (1-\varepsilon) U_s^2 \Delta L}{d_t} \qquad (36)$$

The solid friction factor, f_s, has been obtained by several researchers. Stemerding [43] found the solids friction factor to be:

$$f_s = 0.003 \qquad (37)$$

Reddy and Pie [44] determined that the solids friction factor was given by:

$$f_s = .046(U_s)^{-1} \qquad (38)$$

Van Suaaij et al. [46] obtained the solids friction factor from experiments designed specifically for measurement of the shear stress at the wall due to the solids. The solids friction factor is given by:

$$f_s = .080(U_s)^{-1.22} \qquad (39)$$

Capes and Nakamura [47] obtained the following relation for the solids friction factor from their experimental study:

$$f_s = 0.048 \ (U_s)^{-1} \qquad (40)$$

Yang [45] reviewed the literature data and developed the following correlation for the solids friction factor:

$$f_s = \frac{0.01025 \ (1-\varepsilon)}{\varepsilon^3((1-\varepsilon)\frac{Re_t}{Re_{s1}})^{1.021}} \qquad (41)$$

A.7.4 Riser Section. The riser portion (section F-G) of the high velocity fluidized bed has not been investigated in detail. However, it is assumed that the pressure drop can be expressed as the sum of

the individual contributions due to kinetic energy, potential energy, frictional resistance effects and cluster formation.

$$\Delta P_{F-A} = \Delta P_{SKE} + \Delta P_{SPE} + \Delta P_f + \Delta P_c \qquad (42)$$

The pressure drops ΔP_{SKE} and ΔP_f can be determined from Equation (31) and (32), respectively. The solids velocity U_s used in Equations (31) and (32) is taken to be the time average velocity

$$\bar{U}_s = \frac{G_s}{\overline{\rho_s(1-\epsilon)}} \qquad (43)$$

where $\overline{\rho_s(1-\epsilon)}$ is the time average apparent density in the riser. The potential energy term can be obtained from an equilibrium force balance and is expressed:

$$\Delta P_{SPE} = \overline{\rho_s(1-\epsilon)} \; g \; \Delta L \qquad (44)$$

The pressure drop ΔP_c due to solid cluster formation is actually caused by the continuous particle-gas frictional effects experienced by the solid particles as the clusters form and break apart. This pressure drop contribution is inclued in ΔP_{SWF}.

A.7.5 Pressure Drop Across Orifice Plates. Leung and Jones [17] have reviewed the data and models presented in the literature for gas-solid flow through orifice plates. They present the models:

$$\Delta P = \frac{G_s^2}{C_D^2 \, 2(1-\varepsilon) \, \rho_s} \tag{45}$$

and

$$\Delta P = \frac{G_s^2}{C_D^2 \, [A^2/(A^2 - A_0^2)] \, 2 \, (1-\varepsilon) \, \rho_s} \tag{46}$$

Predictions of the first equation agree with the extensive results by six investigators. The value of C_D ranges from 0.5 to 0.65. The second equation incorporates a term to account for the "non-trivial momentum of a loosely packed bed". The orifice discharge coefficient, C_D, ranges from 0.65 to 0.98. The values of C'_D have been calculated using estimated flowing voidages thus providing the wider range in values. The momentum correction form is approximately 1.15 for an orifice/valve 50% open. The correction provided by this term is negated by the uncertainty in C'_D. Leung and Jones recommend the use of Equation (45) for design and analysis.

A.7.6 Pressure Drop in Bends Due to Gas-Solid Flow. Kunii and Levenspiel [42] present an equation which predicts the pressure drop in bends due to gas-solid flow. This equation is used extensively in pneumatic transport. The pressure drop is given by

$$\Delta P = f_b \, \bar{\rho} \, U_0^2 \tag{47}$$

The bend friction factor, f_b, is 0.375, 0.188, 0.125 for r_b/d_t equal to 2, 4 and 6+, respectively.

B. Coal Combustion

Coal is the world's most abundant resource. The United States has 437 billion tons of coal of which 265 billion tons is recoverable with current mining technology. To utilize coal in the most advantageous way, the chemical-physical make up of coal must be known thoroughly. Coal is a complex heterogeneous material. Coal and its use are being studied throughout the world to supply the ever increasing energy demand.

B.1 Coal

Coal is a complex, solid, heterogeneous material of carbon base, capable of supplying energy for heat and processing. The chemical and physical make-up of coal has been studied extensively and continues to be studied. Coal studies are usually divided into two areas - coal chemistry (chemical and physical make-up) and coal utilization (combustion, gasification, and liquification).

B.1.1 Coal Chemistry. Coal is classified by rank and grade [50]. Coal rank is a method of expressing the progressive metamorphism of coal from lignite (low) to metaanthracit (high). There are four ranks of coal: (1) lignite; (2) subbituminous; (3)

bituminous; and (4) anthracite. Each rank has also been subdivided, based on ash free heating values for low rank coals and moisture-ash free fixed carbon content for high rank coals. The results of the subdivisions, lowest to highest rank are: lignite B, lignite A, subbituminous C, subbituminous B, subbituminous A, high volatile bituminous C, high volatile bituminous B, high volitile bituminous A, medium volatile bituminous, low volatile bituminous, semianthracite, anthracite, and metaanthracite. The heating value increases from 13,900 kJ/kg for lignite B to 34,900 kJ/kg for low volatile bituminous A and then decrease to 30,100 kJ/kg for metaanthracite. The fixed carbon content increases from 25% for lignite B to 90% for metaanthracite.

Coal is also classified by grade. The three factors which cause coal to have a low grade are: high ash content, low ash fusion temperature and high sulfur content. Sulfur is the primary constituent which lowers the grade and thus has been studied extensively. Sulfur in coal lowers the quality of iron and steel, causes corrosion and deposits and promotes air pollution. Sulfur ranges between 0.2% to 7.0% by weight, with the average being between 1% and 2%. Sulfur occurs as inorganic pyrite and marcasite (40% to 80%) with the balance contained in the organic structure. The highest sulfur coals are the bituminous coals of the Pennsylvanian age in the Appalachian, Illinois and Western Interior coal basins. The lowest sulfur coals are the subbituminous coals and lignites in the Rocky Mountain and Northern Great Plains Regions. These coal have less than 1% sulfur. The molecular structure of coal is not

completely known. Investigators (Solomon; Wisner; and Heredy and Wender [51]) have gathered information from infrared measurements, nuclear magnetic resonances, ultimate and proximate analyses and prolylsis data to obtain models for the chemical structure of the organic back bone in coal. This organic back bone of coal is constructed of aromatic and hydro-aromatic units. Some of these units have various functional groups which cross link the units together. The planer nature of the aromatics gives the coal a layered consistency. The layers may be twisted to prevent a perfect laminate. The imperfection in the laminate creates pores which may house ash or other impurities. Low rank coals have about 90% of the carbon associated with five unit layers while high rank coals have about 90% of the carbon associated in 30 unit layers [50, 51, 52, 53].

B.1.2 Coal Utilization Techniques. Coal has been utilized principally by burning (combustion). Coal can also be gasified or liquified. Coal gasification has been conducted on a commercial scale in the past and to a limited extent currently, i.e., Sasol 1, 2 and 3 in South Africa. Coal liquefication has not been commercialized as yet.

Coal is combusted either in fixed bed stoker boilers, fluidized bed boilers, or in pulverized coal boilers [50, 51, 55]. Stoker boilers burn large pieces of coal at high temperatures [50]. Fluidized bed boilers burn coal with a particle size of 1,000 μm at low temperatures to permit sulfur removal during combustion. A

45,500 kg/hr prototype fluidized bed is in operation at Georgetown University, Washington, D.C. Pulverized coal combustors burn particles of coal with a diameter less than 70 μm at high temperatures. Every major utility in the United States uses one of these techniques for coal combustion.

Many processes have been studied for coal gasification and liquefaction [55, 56, 57, 58]. The only commercial gasifiers are the Lurgi design - fixed bed, stokers.

B.2. Engineering Combustion Models

Coal combustion is envisioned to occur in three steps, sequentially and simultaneously. These steps or processes are devolatilization, char oxidation and gas phase oxidation of the volatiles. Engineering models for each process are discussed below.

B.2.1 Devolatilization.

Coal devolatilization has been studied by many investigators and many models have been developed [50]. The models reviewed herein are limited to coal particles less than or equal to 100μm. These models are categorized as: (1) single reaction, (2) multiple parallel reactions, (3) multiple competing reactions, (4) complex schemes, and (5) schemes involving secondary char formation. These models vary from the very simple to the very complex. The details of these models are discussed below.

For the single reaction, coal →solid + volatile, the reaction rate models are simple and quite limited. Both an Arrhenius expression:

$$\frac{dV}{dt} = k(V_\infty - V)^n \tag{48}$$

and a non-Arrhenius expression

$$\frac{dV}{dt} = BV_\infty/t \tag{49}$$

have been developed. The order n in the Arrhenius expression has been estimated to be between 1 and 8 depending on the investigator. The non-Arrhenius expression neglects the observed temperature dependence on devolatilization.

The second category, multiple parallel reactions, are first order Arrhenius expressions. This category has been subdivided by Ubhayakar [50] into two sections, namely two first order Arrhenius models and multiple first order reactions with a statistical distribution of the activation energy. The devolatilization process is modeled by the first of these techniques by the following set of equations:

$$
\begin{aligned}
C_1 &\xrightarrow{k_1} S_1 + V_1 \\
C_2 &\xrightarrow{k_2} S_2 + V_2
\end{aligned}
\tag{50}
$$

where:

$$\frac{d\,C_{1,\,2}}{dt} = -k_{1,\,2}\,C_{1,\,2} \tag{51}$$

The second technique is described by the equations below:

$$\text{Coal} = \sum_{i=1}^{n} C_i + \sum_{i=1}^{n} \overset{k_i}{} (S_i + V_i) + S + V \qquad (52)$$

where:

$$\frac{dV_i}{dt} = k_i (V_{i,\infty} - V_i) \qquad (53)$$

$$k_i = A \exp (-E_i/RT) \qquad (54)$$

$$\int_{o}^{\infty} f (E) dE = 1 \qquad (55)$$

Equation (55) gives a complete statistical distribution of activation energy.

Multiple competing reaction models, the third category, are also used to express the devolatilization process. The reaction is expressed

$$\text{Coal} \quad \overset{k_1}{\underset{k_2}{\overset{k_n}{\searrow}}} \quad \begin{array}{l} (1 - Y_1) \text{ Char} + Y_1 V_1 \\ (1 - Y_2) \text{ Char} + Y_2 V_2 \\ (1 - Y_n) \text{ Char} + Y_n V_n \end{array} \qquad (56)$$
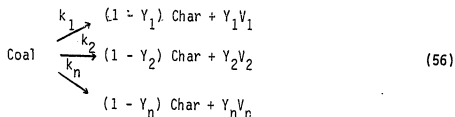
with two rate equations

$$\frac{d (\text{coal})}{dt} = - (\sum_{i=1}^{n} k_i) \text{ Coal} \qquad (57)$$

and

$$\frac{dV}{dt} = (\sum_{i=1}^{n} Y_i V_i) \text{ Coal} \qquad (58)$$

Kobayashi [50, 51] used this model with $n = 2$. Smith and Smoot [51] applied this model in their pulverized coal combustion and gasification models with good success.

The fourth category, complex schemes, include the multiple consecutive parallel first order reaction:

$$\text{Coal} \xrightarrow{k_1} \text{metaplast} \xrightarrow{k_2} \text{residue} \xrightarrow{k_4} \text{primary tar} \qquad (59)$$

with branches:
$$k_3 \downarrow \qquad k_5 \downarrow \text{secondary tar} + \text{gas}$$
$$\text{semi-coke} + \text{gas}$$
$$k_r \downarrow \text{coke} + \text{gas}$$
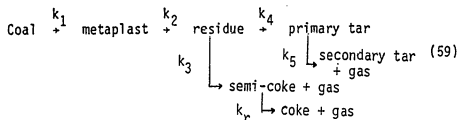
and the parallel competing first order reaction:

$$\text{Coal} \xrightarrow{k_1} \text{Activated Coal} \xrightarrow{k_2} \text{char}$$
$$\xrightarrow{k_3} \text{methane and ethane} \qquad (60)$$
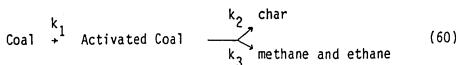
These two mechanisms are complicated, producing several intermediate and final products. A coal combustion model needs a simple, straight forward model of the devolatization process. These two models do not provide these criteria.

In the final category, schemes involving secondary char forming reactions, contains two models: (1) consecutive competing char forming reactions; and (2) parallel competing char forming reactions. These models are prohibitively complex for their inclusion in a combustor model. The first has seven reactions, producing seven product types while the second has n + 2 reactions and a statical distribution of activation energies.

The models presented above indicate that the fraction of volatile matter evolved is a function of both the temperature and the length of time for which devolatilization occurs. For bituminous coals, Kobayashi et al. [51] report that at a temperature of 1260°K and for a time of 200 millinseconds 30% of the coal is volatilized.

B.2.2 Char Oxidation. The devolatilization process produces a solid residue, char. The char consists of the fixed carbon and ash. In actuality, the char is a composite material containing carbon, hydrogen, sulfur, oxygen, nitrogen and ash. An ultimate analysis of the char shows that the fractions of each of these elements are in approximately the same ratios as in the parent coal. Char oxidation is a heterogeneous chemical reaction. Heterogeneous reactions have been studied extensively [42]. The reaction mechanism developed in those studies is discussed below.

B.2.2.1 Heterogeneous char reactions. Char consists of three elements: carbon, hydrogen and sulfur, which are oxidized. The general heterogeneous chemical reaction is expressed as:

$$A_{gas} + bB_{solid} \xrightarrow{k} products \qquad (61)$$
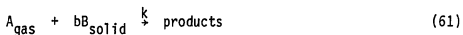
Written in this manner, the reactions for carbon, hydrogen and sulfur become:

$$O_2 + 2C \rightarrow 2CO \qquad (62)$$

$$O_2 + C \rightarrow CO_2 \qquad (63)$$

$$O_2 + 4H \rightarrow 2H_2O \qquad (64)$$

$$O_2 + S \rightarrow SO_2 \qquad (65)$$

This group of reactions is a simplification of possible reactions which have been researched and shown to exist in minor amounts [50].

Smith has reviewed the question as to which product is favored CO or CO_2, and suggests that CO is the most likely [51].

B.2.2.2   Kinetics   of   heterogeneous   char   oxidation.
Heterogeneous chemical reactions have been studied extensively. Levenspiel [59] has proposed a mechanism for gas-solid reactions which has withstood numerous investigations and applications. Heterogeneous reactions are envisioned to proceed by the following steps:

(1) Diffusion of reactant gas from the bulk fluid through the gas film surrounding the particle to the solid surface.

(2) Penetration and diffusion of reactant gas through a blanket of ash (solid product) to the unreacted core.

(3) Chemical reaction of reactant gas with solid at the reaction surface.

(4) Diffusion of the product gas through the ash to the exterior surface of the particle.

(5) Diffusion of the product gas through the gas film surrounding the particle to the bulk fluid.

One or all of these steps may be involved in the chemical reaction sequence. The step(s) which offer the greatest resistance to the propagation of the reaction is(are) called the rate controlling step(s). For reactions such as char oxidation in which a stationary ash layer is not formed, steps 2 and 4 have negligible resistances and can be neglected. The driving force for the product gas between the surface and the bulk fluid is in general quite large since the bulk contains little or no product gas. Thus, step 5 offers negligible resistance and is neglected.

The rate of chemical reaction for the general reaction with steps 1 and 3 controlling is given by:

$$R = \frac{dm_B}{dt} = \frac{A \, b \, M_B \, C_A}{\frac{1}{k_c} + \frac{1}{k_d}} \tag{66}$$

The two terms $\frac{1}{k_c}$ and $\frac{1}{k_d}$ are the chemical reaction resistance and the mass transfer resistance, respectively. The chemical reaction rate constant, k_c has been studied extensively for the carbon-oxygen raction [50, 51]. However, reaction rate constants for the hydrogen-oxygen and sulfur-oxygen reactions are not available in published literature. The mass transfer coefficient, k_d has been studied extensively for a single particle in a fluid [42].

The reaction rate coefficient for the carbon-oxygen reaction has been well studied by investigators [51]. These investigators have used the conventional Arrhenious expression $k = A \exp(-E/RT)$ to model the effect of reaction temperature. Table 1 summarizes the values for the frequency factor A, and activation energy E, along with the type of coal char and particle size used in the experiment. As can be seen in Table 1, the type of coal char greatly influences the values of the frequency factor and activation energy.

The mass transfer coefficient is expressed:

$$k_d = \frac{Sh\ D}{dp} \tag{67}$$

The Sherwood Number, Sh, is modeled by:

$$Sh = 2 + 0.6\ Re^{1/2}\ Sc^{1/3} \tag{68}$$

<div align="center">

Table 1

Carbon-Oxygen Reaction Rate Constants, k_p

$$\text{where} \quad k_p = \frac{k_c \, M_{O_2}}{T_g \, R} = A \exp(-E/RT)$$

</div>

Type of Coal Char	Particle Size (μm)	Frequency Factor ($\frac{g}{cm^2 \, s \, atm \, O_2}$)	Activiation Energy ($\frac{k_{cal}}{kgmol}$)
Bituminous	28	92	21,900
	38		
	82		
	105		
Non-swelling Bituminous	27	45.7	17,263
	38	80.3	21,787
Swelling Bituminous	31	94.3	23,463
	72	1000	35,194
Anthacites and Semi-Anthacites	23 thru 78	20.4	19,000
Flash Pyloysis Char	85	16.3	17,597
Petrolium Coke	-	15	19,000

The Sherwood Number or the mass transfer coefficient modeled by these equations shows good agreement with the experimental data and is an accepted approach to modeling the mass transfer resistance.

B.2.3 Volatile Matter Oxidation. Experimental information on the volatile oxidation rate has not been found in the literature. Experimental research in this area is needed to verify the theoretical predictions [50, 51]. Volatile product combustion times are estimated by considering only mass transfer resistances and chemical reaction rate resistances [52]. The burning time, assuming the volatiles to have a molecular weight of 100 and the coal to have a volatile fraction of 0.5, is 7 milli-seconds for a 50 m coal particle at 1273°K. If the mass transfer resistance is negligible, such that only the chemical reaction is considered and assuming the reaction rate to be that for CO going to CO_2, the slowest step, the combustion time can be estimated. These assumptions provide only an order of magnitude value. The burning time for a 50 m particle and at 1273°K is 3.2 milli-seconds. These two burning time values are approximately the same, such that the volatile oxidation process is neither only diffusion controlled nor reaction rate controlled.

B.2.4 Soot Oxidation. The oxidation time for soot has been estimated [52]. For a soot particle with a 500A° diameter the combustion time is 0.173s at a temperature of 1600°K [52]. Lee, Thring and Beer [52] obtained the following expression for the soot combustion rate:

$$q = 1.085 \times 10^4 \; P_{O_2} \; T^{1/2} \; \exp(-39300/RT) \quad [=] \frac{g}{Cm^2 s} \quad (69)$$

for 400A° soot particles.

C. Desulfurization

The introduction of the Clean Air Act has nurtured the development of sulfur dioxide removal processes. Both wet and dry techniques have been developed to date, with wet processes dominating the market. These processes are expensive to manufacture and operate. Dry processes such as limestone injection systems and fluidized bed coal combustion in a limestone bed are both being researched.

Dry sulfur dioxide removal processes utilize the following chemical reaction.

$$CaO + SO_2 + 1/2 \; O_2 = CaSO_4 \quad\quad\quad (70)$$
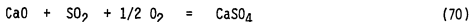
The reaction proceeds forward at temperatures up to 1500°K for sulfurdioxide concentrations approximately 3000 ppm [60]. The calcium oxide is generated by the calcination of limestone ($CaCO_3$) and dolomite ($CaCO_3/MgCO_3$). The calcium oxide and magnesium oxide obtained by calcination are both capable of sulfinating. Formulation of magnesium sulfate occurs at temperatures below 1110°K. However,

experimental evidences show the reaction to occur only slightly in the 700 to 970°K temperature range [60].

The sulfination reaction rate has been found to decay with time. This phenomenon is explained by the observation that pores are created in the stone structure by the calcination process. The actual decay in rate is attributed to the substitution of the much larger sulfurtrioxide molecule for the carbon dioxide molecule. Researchers have taken two approaches towards modeling this phenomenon. Some have used a simple exponential decay models [60, 61, 62] while others have used complicated grain models [63, 64]. The grain models are more theoretical in nature and probably describe the actual decay phenomenon as it truly is. However, the grain models' complexities limit their use in a combustion process model.

Lee et al. [61, 62] have developed a simple model based on two experimental parameters, which predicts the time decay quite well, and is discussed below. The rate of reaction is expressed by the product of the initial rate and an exponential decay term.

$$R = R_0 \ e^{-t/\tau_p} \tag{71}$$

The exponential decay term contains the pore plugging time constant, τ_p, which is taken as one third the pore plugging time.

$$\tau_p = \frac{t_p}{3} \tag{72}$$

The pore plugging time has been shown to be inversely proportional to the sulfur dioxide concentration, thus τ_p can be expressed by:

$$\tau_p = \frac{P^*}{C_{SO_2}} \qquad (73)$$

where P^* is the pure plugging constant. The initial rate R_o, is expressed by:

$$R_o = \frac{\pi d_p^3}{6} \rho_s \, k \, S_n \, C_{SO_2} \qquad (74)$$

The group $\rho_s k S_n$ is combined into one constant τ_{SF} which has been provided for a number of limestone and dolomite stones. Upon substituting, Lee et al. obtained the following equation:

$$R = \frac{\pi d_p^3}{6} \frac{C_{SO_2}}{\tau_{SF}} e^{(-tC_{SO_2}/P^*)} \qquad (75)$$

The only parameters needed from experimental data are P^* and τ_{SF}. Lee et al. has provided these data [61]. They conducted all their experimental work using 1000 µm particles.

Borgwardt [60] has conducted extensive experimental studies on stone sulfination. He has modeled the reaction rate time delay phenomenon by modifying the conventional Arrhenious frequency factor. Borgwardt presented the following model:

$$R = \frac{n}{\rho_s} A_0 \, e^{-\beta n'/w} \, e^{-E/RT} \, C_{SO_2}^m \qquad (76)$$

He presents a method to obtain β, the exponential decay coefficient. However, the number of parameters is greater than those needed in the model by Lee et al. and typical values have not been provided.

4. EXPERIMENTAL SET-UP AND PROCEDURE

The experimental unit shown in Fig. 3 has been assembled from a 0.038 m (1-1/2 in) pyrex brand glass pipe. There are four nozzles, N_1, N_2, N_3 and N_4 located at the lower part of the loop which supply air at high velocity to fluidize the solid particles. Solid particles are placed in the feed hopper. These solids are fed manually to the LFB at the top of the standpipe through a ball valve. The particles traverse the standpipe as moving bed flow, entering the eductor zone. The particles are entrained in the high velocity air stream at this zone. The air is supplied from an Ingersoll-Rand compressor. The flow rate is measured with four Dwyer rotameters. The particles conveyed upwards travel through an Auburn mass fraction monitor. The monitor continuously measures the percent solids of the two-phase stream as it flows past. The pressure drop across the monitor is monitored with a Validyne differential pressure transducer - indicator system. These instruments give analog outputs proportional to the corresponding variables. The analog outputs are recorded by a Cole-Palmer strip chart recorder. The solid particles and gas travel through the remainder of the riser and then loop around the top via a 135° bend and a 45° bend. The gas exits via a 135° bend while the solid particles return to the standpipe. The air containing a small amount of solid particles flows through a cyclone and a bag filter (not shown in figure); solids leave the loop through

45

FIG 3 HIGH VELOCITY FLUIDIZED BED EXPERIMENTAL UNIT

D.P.T. = DIFFERENTIAL PRESSURE TRANSDUCER
N = NOZZLES
P = PRESSURE PORTS

46

the cyclone bottom. Pressure ports are provided approximately every 1/3 of a meter around the loop for pressure monitoring with water manometers.

4.1 Details of the LFB System

Each component in the LFB system is discussed in detail below.

4.1.1 Loop.

The test loop is constructed out of a corning 0.038 m (1-1/2 in) glass process pipe. The glass pipe sections are connected to one another with one bolt couplings. The loop is capable of operating at pressures up to 120 kPa gauge and temperatures between 290°K and 480°K. Pressure taps have been provided to the glass pipe, so that the pressure can be monitored approximately every one-third of a meter. The detailed dimensions are given in Table 2.

4.1.2 Nozzles.

The primary air nozzles, N_1 through N_4, have been designed to connect directly to the glass loop reducing the dead zones. They are made of carbon steel and cut at 45° angles to promote smooth flow around the bend. Nozzle, N_0 is made of glass and permanently attached to the standpipe.

4.1.3 Auburn Monitor.

The Auburn monitor consists of two separate units, the sensor spool and the electronics. The sensor spool is constructed from a heavy steel pipe which has an inner

Table 2

Equipment Dimensions

Diameter	0.038 m
Nozzle Diameter	0.0064 m
Riser Height	2.1 m
Standpipe Height	
Total	1.2 m
Solids Level	0.5 to 1.0 m
Total Length (between lower upper loop)	2.3 m

Pressure Port Number	Sand	Height, m Limestone and Gypsum
P_1	0.0	0.0
P_2	0.26	0.26
P_3	0.36	0.61
P_4	0.61	0.85
P_5	1.46	1.46
P_6	2.10	2.10
P_7	2.05	2.05
P_8	0.99	0.99
P_9	0.35	0.35

diameter of 0.038 m (1-1/2 in). Six individual sensor points are supplied around the spool. The electronics monitor the signals and analyze them to give an output voltage proportional to the voidage of the flowing suspension.

For the proper operation of the Auburn monitor, the following precautions must be taken [38]:

(1) Particles/solids should be bone dry.

(2) Gas bubbles should not be present. These bubbles may distort the electric field lines near the sensing electrodes.

(3) Temperature and pressure should not exceed 623°K and 10,000 kPa (1500 psig), respectively. These thermo-dynamic variables for this study are at room tempera-ture and atmospheric pressure.

4.1.4   Differential Pressure Measurement.   The differential pressure across the Auburn monitor is obtained via a Validyne differential pressure transducer (model DP45). Model DP45 is capable of measuring pressure drops as low as 0.0055 m (0.22 in) H_2O. The signal generated by the transducer is sent to a Validyne model CD12 transducer indicator. The indicator also supplies a 0 to 10 VDC analog output proportional to the differential pressure.

4.1.5 Stripchart Recorder. The analog output supplied by the Auburn monitor and the Validyne transducer indicator is recorded by Cole-Parmer three channel laboratory stripchart recorder model K-8373-30. The recorder has 22 speeds, ranging from 1 cm/hr to 1800 cm/hr. The full scale reading of each channel can be independently set at one of ten ranges, 1 mv to 5 V. The channel is also supplied with a 10:1 attenuator allowing voltages up to 50 V to be recorded.

4.1.6 Air Supply. Air is supplied from an Ingersol-Rand model T30 two stage compressor. The compressor is capable of supplying 1.15 m^3/min (40 scfm) at 346 kPA (50 psi). An 0.31 m^3 (80 gallon) receiving tank is provided to reduce pressure fluctuations. Also, the compressor system is supplied with constant speed control to reduce the receiver pressure fluctuations.

4.2 Modifications to the Equipment (Standpipe)

During the experiments it was observed that the flow rate through the air nozzles was not adequate to keep the solids properly fluidized. Consequently, higher capacity rotameters and manometers were installed.

The solid mass flux in the LFB was found to be relatively insensitive to the gas mass flux. This inability to regulate the solid mass flux was considered to be a severe limitation. In most studies [1, 2] on recirculating fluidized beds the solid mass flux was regulated with a slide valve. Considering the mechanical problems associated with valves in high temperature environments, an alternate solution was sought. A review of the literature on

standpipe flow revealed that air injected at the bottom of a standpipe above an orifice plate could vary the solid mass flux (18, 40, 41]. Thus, it was decided to modify the standpipe with an orifice plate and air injection system to regulate the solids mass flux.

5. EXPERIMENTAL OPERATING CONDITIONS

With the modifications discussed earlier there are a total of five nozzles, N_0 through N_4, in the experimental LFB test unit as shown in Figure 4. These may be operated at different flow combinations. Each nozzle has a specific function. N_0 regulates the solids mass flux, to be discussed later. Nozzles N_1 and N_2 provide solid transportation through the LFB. Nozzle N_3 reduces the saltation in the eductor section (horizontal to vertical bend towards the riser). Finally, nozzle N_4 provides gas mass flow control and is used in conjunction with nozzles N_0, N_2 and N_3.

Experiments are carried out using the operating conditions listed in Table 3. The solids used in this study are sand, limestone and gypsum particles. Limestone and gypsum have been chosen since these will be present in an HVFB coal combustion system. The characteristics of these solids are presented in Table 4.

52
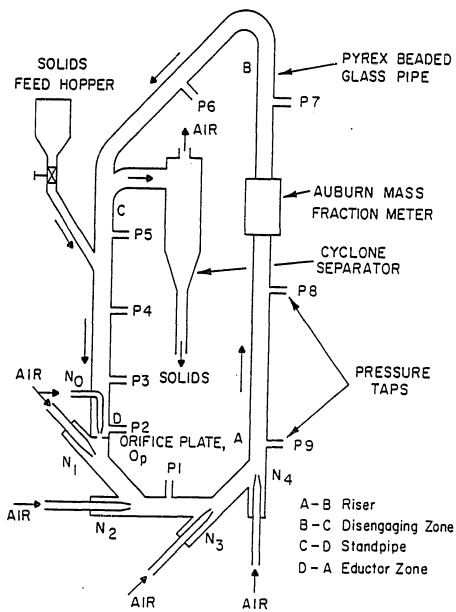
FIG 4 MODIFIED LOOP FLUIDIZED BED

Table 3

Nozzle Flow Rates

Temperature	298°K
Pressure	10-50 kPa Gauge

Nozzle Air Velocity	Air Volume
N_1 0 - 237 ms^{-1}	0 - 7.5 x 10^{-3} m^3s^{-1}
N_2 0 - 237 ms^{-1}	0 - 7.5 x $10^{-3}m^3s^{-1}$
N_3 0 - 118 ms^{-1}	0 - 3.8 x 10^{-3} m^3s^{-1}
N_4 0 - 118 ms^{-1}	0 - 3.8 x 10^{-3} m^3s^{-1}
N_0 0 - 49 ms^{-1}	0 - 1.58 x 10^{-3} m^3s^{-1}

Superficial Velocity in Riser	3.9 - 7.6 ms^{-1}

Table 4

Particle Characteristics

	Sand	Limestone	Gypsum
Average size (μm)	300	452	296
Particle density (kg/m^3)	2575	2737	2244
Bulk density (kg/m^3)	1455	1394	1104

Size Distribution

Mesh	d(μm)	Sand	Wt. Fraction Limestone	Gypsum
-16 + 18	1090	–	0.03	0.11
-18 + 30	800	0.20	0.33	0.28
-30 + 40	510	0.26	0.40	0.16
-40 + 50	360	0.23	0.16	0.12
-50 + 60	275	0.09	0.03	0.05
-60 + 80	215	0.11	0.02	0.10
-80	110	0.11	0.04	0.18

6. HYRODYNAMIC EXPERIMENTAL RESULTS AND COMBUSTION MODELING

The overall objectives of this investigation have been to study the hydrodynamic characteristics of a loop fluidized bed system and to develop coal combustion and desulfurization models using the fast fluidization principle. In order to accomplish these objectives the investigation has been conducted in two parts. In the first part, an experimental cold flow bench scale unit was designed and assembled as discussed in Chapters 4 and 5. This experimental investigation is undertaken to obtain pressure drop data for the development of a model predicting the hydrodynamics of the high velocity fluidized bed system. The experimental results and discussion of this study are presented in Section A.

In the second part of this thesis, the development of coal combustion and desulfurization models for the LFB combustor has been undertaken. These models include the conversion of carbon, sulfur and hydrogen contained in the coal particle as a function of the combustor length. The net sulfur dioxide gas evolved by combustion less the sulfur dioxide absorbed in the calcium sorbent is also estimated as a function of the combustor length by the model. It may be mentioned here that no experimental work was conducted on LFB the combustion process. However, the HVFB combustion model developed has been applied to the bubbling fluidized bed combustor and the pulverized coal combustor. The predicted results are compared against the literature values for these systems.

56

The following chapter gives the conceptual design of a LFB combustor for processing coal. The use of the models developed in this chapter is demonstrated in designing the LFB combustor unit. The results from the designed unit are compared with the results from existing combustion systems.

A. Hydrodynamic Experimental Results and Pressure Drop Model

The objective of the experimental investigation has been essentially to study gas-solid flow characteristics in a Loop Fluidized Bed. The experiments have been conducted in an experimental set-up as discussed earlier. Initial experiments have been conducted without the use of an orifice plate and nozzle N_0 in the standpipe. These experiments helped in fixing nozzle positions and studying their effect on LFB performance. An orifice plate and nozzle when introduced in the standpipe reduced the void fraction (increased the solid throughput) in the riser section. The major part of this study has been conducted using the standpipe with the orifice plate.

A.1 Work Without the Orifice Plate

Experiments have been conducted to study the gas-solid flow characteristics in the LFB. The data from these experimental runs are to define good operating regions for the system. A good operating region is that when the LFB can be operated at various flow rates through the nozzles with no slugging in the standpipe, choking

in the riser, or significant saltation in the eductor. The main emphasis of the work has been to study the solids flow behavior in the riser since it is in this zone that coal combustion and SO_2 removal would occur.

A.1.1   Selection of Nozzle Positions in the LFB.   The initial experimental efforts are directed to study the effect of air flow rate through nozzles (N_1 through N_4 as shown in Figure 4) on the flow characteristics of sand-air system circulating through the loop. The equipment dimensions, nozzle flow rates, and particle characteristics are presented in Tables 1, 2 and 3.   Experiments are conducted injecting air through nozzles individually as well as in combinations.   The results are presented in Tables 5 and 6.   When conducting experiments with individual nozzles, the best results are obtained with nozzle, N_2 with an air flow rate of 6.2×10^{-3} m^3/s. The void fraction could be reduced to 0.98 by decreasing the air flow rate to 4.4×10^{-3} m^3/s Using a nozzle combination N_2 and N_3 the void fraction could be further reduced to 0.975. A reduction in void fraction means an increase in solid content which is one of the desired objectives.

A.1.2   Effect of Standpipe Height on Riser Void Fraction. Efforts have been made to decrease the riser void fraction and thus increase the solids flow content through the riser by controlling air flow rate through the nozzles. It is found that standpipe height for the nozzle combinations studied restricted the extent to which the

Table 6

LFB Performance at Various Nozzle Flow Rates

Nozzle	Air Rate ($m^3 s^{-1}$)	ε^*	Eductor	Riser	Standpipe
N_1	7.5×10^{-3}	0.99	No Saltation	No Mixing	Steady
	6.7×10^{-3}	0.985	Solids Saltation in N_3-N_4 Region	Good Mixing	Bubbling
	6.5×10^{-3}	----	N O S O L I D S F L O W	----	Slugging
N_2	7.5×10^{-3}	0.99	No Saltation	No Mixing	Steady
	6.2×10^{-3}	0.985	No Saltation	Good Mixing	Steady
	4.4×10^{-3}	0.98	Saltation in N_3-N_4 Region	Good Mixing	Steady
	4.0×10^{-3}	----	N O S O L I D S F L O W	----	Slugging
N_3	All Gas Flows	----	N O S O L I D S F L O W	----	
N_4	All Gas Flows	----	N O S O L I D S F L O W	----	

*In riser section

Table 6

LFB Performance for Various Nozzle Flow Rate Combinations

Nozzles	Air Rates (m^3s^{-1})		ε^*	Eductor	Riser	Standpipe
	1st	2nd				
N_1 & N_2	4.17×10^{-3} to 7.5×10^{-3}	$.1 \times 10^{-3}$ to 1.57×10^{-3}	----	N O S O L I D S F L O W ----		Slugging
N_1 & N_3	7.5×10^{-3}	0.9×10^{-3}	0.98	Saltation in N_3-N_4 Region	Good Mixing	Steady
	7.0×10^{-3}	0.9×10^{-3}	----	N O S O L I D S F L O W ----		Slugging
	7.0×10^{-3}	1.8×10^{-3}	0.98	Saltation in N_3-N_4 Region	Good Mixing	Steady
N_2 & N_3	5.0×10^{-3}	0.9×10^{-3}	0.99	Saltation Over Entire Eductor (1/4 Pipe filled)	Good Mixing	Steady
	4.13×10^{-3}	0.9×10^{-3}	0.985	Same	Same	Same
	3.12×10^{-3}	1.8×10^{-3}	0.98	Same	Same	Same
	3.12×10^{-3}	1.3×10^{-3}	0.975	Same	Same	Same

*In riser section
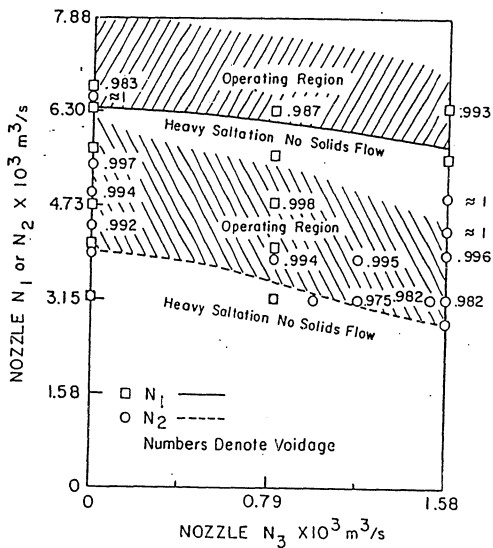
FIG. 5 LFB OPERATING REGIONS FOR NOZZLES N_1, N_2, AND N_3 FLOW RATES

void fraction could be reduced in the riser section. The experimental results agree with the estimated void fraction values from the mathematical equation proposed by Singh [48].

A.1.3 Effect of Air Flow Rates Through Nozzles on LFB Performance.

Experiments using the nozzle combinations N_1 & N_3 and N_2 & N_3 were conducted. The data are presented in Table A1 of Appendix A. In Fig. 5 flow rates through nozzles N_1 and N_2 are plotted against flow rates through nozzle N_3. Void fractions are also indicated at appropriate points. The operating regions are shown by the hatch lines for the two nozzle combinations N_1 & N_3 and N_2 & N_3. It is seen that the operating region for nozzle combination N_1 & N_3 is narrower (smaller range in voidage) than for nozzle combination N_2 & N_3. The LFB can be operated satisfactorily with any flow rate combination within these operating regions.

The LFB, as stated above, can be operated with a stable gas-solid flow for a number of nozzle flow rate combinations. However, the performance of nozzle combination N_2 & N_3 is found to be superior as it gave higher solids flux and solids loading over a wide range of air flow rates. Nozzle combinations of N_2, N_3 and N_4 can be used when a constant gas flux through the riser is required. This combination does not provide gas-solid flow with a low voidage due to extra air flow through nozzle N_4. However, the gas mass flux through the riser can be better regulated with the nozzle combination N_2, N_3 and N_4 due to the use of nozzle N_4.

A.2 Experimental Work with Orifice Plate and Nozzle N_0

In an effort to achieve a better regulation of solid mass flux, an orifice plate and a nozzle at the bottom of standpipe have been introduced as discussed earlier. Experiments are conducted to study the effect of the orifice plate and nozzle on solids flux. Three orifice plates with diameters 0.013 m (0.5 in), 0.019 m (0.75 in), and 0.025 m (1.0 in) are used.

A.2.1 Effect of Orifice Plate.

The use of the orifice plates with diameters 0.013 m (0.5 in) and 0.019 m (0.75 in) resulted in a flow through the riser with void fractions greater than 0.99 which are much higher than desired. The use of the 0.025 m (1.0 in) orifice plate reduced the void fractions to 0.975 which is the same as that obtained using no orifice plate. However, this orifice plate considerably helped in regulating the solids mass flux. It should be noted that the standpipe nozzle, N_0 is not used in these experiments.

The experimental data using the 0.025 m (1.0 in) orifice plate and nozzle combination N_2 & N_3 are presented in Table A2 of Appendix A. These data are plotted on a three dimensional diagram in Fig. 6. The three dimensional figure provides better estimates of the void fraction than can be obtained from a plot similar to Fig. 5. The operating region is the surface ABEFGHH' contained within the cube ABCD-A'B'C'D'. Nozzle N_3 flow rates are plotted along C'D' and those of nozzle N_2 are plotted along C'B'. The voidage is plotted along BB'. Nozzle N_2 flow rates are labeled as lines of constant flow rate. These lines are HH', GG', FF', EE' and II'. Nozzle N_3
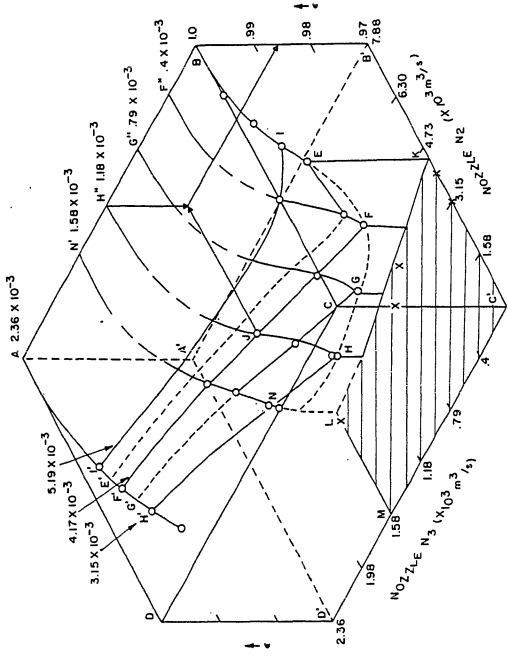
FIG. 6 OPERATING REGION FOR NOZZLES N$_2$ & N$_3$ WITH ORIFICE PLATE, O$_p$ (d = 0.025 m)
FOR SAND PARTICLES
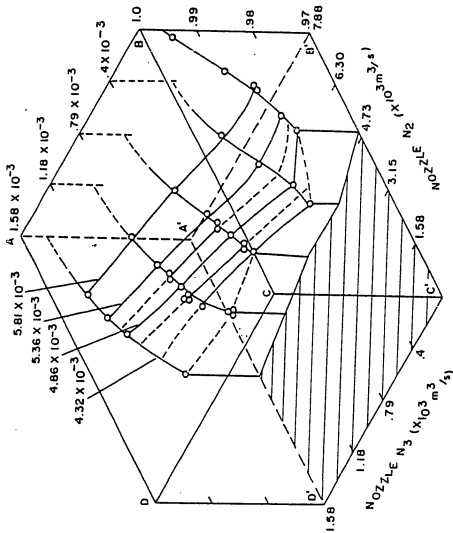
FIG. 7 OPERATING REGION FOR NOZZLES N_2 & N_3 WITH ORIFICE PLATE, O_p (d = 0.025m) FOR LIMESTONE PARTICLES
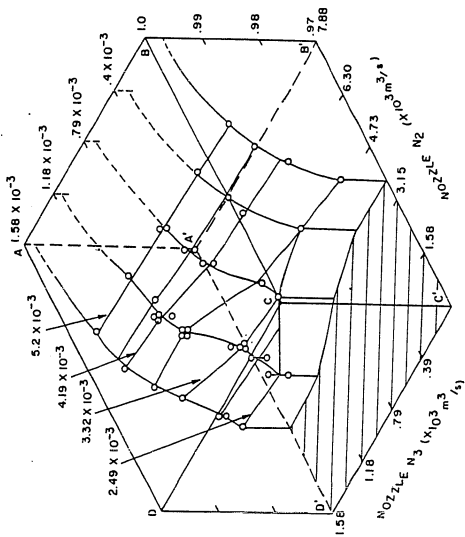
FIG. 8 OPERATING REGION FOR NOZZLES N_2 & N_3 WITH ORIFICE PLATE, O_P ($d = 0.025$ m) FOR GYPSUM PARTICLES

flow rates are also labeled as lines of constant flow rate on the surface. These lines are H'A, NN', HH', GG', FF' and EB.

Using Figure 6, the voidage can be estimated at any point in the operating region, say point J at the nozzle flow rates $N_2 = 4.17 \times 10^{-3}$ m^3/s and $N_3 = 1.18 \times 10^{-3}$ m^3/s, performing the following steps:

(1) On the plane ABB'A' draw a line parallel to BB' at the desired flow rate of nozzle N_3, say 1.18×10^{-3} m^3/s.

(2) Draw a line from point J parallel to CB to intersect the line constructed in Step 1.

(3) From the intersection point of these two lines, draw a line parallel to AB to intersect BB'.

(4) Read the voidage off BB'.

The area C'KLM (hatch lines) indicates nozzle flow rate combinations of N_2 & N_3 for which no flow could be obtained. The region of low void fraction and high solid mass flux is the surface EFGHJ and is of the most practical importance.

Similar data are also taken for the limestone and gypsum particles. These data are presented in Tables A3 and A4 of Appendix A, respectively. The operating regions for the limestone and gypsum particles are shown in Fig. 7 and 8. These regions are different for the three solids, however the general characteristics are the same. The actual differences are discussed in the following two paragraphs.

The operating region of limestone originates at larger air flow rates through nozzle N_2 than for sand. The use of nozzle N_3 does not have the marked effect in reducing the voidage in the limestone-air system as in the case of sand-air since the void fractions are lower

over the entire operating region. Furthermore, the region of high mass flux and low void fraction labeled EFGHJ on Figure 6 is much flatter for the limestone system. This increases the ease of operating the system in this high solid mass flux and low void fraction region. The operating region originates at larger air flow rates through nozzle N_2 since the limestone particles are both larger and more dense than the sand particles. The void fraction is lower for the entire operating region for the same reasons. The gas velocity in the riser provided by the flow through nozzles N_2 and N_3 is not sufficient to convey the heavier limestone particles through the riser at the same velocity as it does for the sand. Thus, for the similar solids flux values, the void fraction will be lower for limestone than for sand particles.

The operating region for gypsum is more similar to that for sand than for limestone. The minimum air flow rate through nozzle N_2 is lower for gypsum than for either sand or limestone particles. This is due to the lower density of gypsum. The high solids and flux low void fraction region is shaped very similar to that of sand. Considering the particle size and density for three solids, it is considered that the particle size is more responsible than the particle density for the steepness of this portion of the operating region.

A.2.2 Effect of Orifice Plate and Nozzle N_0. Experiments for sand particles are conducted using nozzle N_0 with each of the three orifice plates. The use of nozzle N_0 with air flow rates in the

range of 0 - 1.58 x 10^{-3} m^3/s could regulate solid mass flux for each of the three orifice plates. The flow rates through nozzle N_0 greater than 1.18 x 10^{-3} m^3/s could completely stop the solid mass flux for the 0.013 m (0.5 in) and the 0.019 m (0.75 in) orifice plates. However, the solids mass flux could not be completely stopped for the 0.025 m (1 in) orifice plate probably because of the large orifice diameter. Also, the use of nozzle N_0 with no orifice plate resulted in no solids mass flow.

Data for solids mass flux vs. air flow rates through nozzle N_0 for the two nozzle combinations N_2 & N_3 and N_2, N_3 & N_4 are presented in Tables A5, A6 and A7 of Appendix A. These data are plotted as solid mass flux vs. air flow rate through nozzle N_0 in Fig. 9. The solids mass flux is approximately 53 kg/m^2s (10.8 lb/ft^2s) when no air is supplied through nozzle N_0 (i.e., N_0 = 0). As the air flow rate through nozzle N_0 is increased, the solids mass flux for all three flow combinations passes through a maximum. For example, the solid mass flux for the N_2, N_3 & N_4 combination increased 40% from 52 kg/m^2s (10.6 lb/ft^2s) to 73 kg/m^2s (15.2 lb/ft^2s) for an increase in nozzle N_0 air flow rate from zero to 0.394 x 10^{-3} m^3/s (50 SCFH). The solids mass flux then decreased for further increases in nozzle N_0 flow rate. The solid loading, solids mass flux divided by gas mass flux, correspondingly increased from 7.75 to 11 and then decreased to 4.8 as the flow rate through nozzle N_0 increased.

Similar experiments have also been conducted using limestone and gypsum particles (Tables A8, A9, A10 and A11 of Appendix A). The data are presented in Fig. 10 and 11. In both cases solid mass flux
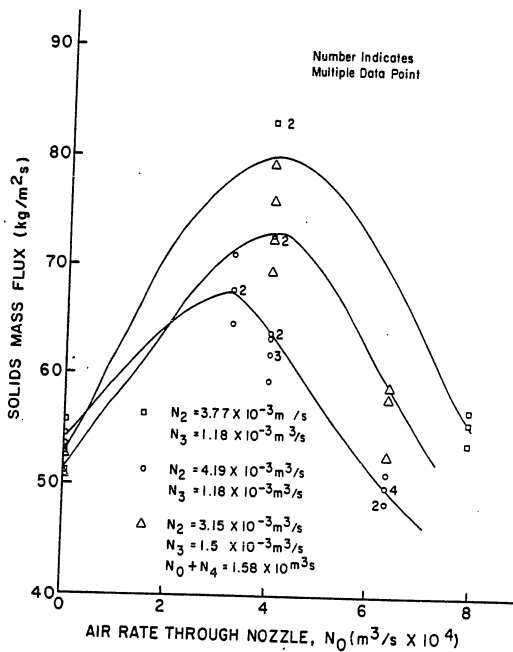
FIG. 9 SOLID MASS FLUX VS AIR RATE THROUGH
NOZZLE N_0 FOR SAND PARTICLES
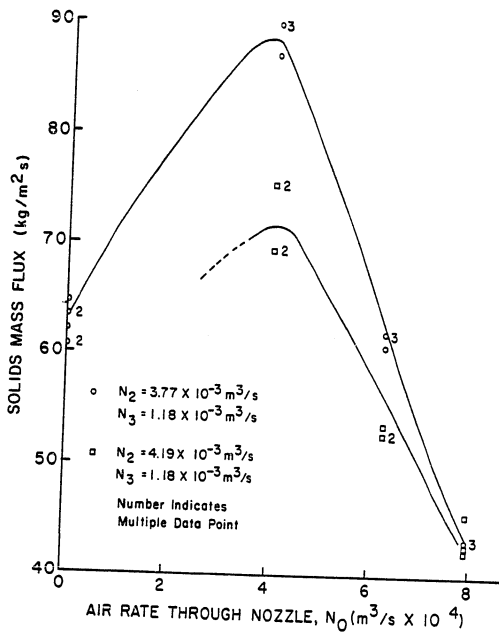
FIG. 10 SOLID MASS FLUX VS AIR RATE THROUGH
NOZZLE N_0 FOR LIMESTONE PARTICLES

SOLIDS MASS FLUX (kg / m^{2}s)

AIR RATE THROUGH NOZZLE, N_0 (m^3/s X 10^4)

$N_2 = 3.77 \times 10^{-3}$ m /s
$N_3 = 1.18 \times 10^{-3}$ m^3/s

$N_2 = 4.19 \times 10^{-3}$ m^3/s
$N_3 = 1.18 \times 10^{-3}$ m^3/s

Number Indicates
Multiple Data Point
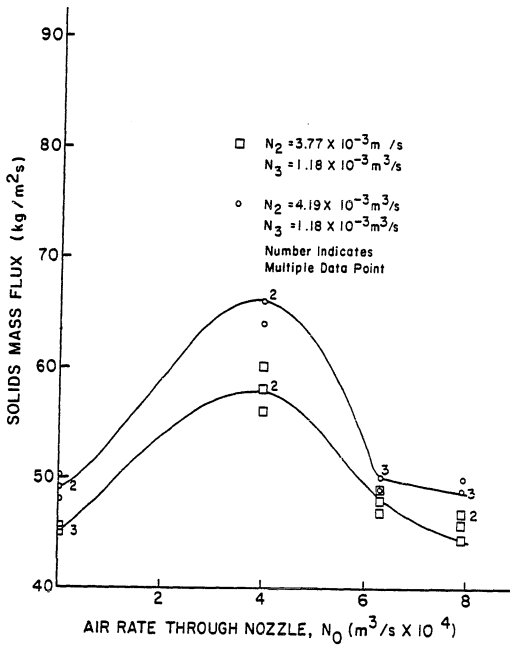
FIG. II SOLID MASS FLUX VS AIR RATE THROUGH
NOZZLE N_0 FOR GYPSUM PARTICLES

could be increased by the use of nozzle N_0. In all three cases solid flux appears to peak at an air flow rate through nozzle N_0 equal to approximately 4×10^{-4} m^3/s. A further increase in flow rate through nozzle N_0 sharply decreases the solid flux, negating the nozzle effect altogether at a flow rate of about 8×10^{-4} m^3/s. It should be noted that useful effect of nozzle N_0 in the case of limestone is eliminated at a lower value of about 6×10^{-3} m^3/s as compared to other two solid particles. Limestone has the highest solid density and largest particle size which are considered responsible for this behavior.

A.2.3 Pressure Drop in the Riser of a High Velocity Fluidized Bed.

The riser is the key section of a high velocity fluidized bed combustor, since it is in this regions that coal combustion and sulfur removal occurs. The riser operates in the fast fluidization mode which lies between the regimes of pneumatic transport and fluidized bed flow. No suitable model representing the flow behavior and pressure drop in this region is available in the literature. Many investigators [42, 43, 44, 45, 46, 47] have proposed additive pressure drop models based on the Bernoulli force balance. In these models, the total pressure is considered to be the sum of the pressure drop contributions from the solids and gas kinetic energy changes, the solid and gas potential energy changes, the solids and gas interphase friction, the particle-particle friction, and the solids and gas wall friction. These mathematical models are represented in the most general form by the equation:

$$\Delta P_T = \Delta P_{SKE} + \Delta P_{GKE} + \Delta P_{SPE} + \Delta P_{GPE} + \Delta P_{SGF} \tag{77}$$
$$+ \Delta P_{SSF} + \Delta P_{SWF} + \Delta P_{GWF}$$

The high velocity fluidized bed will in general be operating in steady state fashion. Therefore the changes in solid and gas kinetic energy are zero. The resulting equation for the pressure drop is then becomes:

$$\Delta P_T = \Delta P_{SPE} + \Delta P_{GPE} + \Delta P_{SGF} + \Delta P_{SSF} + \Delta P_{SWF} + \Delta P_{GWF} \tag{78}$$

The first two terms on the right in Equation (78) are the solid and gas potential energy changes, commonly referred to as the solids and gas head, respectively. The third term ΔP_{SGF} represents the interphase solid and gas frictional losses. The fourth term ΔP_{SSF} represents the solid-solid particle interaction frictional losses. To date these two terms, third and fourth, have been considered negligble when compared to the head terms and wall frictional losses. The fifth and sixth terms represent the solids-wall and gas-wall frictional losses, respectively. The solids-wall frictional losses have been extensively studied for pneumatic transport, however, no uniformly agreed upon single model exists for this term. The gas-wall friction factor is usually modeled by the familiar Fanning Equation.

Pressure drop data are obtained for the riser section using sand, limestone and gypsum particles in order to develop a mathematical model for this section. These measurements are made across the Auburn Monitor to simultaneously obtain accurate solid fraction data as well (Tables A12, A13 and A14 of Appendix A).

To illustrate the deficiency of existing gas-solid flow models to predict the pressure drop in HVFB flow a comparison of the predicted results using the mathematical models obtained from the literature and the experimental data is made. In general, these models are represented by the equation:

$$\Delta P_T = \Delta P_{SPE} + \Delta P_{GPE} + \Delta P_{GWF} + \Delta P_{SWF} \qquad (79)$$

The solid potential energy loss term, ΔP_{SPE}, is obtained from Equation (44). The gas potential energy loss term, ΔP_{GWF} is obtained from Equation (44) by substituting $\rho_g \varepsilon$ for $\rho_s(1 - \varepsilon)$. The solids wall friction loss, ΔP_{SWF}, is obtained from Equation (36) with the solids wall friction factor obtained from Equation (37) through (41). The gas wall frictional loss, ΔP_{GWF}, is obtained from Equation (33).

The predicted pressure drop values for each model are plotted against the corresponding experimental values in Figures 12, 13, 14, 15 and 16. The absolute average percent deviation (AAPD) between the model predictions and the experimental data range from 23.78 to 58.67 percent as shown in Table 7. Klinzing [49] reviewed the existing
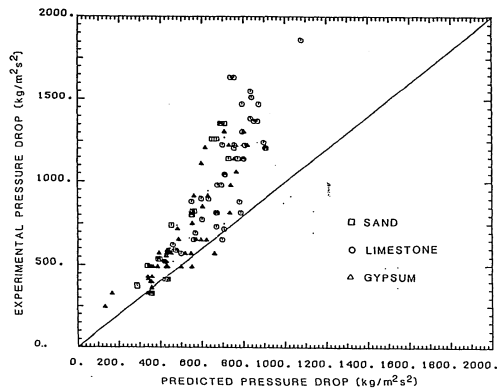
FIG. 12 EXPERIMENTAL PRESSURE DROP IN THE RISER VS PREDICTED

WITH VAN SWAAIJ'S SOLIDS FRICTION FACTOR
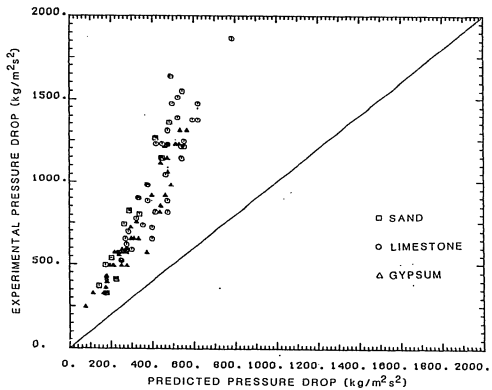
FIG. 13 EXPERIMENTAL PRESSURE DROP IN THE RISER VS PREDICTED

WITH STEMERDING'S SOLIDS FRICTION FACTOR

77
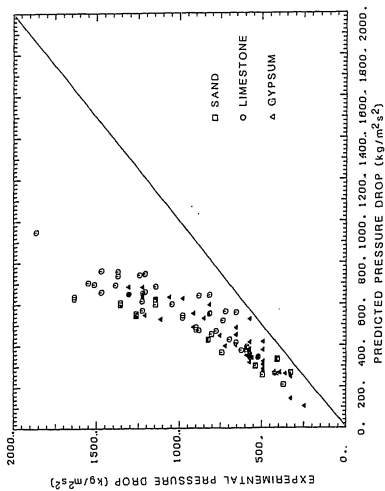
FIG. 14 EXPERIMENTAL PRESSURE DROP IN THE RISER VS PREDICTED
WITH REDDY AND PEI'S SOLIDS FRICTION FACTOR
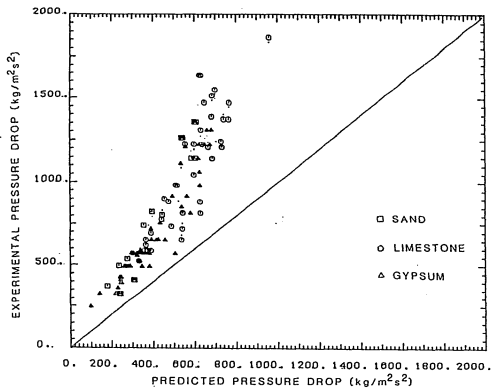
FIG. 15 EXPERIMENTAL PRESSURE DROP IN THE RISER VS PREDICTED

WITH CAPES AND NAKAMURA'S SOLIDS FRICTION FACTOR
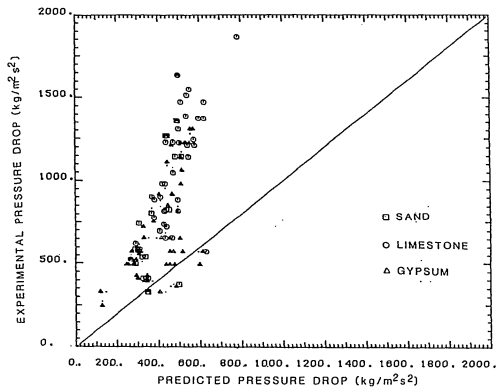
FIG. 16 EXPERIMENTAL PRESSURE DROP IN THE RISER VS PREDICTED

WITH YANG'S SOLIDS FRICTION FACTOR

Table 7

Absolute Average Percent Deviation Between Experimental

and Predicted Pressure Drop

	Sand	Limestone	Gypsum
Van Swaaij	29.58	28.67	23.78
Stemerding	58.67	56.53	55.10
Reddy and Pie	41.51	41.37	37.95
Capes and Nakamura	45.05	43.15	40.93
Yang	43.31	52.41	40.31

literature data and models proposed by seven investigators. He found that the deviation in experimental pressure drop vs. predicted pressure drop was between -30% and +50%. The percent deviation in most of the models in Table 7 agree with this error range.

The AAPD for the predicted pressure drop using the correlation by Van Swaaij et al. range from 23.78 for gypsum to 29.58 for sand particles. The error magnitude is quite reasonable considering the application of this model outside the region for which it was originally developed. However, the plot of the experimental data versus the predicted values by this model (Fig. 12), shows the agreement to be acceptable below 600 kg/m^2s^2, but unacceptable above this value. The large deviation at high pressure drop between the data and the model predictions is due to the inadequacy of the solids friction factor model to account for the solid-solid particle interaction, the solid-gas interaction and the effect of solids fraction.

The AAPD in the predicted pressure drop using the correlation developed by Stemerding [43] range from 55.11 for gypsum to 58.67 for sand particles. The experimental data is plotted against the predictions in Fig. 13. As can be seen, the model always under predicts the observed pressure drop. By comparing Fig. 12 to Fig. 13, the effect of solids velocity can be clearly seen. The use of a constant solids friction factor gives unacceptable pressure drop predictions.

The pressure drop predictions using the solid friction factor correlation developed by Reddy and Pei [44] are plotted against the

experimental data in Fig. 14. The AAPD ranged from 37.95 for gypsum

to 41.51 for sand. The friction factor correlation has the same form

as that by Van Swaaij et al. except that the proportionality constant

is approximately 40% lower in this model. As a result, the error is

larger. The resemblance of Fig. 14 to Fig. 12, and the associated

AAPD for both correlations strengthens the concept of the inverse

proportionality of the solids friction factor with solids velocity.

Capes and Nakamura [47] obtained a correlation for the solids

friction factor which stated that the solids friction factor was

inversely proportional to the solids velocity raised to the 1.22

power. The AAPD for this correlation ranged from 40.93 for gypsum to

45.05 for sand. The experimental data are plotted against the

predictions in Fig. 15. The proportionality constant for this model

and that by Reddy and Pei is approximately the same. The larger APPD

for this correlation suggests that raising the power of the solids

velocity term is inappropriate.

The correlation by Yang was developed using data available in

the literature. Yang's model incorporates the solids fraction and

the slip velocity. The experimental data versus the predictions are

plotted in Fig. 16. The AAPD ranged from 40.31 for gypsum to 52.41

for limestone particles. The agreement at low pressure drop values

is acceptable. The error increases greatly for experimental pressure

drops in excess of 500 kg/m^{2}s^2. The agreement at low pressure drops

suggest that solids friction factor should be a function of the slip

velocity, and the solids fraction as well as the solids velocity.

The values of solids fraction and slip velocity are unavailable in

the literature from which Yang developed the model. It is possible that greater error was introduced due to erroneous estimates of these values.

The large deviation between the predictions and the experimental data suggests that the existing models are not correctly describing the physical phenomena occurring in high velocity fluidization. High velocity fluidization is a special case of gas solid transport. High velocity fluidization is the term used to describe the phenomena of dense strands and clusters moving to and fro, rising and falling, and forming and breaking apart, as the particles are conveyed through the riser. The pressure energy losses associated with such a flow behavior must be greater than those losses due to solids transported pneumatically where the solids flow in stream lines with very little or no interaction between the particles. The frictional pressure drop terms which incorporate the losses due to the complicated flow phenomena in HVFB's are: (1) ΔP_{SWF} (the solid wall friction); (2) ΔP_{SSF} (solid-solid friction); and (3) ΔP_{SGF} (solid-gas friction). The effect of these three terms has been neglected in the past. This omission would cause erroneous estimates of the solids fraction and solids velocity. The solids fraction would be estimated higher than it actually is, while the solids velocity would be lower than it is. Errors in the estimates of these parameters have not caused serious problems when the equipment is used only to transport solids. However, the solids fraction and solids velocity are very critical parameters in the high velocity fluidized bed combustion of coal. The pressure losses due to ΔP_{SWF}, ΔP_{SSF} and ΔP_{SGF} must be

considered when modeling solids-gas reacting flow systems. The solid wall frictional pressure loss is the only one of these three terms which has been studied to date.

The effects of each of the above terms on the total pressure drop have not been separated. These are combined into one term, the solids frictional loss term, which is modeled by the friction factor approach. This term has principally been considered to be only wall friction. The solids frictional loss term will be influenced by the solids velocity, the solids fraction, and the gas-solid slip velocity. It is expected that increasing the solids velocity would decrease the frictional losses as is the case for gases. Increasing the solids fraction should increase the friction factor since more solids are available for collision. Similarly, increasing the slip velocity should increase the friction factor since greater drag will be exterted on the particles. The solids friction factor models available in the literature and the effects of the above parameters on the friction factor are shown in Table 8.

Table 8 shows that only the model developed by Yang [45] even considered the effect of the solids-fraction on the solids friction factor. Yang's model predicts the expected increase in the solids friction factor for an increase in the solids fraction. The models by Van Swaaij et al. [46], Reddy and Pie [44], and Capes and Nakamura [47] predict the expected decrease in the solids friction factor for an increase in solids velocity. The Stemerding [43] and Yang [45] models do not consider the effects of solids velocity. The only

Table 8

Solids Friction Factor Correlations

| Investigation[a] | Solid Model | Effects of Increasing | | |
		Solid Fraction	Slip Velocity	Velocity
Van Swaaij et al.	$f_s = .08/U_s$	no effect	decrease	no effect
Stermerding	$f_s = .003$	no effect	no effect	no effect
Reddy & Pei	$f_s = .046/U_s$	no effect	decrease	no effect
Cape & Nakamura	$f_s = 0.48/U_s^{1.22}$	no effect	decrease	no effect
Yang[b]	$f_s = \dfrac{0.01025\ (1-\epsilon)}{\epsilon^3\ ((1-\epsilon)\ \overline{Re_{sL}})} \dfrac{Re_t}{1.021}$	increase	no effect	increase

[a] all taken from [28]

[b] taken from [46]

model which considers the influence of the slip velocity on the solids friction factor is by Yang. This model predicts the expected increase in the solids friction factor for an increase in the slip velocity. The solids friction factor models are in disasgreement when extrapolated to the conditions of high velocity fluidization, namely solids velocity equal to 1m/s,solids fraction equal to 0.003, and slip velocity equal to 5m/s. As seen from Table 7 solids friction factors differ widely for these models. Disagreement of such magnitude eliminates all possibility of using these equations to develop correlations for predicting losses due to solid-solid and solid-gas effects. Therefore, the model developed for predicting the overall pressure drop due to the solids frictional effects has not considered these two losses separately but included them in the solids-wall frictional term.

The developed mathematical model is presented in Equation (80)

$$\Delta P_{SF} = \Delta P_{SWF} + \Delta P_{SSF} + \Delta P_{SGF} \qquad (80)$$

The pressure loss ΔP_{SF} is modeled by a Fanning type equation similar to that used by previous investigators. Equation (80) becomes:

$$\Delta P_{SF} = 2 \, f_s U_s^2 \, \rho s (1 - \epsilon) \, \Delta L/d_t \qquad (81)$$

The solids friction factor, f_s in the above equation is a function of the solids velocity, the solids fraction, and the slip velocity. The slip velocity contributes primarily to the term describing the solid-gas losses, which are assumed to be negligble. Thus, the solids friction factor is expressed:

$$f_s = aU_s^b (1-\epsilon)^c \epsilon^d \qquad (82)$$

Information from the literature and experimental data from the present study have been used to estimate values of the constants "a", "b", "c" and "d". The model for the solids friction factor by Van Swaaij et al. predicts that the solids friction factor varies inversely with the solids velocity $(f_s \propto U_s^{-1})$. Since this model provides the best agreement with the present experimental data for pressure drop (See Table 6) the value of "b" is taken as -1.0. The Ergun Equation in the viscous dominated region of packed bed flow states that the solids friction factor is proportional to $(1 - \epsilon)/\epsilon^3$. Thus, the values of "c" and "d" are taken to be 1.0 and -3.0, respectively. Therefore, the solids friction factor is represented by:

$$f_s = a (1 - \epsilon) /U_s\epsilon^3 \qquad (83)$$

This leaves only one unknown constant "a". The sand and limestone data are used to determine "a", by a least squares regression

technique. The regression estimated a value of "a" to be 12.2 which
resulted in the AAPD for sand and limestone to be 17.266 and 16.312,
respectively (Fig. 17).

     To check this model, the pressure drop data for the gypsum-air
system are plotted versus the model predictions in Fig. 18. The
agreement is quite acceptable with an AADP of 20.389.

     A.2.4   Pressure Profile in the LFB. Pressure measurements for
sand particles are taken at pressure ports P_1 through P_9 as shown in
Fig. 4. The pressure at the gas inlet to the LFB (pressure port P_1)
is the highest, while the pressure at the gas outlet (pressure port
P_5) is the least compared to any other point in the LFB. This means
that the gas entering the LFB has two paths that it may take enroute
to the exit. The gas flow up the standpipe creates a pressure drop
equal to that produced by the gas-solid flow through the riser.

     Experiments for pressure measurements in the LFB for sand,
limestone, and gypsum particles at various solid flux, air flux
including flow rate through nozzle N_0, solids fraction in the riser,
and standpipe height have been conducted. The operating data are
listed in Tables A15, A16 and A17 of Appendix A. The corresponding
pressures at various LFB pressure ports are presented in Tables A18,
A19 and A20 of Appendix A.

     The pressure profiles (static pressure vs. loop height) for
sand, limestone and gypsum particles are presented in Fig. 19, 20 and
21. These agree with the theoretical concept shown in Fig. 2. The
profiles for all three solid particles exhibit the same general
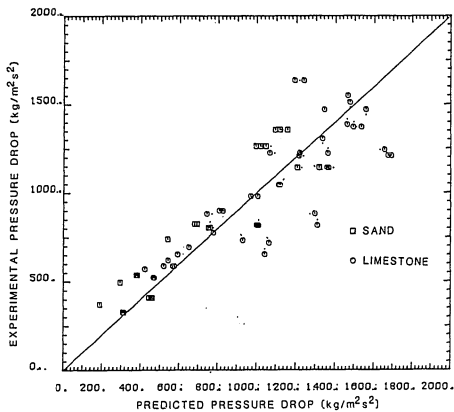
FIG. 17 EXPERIMENTAL PRESSURE DROP IN THE RISER VS PREDICTED

USING THE SOLIDS FRICTION FACTOR DEVELOPED
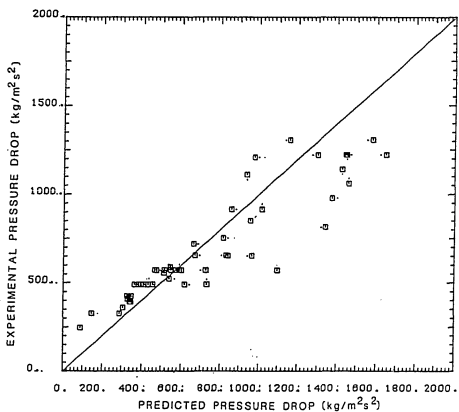
FIG. 18 EXPERIMENTAL PRESSURE DROP IN THE RISER VS PREDICTED USING THE SOLIDS FRICTION FACTOR DEVELOPED IN THIS STUDY FOR SAND AND LIMESTONE APPLIED TO GYPSUM
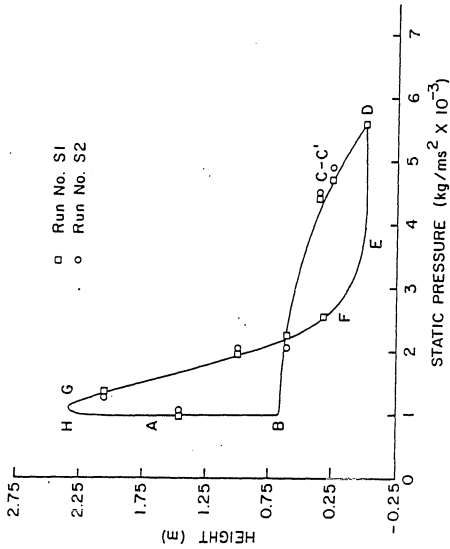
FIG. 19 PRESSURE PROFILE IN LFB FOR SAND PARTICLES
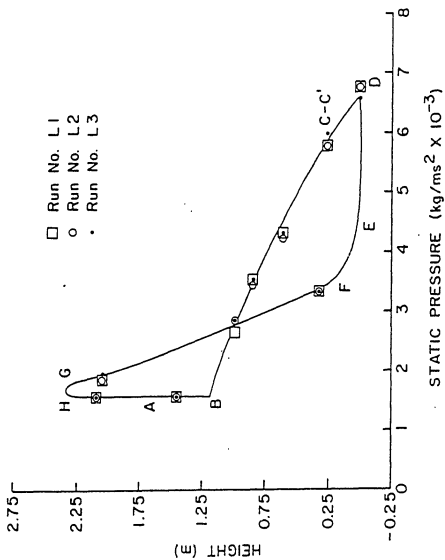
FIG. 20 PRESSURE PROFILE IN LFB FOR LIMESTONE PARTICLES

□ Run No. L1
o Run No. L2
• Run No. L3

HEIGHT (m)

STATIC PRESSURE (kg/ms² x 10⁻³)
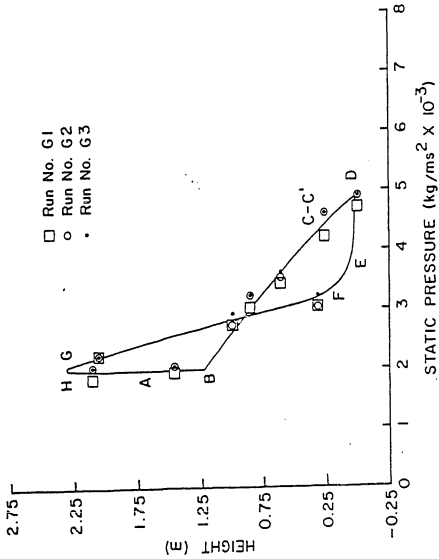
FIG. 2 1 PRESSURE PROFILE IN LFB FOR GYPSUM PARTICLES

behavior. Static pressure at point D (solids entrance to horizontal bottom loop) varies from 5000 to 6700 kg/ms^2. This variation is considered due to the effect of operating parameters in general and solids fraction in the riser in particular. The static pressure variation at point A is considered due to down stream pressure drop in the cyclone and bag filters. The vertical B position is the height of the solids in the standpipe which is controlled by the amount of solids charged to the system.

A model is developed to construct the pressure-height profile based on the physical and operating parameters in the HVFB. The model is based on pressure drop correlations for the various flow regimes from the literature. Pressure drop for the riser in the high velocity fluidized bed is estimated by the model developed in Chapter 6, Section A.2.3.

The HVFB is simplified for the model development, and is shown in Fig. 22. The simplification involves primarily the air nozzle system. The model developed utilizes only one nozzle through which all air is introduced to the HVFB. As shown later, this simplification greatly reduces model complexity without sacrificing the accuracy of the model.

The model consists of two parts. These are a riser section ABCDEFGH as shown in Fig. 22, and a standpipe section AJ'JIH as indicated Fig. 22. The portion, ABCDEFGH of the HVFB consists of a horizontal pneumatic transport section, a 90° bend, the riser, a 135° bend, and an angled pneumatic transport section. The correlations which represent each of these sections have been previously
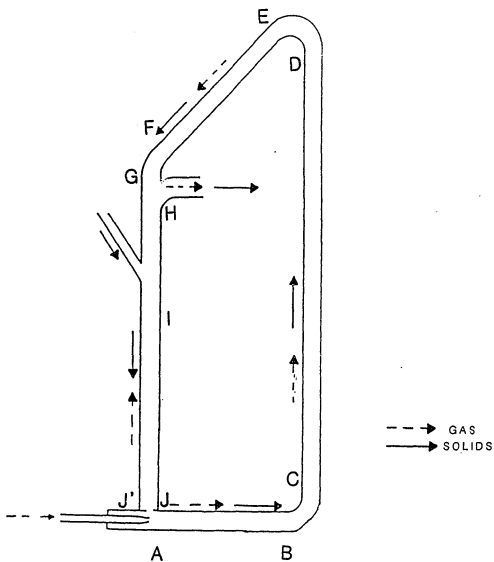
FIG. 22 LOOP FLUIDIZED BED MODELED BY HVFBPP

discussed. These equations have been rearranged and incorporated in a subroutine RISER to predict the pressure at the points of interest. The subroutine RISER calls subroutines written for each section. The subroutines and the main program are presented in Appendix B. A calculation flow chart of subroutine RISER is presented in Fig. 23.

The portion, AJ'JIH, of the HVFB consists of the following sections: an aerated solids flow section, an orifice, a standpipe, and an aerated solids flow section. The equations used have previously been discussed in Chapter 3, Section A. They are arranged to predict the pressure at the points of interest. The subroutines for estimating the pressure in the standpipe are assembled in a Subroutine STNDPP (STANDPIPE) (Appendix B). The calculation flow chart is presented in Figure 24.

The flow chart for the HVFB flow model HVFBPP (High Velocity Fluidized Bed Pressure Profile) is presented in Fig. 25. The Subroutines RISER and STNDPP develop the height versus static pressure plot as shown in Fig. 2, 19, 20 and 21. The data for sand, limestone and gypsum particles at three values of gas mass flux (low, medium and high) are compared with the predicted pressure profile using the model. The AAPD values are presented in Table 9. The AAPD ranges from 4.90 for limestone runs L1, L2 and L3 to 21.33 for sand runs S9, S10 and S11. It should be noted that only two groups of data have AAPD values exceeding 10. This deviation is possibly due
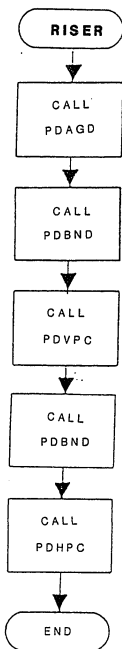
FIG. 23 RISER CALCULATION FLOWCHART
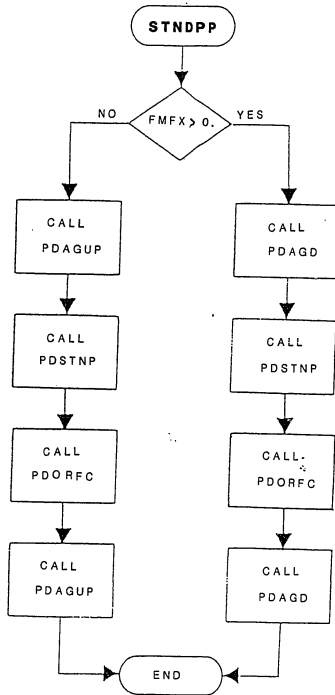
FIG. 24 STNDPP CALCULATION FLOWCHART
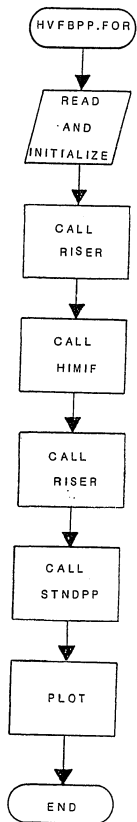
FIG. 25 HVFBPP CALCULATION FLOWCHART

Table 9

Absolute Average Percent Deviation Between

Pressure Profile Model and Data

Gas Flux	Sand[a]		Limestone[b]		Gypsum[c]	
	Runs	AAPD	Runs	AAPD	Runs	AAPD
Low	S 9		L 6		G 7	
	S10	21.33	L 7	6.22	G 8	6.81
	S11		L 8		G 9	
Medium	S 1		L 1		G 4	
	S 2	6.25	L 2	4.80	G 5	13.31
			L 3		G 6	
High	S18		L20		G 1	
	S19	6.99		7.62	G 2	5.59
	S20				G 3	

(a) Run numbers as per Table A15

(b) Run numbers as per Table A16

(c) Run numbers as per Table A17

to plugging of the pressure ports, P_3 and P_4. Elimination of poor data at these ports considerably reduces the error.

The predicted static pressure by the model for sand runs S1 and S2 are plotted in Fig. 26 along with the experimental data points. The largest error (horizontal deviation between points and line) is seen to be in the standpipe with the experimental values being low. The riser prediction agrees well with the data. The model prediction for limestone runs L1, L2 and L3 are shown with the experimental data in Fig. 27. The deviation is divided evenly between the standpipe and the riser, showing very good agreement with an AAPD of 4.90. The model pressure predictions for gypsum runs G1, G2 and G3 are shown in Fig. 28 along with the data. The predicted values show deviations similar to those of the limestone runs.

B. Combustion Model

The coal combustion model for the loop fluidized bed combustor is discussed in two sections. The first section describes the coal oxidation model. It provides mass data for various species (i.e. C, H,) in the coal at any height in the LFB combustor. The respective species conversion rates are also generated. The second section describes the desulfurization model used to estimate the sulfur dioxide retained in the limestone/dolomite particles.

The combustion model is extrapolated to bubbling fluidized bed coal combustion and to pulverized coal combustion to check its validity since no experimental data is available for the LFB. The
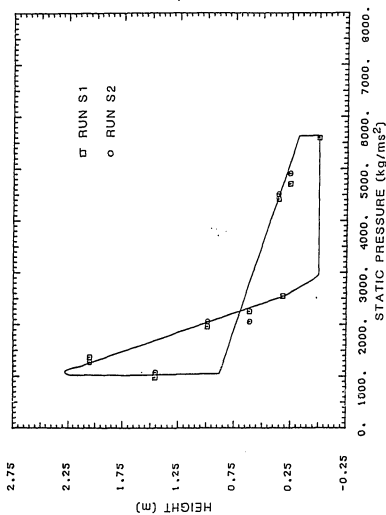
FIG. 26 PRESSURE PROFILE MODEL PREDICTION COMPARED TO THE DATA FOR SAND RUNS S1 AND S2
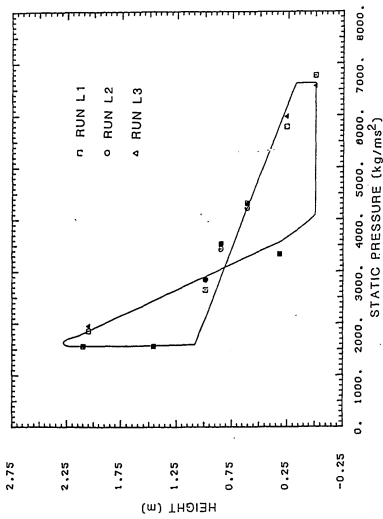
FIG. 27 PRESSURE PROFILE MODEL PREDICTION COMPARED TO THE
DATA FOR LIMESTONE RUNS L1, L2, AND L3
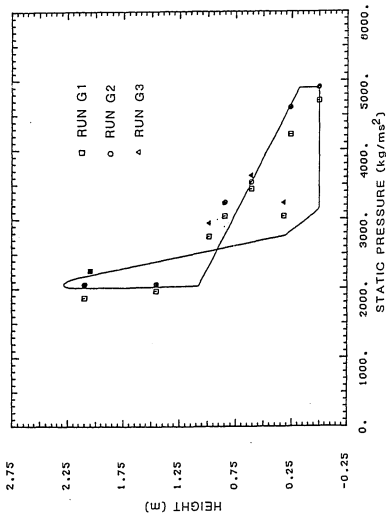
FIG. 28 PRESSURE PROFILE MODEL PREDICTION COMPARED TO THE
DATA FOR GYPSUM RUNS G1, G2, AND G3

□ RUN G1

○ RUN G2

△ RUN G3

STATIC PRESSURE (kg/ms²)

HEIGHT (m)

predicted exit values of coal conversion efficiency and sulfur removal from both the models are compared against literature data for circulating fluidized beds, pulverized coal combustors and bubbling fluidized bed coal combustors [50, 51, 56, 67, 68, 69].

B.1 High Velocity Fluidized Bed Combustion Model

The High Velocity Fluidized Bed Combustor burns pulverized coal in the presence of calcium carbonate such that sulfur can be captured from the gaseous products in the reactor, thus eliminating downstream clean up. High velocity fluidized bed combustion can be considered as to occur between pulverized coal entrained flow combustion and bubbling fluidized bed combustion. A good model for the HVFBC when reduced to these two extreme cases by suitable changes in particle size and temperature should predict satisfactory results.

The combustion model developed in this thesis is quite simple. The assumptions made in the development of the model appear to contradict each other. However, initially the complexity of the process requires a simple model.

One of the objectives of this thesis has been to develop a model which would predict coal combustion efficiency for the design of commercial HVFBC units. The assumptions used in the development of this model are summarized in Table 10. The process is assumed to occur as shown in Fig. 29. A coal particle consisting of fixed carbon, hydrogen, sulfur and ash moves through the riser at a velocity, U_s. The gas moves through the riser at a velocity, U_g.

Table 10

HVFBC Model Assumptions

1. Plug flow

2. Uniform spherical coal particles

3. Coal-char particle traveling at velocity U_s and flux $G_{s,c}$

4. Gas flowing at velocity U_s and flux G_g

5. The relative velocity between the coal and gas is U_{s1}

6. The gas temperature of the coal particle is equal to the surrounding gas at temperature T

7. The temperature of the combustor is determined by quantity of excess air needed to operate it at the specified temperature T

8. Volatile products are instantaneously oxidized into H_2O and CO_2

9. Nitrogen, oxygen, volatile products, and moisture are instantaneously released from the coal-char particle

10. Hydrogen and sulfur oxidation rate constants are assumed equal to the carbon oxidation rate constant.
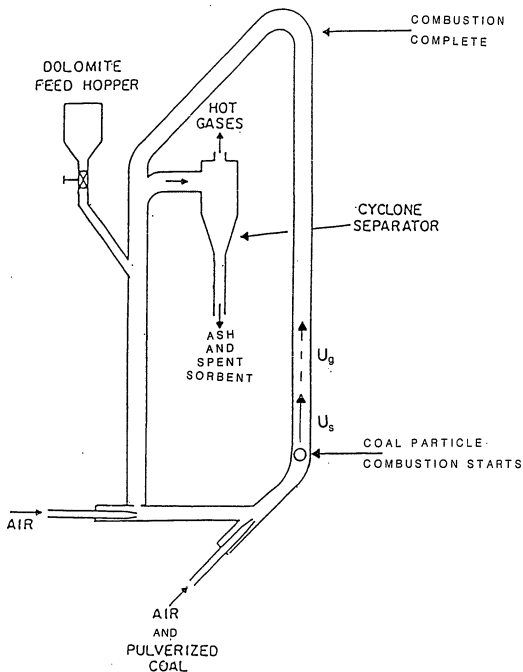
FIG. 29   LOOP FLUIDIZED BED COAL COMBUSTION

MODEL SYSTEM

This results in a slip velocity U_{s1}, equal to the gas velocity less the solids velocity, controlling mass transfer of oxygen to the

Based on the assumptions listed in Table 10 the following oxidation reactions take place in the combustion system:

$$O_2 + 2C \rightarrow 2CO \tag{84}$$

$$O_2 + 4H \rightarrow 2H_2O \tag{85}$$

$$O_2 + S \rightarrow SO_2 \tag{86}$$
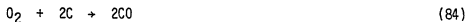
The coal combustion HVFB process will take place as shown in Fig. 29. Pulverized coal will be fed pneumatically through nozzel N_2 which is located at the bottom of HVFB. The coal will combust as it flows with the limestone through the riser section in the high velocity fluidized bed. Combustion will be complete by the time the coal particles reach the 135° bend at the top of the riser. The ash and spent sorbent will flow through the remainder of the system and exit with the gas to the cyclone.

The differential equations resulting from the earlier stated assumptions have been developed in Section 3, and are presented below as Equations 87, 88 and 89.

$$\frac{d_{mc}}{dt} = \frac{(\frac{m_c}{m} A)\, \phi_C\, M_C\, C_{O_2}}{\frac{1}{k_{c,C}} + \frac{1}{k_{d,O_2}}} \tag{87}$$

$$\frac{dm_s}{d_t} = \frac{(\frac{m_s}{m} A) \; \phi_S \; M_S \; C_{O_2}}{\frac{1}{k_{c,S}} + \frac{1}{k_{d,O_2}}} \tag{88}$$

$$\frac{dm_H}{d_t} = \frac{(\frac{m_H}{m} A) \; \phi_H \; M_H \; C_{O_2}}{\frac{1}{k_{c,H}} + \frac{1}{k_{d,O_2}}} \tag{89}$$

Equation 87 represents the rate of carbon oxidation (loss) with time. The term $\frac{m_c A}{m}$ represents the mass weighted area of the particle available for carbon conversion. Similarly, Equations 88 and 89 are for sulfur and hydrogen oxidation, respectively. These differential equations have been assembled in a computer model HVFBCC.FOR (High Velocity Fluidized Bed Coal Combustion). This model makes use of a program called DYSIM developed by Farag [72] to solve a set of equations using a fourth order Runge and Kutta method. The flowchart is presented in Fig. 30.

The program HVFBCC.FOR has been run for high velocity fluidized bed coal combustion, bubbling fluidized bed coal combustion (BFBCC), and pulverized coal combustion (PCC) as per scheme shown in Fig. 31. The computer program and the input data are discussed in Appendixes 2 and 3. The results for these three cases and experimental data from the literature are presented in Table 11. The predicted percent conversions by the HVFBCC.FOR for the BFBCC and PCC show close agreement with the experimental data. Use of this model for designing LFB or other once through coal combustors is recommended.
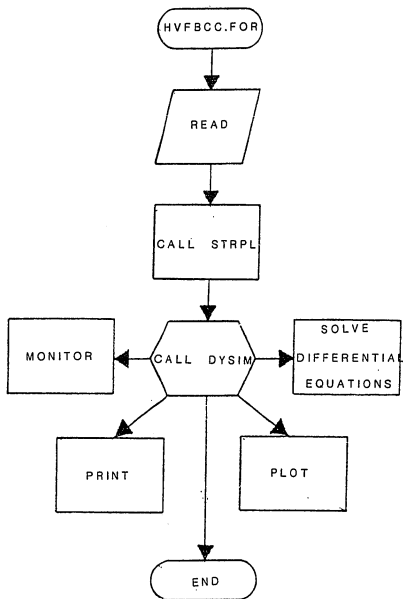
FIG. 30 HVFBCC CALCULATION FLOWCHART
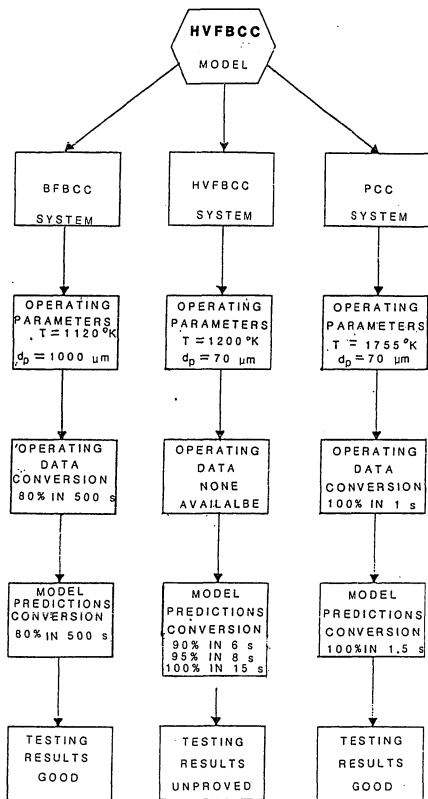
FIG. 31   MODEL TESTING PROCEDURE

Table 11

Comparison of Predicted Estimates
with Experimental Coal Conversion Data

Paramater		HVFBCC	BFBCC [51]	PCC [51]
Data				
Particle Size	(μm)	70	1,000 m	70
Residence Time	(s)	8	500	1
Temperature	($^\circ$K)	1200	1120	1755
Conversions	(%)	-	80	100
Predicted % Coal Conversion by the HVFBCC Model		95	80	100 (residence time 1.5s)

B. 2 High Velocity Fluidized Bed Desulfurization Model

A fluidized bed, whether bubbling or high velocity can be used for its unique ability to remove sulfur dioxide from coal combustion products during the combustion process. The bubbling fluidized bed desulfurization process has been modeled extensively [62, 63, 64, 65, 66, 67]. On the other hand the high velocity fluidized bed desulfurization process has been modeled for the first time as part of this thesis. This model for sulfur removal is developed using Equation 88 for sulfur dioxide production during coal combustion.

The coal desulfurization is considered to occur in the riser of the HVFB as shown in Figure 32. The net rate of sulfur dioxide formation at any position is expressed by the relation:

$$
\begin{matrix}
\text{Net} & & \text{Total} & & \text{Rate} \\
\text{Rate} & = & \text{Rate} & - & \text{of} \\
\text{of} & & \text{of} & & SO_2 \\
SO_2 & & SO_2 & & \text{Absorption by} \\
\text{Generation} & & \text{Formation} & & \text{Stone Particles}
\end{matrix}
\qquad (90)
$$

The rate of sulfur oxidation has been developed in Chapter 6 Section B.1 and is:

$$
\frac{dm_S}{dt} = \frac{(\frac{m_S}{m} A)\,\phi_S\,M_S\,CO_2}{\frac{1}{K_{c,S}} + \frac{1}{K_{d,O_2}}} = R_{SOX}
\qquad (88)
$$

for a single coal particle. The total rate of sulfur oxidation is:

$$
R_{SOXT} = R_{SOX}\,N_{PC}
\qquad (91)
$$
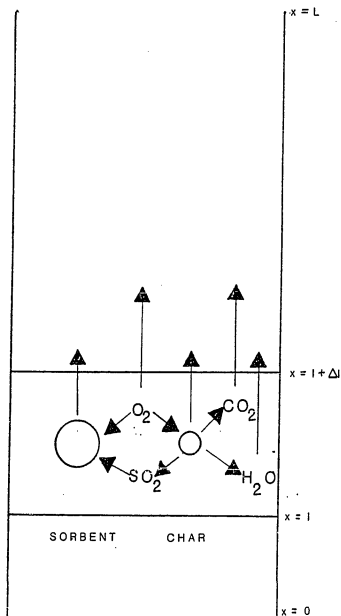
FIG. 32 HIGH VELOCITY FLUIDIZED BED COMBUSTION AND

DESULFURIZATION REACTION MODEL SCHEMATIC

where N_{PC} is the number of coal particles in the cylindrical volume $\pi d_t^2 \Delta L/4$. The number of coal particles can be expressed as:

$$N_{PC} = \frac{(\text{Volume in Consideration})(\text{Volume Fraction of Coal})}{(\text{Volume of One Coal Particle})} \quad (92)$$

$$= \frac{3}{2} \frac{d_t^2 \Delta L (1 - \varepsilon)_C}{d_{pC}^3}$$

The kinetic model developed by Lee et al. [66, 67] is used to simulate the desulfurization process since it is both simple and accurate. The SO_2 rate adsorption for a single stone particle, R_{SBNT} has been discussed in Chapter 3, Section C and is:

$$R_{SBNT} = \frac{\frac{\pi}{6} d_{pSBNT} M_{SO_2} C_{SO_2} e^{\tau/\tau p}}{\tau_{SF}} \quad (93)$$

The total rate of SO_2 adsorption is obtained by multiplying the adsorption rate of one particle by the number of limestone particles, N_{pSBNT}, in the volume under consideration.

$$R_{SBNTT} = R_{SBNT} \, N_{PSBNT}$$

The number of limestone particles is calculated as:

$$N_{pSBNT} = \frac{(\text{Volume in Consideration})(\text{Volume Fraction of Sorbent})}{(\text{Volume of Sorbent Particle})} \quad (94)$$

In mathematical symbols this becomes:

$$= \frac{3}{2} \frac{d_t^2}{d_{PSBNT}^3} \Delta L (1 - \varepsilon)_{SBNT} \quad (95)$$

In order to solve Equation (93) for the mass of sulfur dioxide adsorbed, the concentration of sulfur dioxide is estimated from the following equation:

$$C_{SO_2} = \frac{m_{SO_2}}{M_{SO_2} U_g \Delta t \frac{\pi d_t^2}{4}} \quad (96)$$

This equation has been added to the Combustion Model HFBCC.FOR. The model predicts the fraction of the total sulfur dioxide that is removed from the coal combustion process. The verification of this model is discussed in the next chapter.

7.0 CONCEPTUAL DESIGN OF THE

LOOP FLUIDIZED BED

The hydrodynamic experimental results and the models developed earlier have been used to design a conceptual LFB combustor with a coal feed rate of 1000 kg/hr operating at 1200°K and 405 kPa. This is about the size of one pulverized coal burner within a commercial furnace unit. The conceptual design is obtained using three computer programs as shown in Fig. 33. The first program determines the gas flow rate from the overall energy balance for the specified coal flow rate and combustion temperature. The second program calculates the pressure profile in the LFB equipment from the model developed based on the experimental data in Chapter 6. The third program calculates the percent coal conversion and sulfur removal from the models developed earlier.

The conceptual LFB combustor is shown in Fig. 34 and operates as follows:

(1) Fresh limestone enters the standpipe through a screw feeder located above the solids flux regulator (orifice plate and air injector nozzle).

(2) The limestone calcines and flows down the standpipe with the recirculating solids.

(3) The rate of circulation is regulated by the rate of air flow through nozzle N_0 and orifice at the bottom of the standpipe.

118
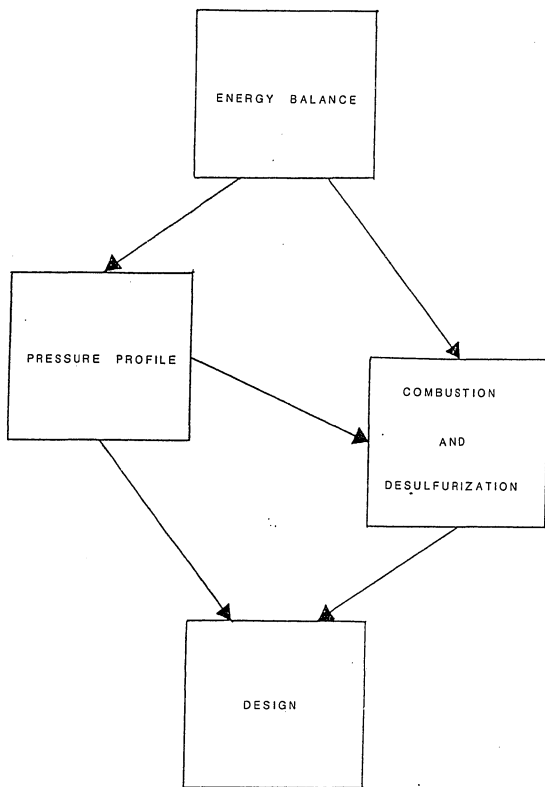
FIG. 33 FLOWCHART FOR THE DESIGN
OF A HVFBCC SYSTEM
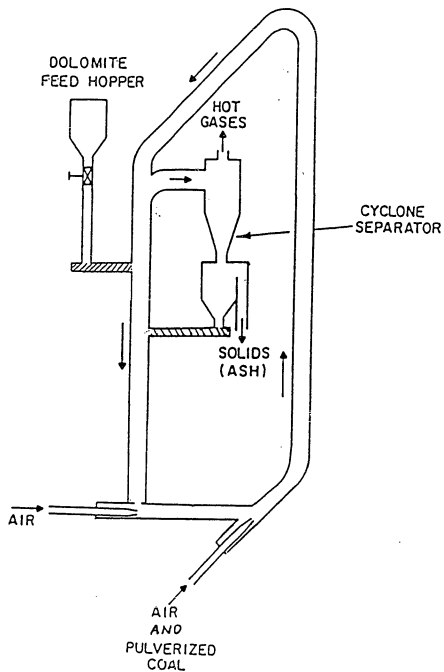
FIG. 34 CONCEPTAL LFB COAL COMBUSTION SYSTEM

FOR 1000 kg/hr OF COAL FEED

(4) The primary air from nozzle N_1, entrains the solid sorbent particles and conveys them through the eductor.

(5) The secondary air and coal are introduced by nozzle N_2.

(6) Combustion and desulfurization occurs in the riser. The length of the riser is estimated by the combustion model to insure that 85% sulfur removal and 95% carbon conversion are achieved.

(7) The gas and entrained fines exit to a cyclone.

(8) The spent solids and ash exit the process through the hopper overflow.

(9) The fines containing unburned coal and unused sorbent are reinjected to the standpipe for additional conversion of each.

This chapter discusses various aspects of the conceptual design, namely: (1) energy balance, (2) pressure profile, (3) combustion and desulfurization, and (4) comparison of the predicted data with existing commercial bubbling fluidized bed coal combustors, pulverized coal combustors, and circulating fluidized bed coal combustors. No efforts have been made towards sizing auxiliary equipment cyclone, compressor screw feeders, etc.). The design shows only the feasibility of the LFB combustion process when compared to other commercial coal combustors.

7.1 Energy Balance

The overall energy balance is obtained using the program OAEB.FOR (Over All Energy Balance). This program estimates the necessary solid flux and gas flux in the LFB combustor for the specified operating temperature. The needed input consists of the desired coal flow rate, heat of combustion, physical properties of the coal, thermal efficiency (% heat loss through walls), coal proximate and ultimate analyses, species molecular weights, heat of calcination, physical properties of sorbent, physical properties of air, combustor diameter, the solids loading (solids flux to gas flux ratio), and the calcium/sulfur molar ratio in the feed streams. This design is based on bituminous coal from the Blacksville No. 8 mine and the Pittsburgh No. 8 bed. The ultimate and proximate analyses values are presented in Table 12.

The program OAEB.FOR calculates the gas flux from the energy balance equation:

$$G = \frac{(1-\eta)\dot{m}_C(-\Delta H_C)-(\dot{m}_C Cp_C + \dot{m}_{SBNT}Cp_{SBNT})(Ts-300)-\dot{m}_{SBNT}(-\Delta H_{CAL})}{Cp_A(Ts-300)(\frac{\pi d_t^2}{4})} \quad (97)$$

The first term in the numerator of Equation (97) is the net energy released during coal combustion. The difference $(1-\eta)$ represents the energy fraction not lost through the walls. The second term in the numerator represents the sensible energy needed to raise the coal and limestone to the combustion temperature. The third term accounts for

122

Table 12

Proximate and Ultimate Analyses

Proximate Analysis

		Weight %
Volatile matter		35.2
Fixed carbon		51.5
Moisture		1.74
Ash		11.56
	Total	100%

Ultimate Analysis

		Moisture-Ash Free Weight %
Carbon		82.4
Hydrogen		5.5
Sulfur		1.4
Oxygen		7.6
Nitrogen		3.1
	Total	100%

$\Delta H_c = -24000$ kJ/kg

the energy used in calcining the limestone. The denominator is the product of the thermal capacity of the air and the flow area. The solids flux is obtained from the following expression:

$$Gs = (\frac{Gs}{G}) G \qquad (98)$$

The solids loading (Gs/G) is provided as input to the program, this enables the solids mass flux to be calculated from Equation (98).

The LFB combustor design data as specified (lengths, diameters, loading, etc.) are given in Table 13. The information contained in Tables 12 and 13 is used as input to the program OAEB.FOR. The program estimates the solids mass flux and gas mass flux to be 63.76 and 7.97 kg/m^2s, respectively. A program listing is provided in Appendix B. The program input is presented in tabular form in Appendx C.

7.2 Pressure Profile

The pressure profile model developed earlier is utilized to estimate the energy consumption associated with circulating the solids in the LFB combustor. The application of this model to the LFB combustor is an extrapolation of only the solids friction factor correlation. This is only a small part of the overall pressure profile model and should not effect the results significantly. The remaining sections of the model are from the literature and used extensively in solid circulating systems by the petroleum industry. The equipment dimensions used by the model are listed in Table 13.

Table 13

1000 kg/hr LFB COMBUSTOR DESIGN SPECIFICATIONS

Riser Height	30.0	m
Standpipe Dense Bed Height	20.0	m
Gas Exit Height	25.0	m
Overall Height	32.0	m
Riser Diameter	1.0	m
Standpipe Diameter	1.0	m
Gas-Solid Disengaging Zone Diameter	1.0	m
Eductor Diameter	0.25	m
Orifice Diameter	0.75	m
LFB Exit Pressure	405.0	kPa
Maximum LFB Pressure Drop	50.0	kPa
Solids Loading	8.0	
Ca/S Molar Ratio	2.0	
Coal Flow Rate	0.278	kg/s

The solids and gas mass flux values have been estimated by the overall energy balance.

The pressure profile output is shown in Fig. 35. The pressure drop across the loop is 32 kPa. The pressure drop across each section of the loop is summarized in Table 14.

7.3 Combustion and Desulfurization

The combustion and desulfurization models are used to obtain the riser height such that a minimum of 90% carbon conversion and minimum of 85% sulfur removal are obtained in one pass as discussed later. The model also estimates the particle weight fraction, solid species weight fraction, and the associated conversion values of carbon, hydrogen and sulfur at each point along the length of the riser. The sulfur dioxide conversion to calcium sulfate at each point along the length of the riser is also given as output from the model. The input to the combustion and sulfur removal program HVFBCC.FOR is presented in tabular form in Appendix C.

The program HVFBCC.FOR is run to obtain the riser length which meets the carbon conversion and sulfur removal criteria. The coal conversion is found to be +99% and the sulfur removal is 86% for a riser length of 30 m. The pressure profile is acceptable since the sulfur removal is greater than 85%. If the conversion criteria had not been met with the equipment dimensions listed in Table 13, these values, particularly the riser height, would have to be changed and the pressure profile and conversion programs rerun. The weight a coal particle changes with riser height is shown in Fig. 36. The

127
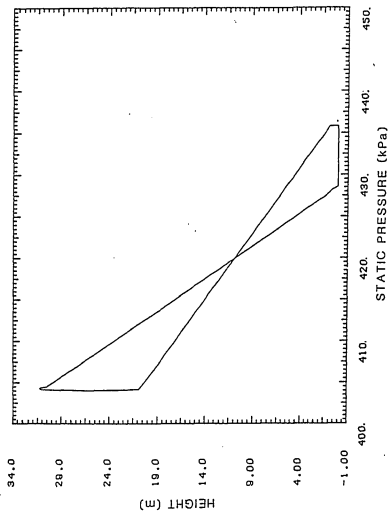
FIG. 35 LOOP FLUIDIZED BED COMBUSTOR PRESSURE PROFILE

Table 14

LFB COMBUSTOR PRESSURE DROP SUMMARY

Overall Pressure Drop	32.0	kPa
Eductor	7.5	kPa
Riser	24.0	kPa
Gas-Solid Disengaging Zone	0.5	kPa
Standpipe	32.0	kPa
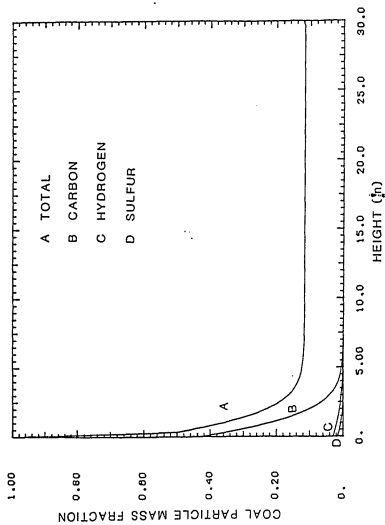
FIG. 36 COAL PARTICLE MASS FRACTION VS HEIGHT IN THE LFB COMBUSTOR

A TOTAL
B CARBON
C HYDROGEN
D SULFUR
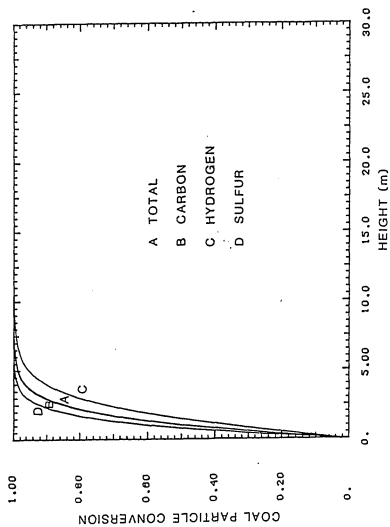
FIG. 37 COAL PARTICLE CONVERSION VS HEIGHT IN THE LFB COMBUSTOR

A TOTAL
B CARBON
C HYDROGEN
D SULFUR
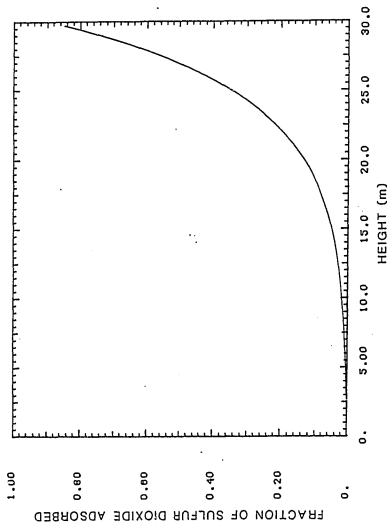
FIG. 38   FRACTION OF SULFUR DIOXIDE ADSORBED IN THE LFB COMBUSTOR

associated particle conversion is shown in Fig. 37. Approximately
100% carbon conversion is found to occur at a height of 8 m. The
percent sulfur removed is presented in Fig. 38 as a function of the
riser height. It is seen that 86% of the sulfur dioxide is absorbed
in the sorbent at a height of 30 m.

7.4 Discussion of Conceptual LFB Design Predictions

The conceptual design has been provided to illustrate the use of
the models developed in this thesis. The predicted estimates are
compared with published date for the following: (1) the Lurgi Chemie
and Huttentechnik GmbIt semi-industrial circulating fluidized bed
plant at the Lurgi Research Center, (2) the Battelle multisolids
fluidized bed pilot plant, (3) typical pulverized coal combustors
with both wet and dry sulfur removal processes, and (4) the
Georgetown University fluidized bed coal combustor, Washington, D.
C. The predicted and published data are summarized in Table 15. It
is seen from Table 15 that the LFB combustor is comparable to the
other circulating fluidized processes. It also has much better
carbon conversion than the BFBCC and better sulfur removal abilities
than the PCC with limestone injection.

Table 15

Comparison of Combustion Systems*

| Paramater | Circulating FBCC | | | | PCC | | |
	LFB Model Prediction	Lurgi Data	Lurgi**	Battelle Multi Solid	Limestone Injection	Unit Scrubbers	Georgetown BFBCC
Carbon Conversion (%)	+99	+96	+99	95-99	+99	+99	80 w/o recycle
SO_2 Removal (%)	85	85	+90	85	<50	+90	85
NO_x Commissions (ppm)	–	90-100	100-200	<100	300-600	–	300-400
Gas Velocity (m/s)	5-8	–	5-8	9	3-4	–	1
Coal Residence Time (s)	30	–	20-30	5-14	1	–	–
Coal Size μm	<70	240	300	1-1/2" x 0	70	<70	1000
Sorbent Size μm	300	240	300	1000	<70	1000	1000
Temperature °K	1200	1173	1173	1170	2000	2000	1120

* References [50, 51, 56, 67, 68, 69]

** Estimated for a commercial unit

133

8.0 CONCLUSIONS

During the past few years considerable efforts have been made on the research and development of fluidized bed combustion of coal. This technology holds a number of attractions all stemming from the concept of maintaining low temperatures in the range of 1100 to 1200°K in the combustion chamber. However, a fluidized bed cannot be operated over a wide range of velocity.

A high velocity fluidized bed can operate over a wide range of gas throughputs. A special case of this high velocity fluidized bed concept recently was develped at the Morgantown Energy Technology Center, Morgantown, West Virginia, in the Loop Fluidized Bed (LFB). In this system a mixture of powdered coal and dolomite or limestone flows in a loop at high velocity. The sulfur dioxide generated is absorbed by the fine dolomite or limestone particles. The fluidizng medium (air) is injected into the system at a high velocity through a set of nozzles.

In this study a bench scale loop fluidized bed made of pyrex glass has been designed, fabricated, and installed. The LFB has been operated using sand, limestone, and gypsum particles. Data were obtained to study the effect of particle size, particle density, air flux, and solids flux on fluidizing characteristics of the above mentioned solid particles. A correlation is developed to describe

134

the pressure drop in the riser. A computer model is developed to predict the pressure profile in the LFB for a particular geometry and flux values. Computer models representing the combustion and desulfurization processes in HVFB systems have also been developed. Our major findings are as follows:

(1) Flow characteristics of sand, limestone, and gypsum in LFB are sensitive to nozzle positions and nozzle air flow rates.

(2) Introduction of an orifice plate and nozzle at the bottom of the standpipe assists in the solids flow regulation and in increasing the solids mass fraction in the riser section.

(3) An LFB is considered to be operating in a satisfactory manner when there is no slugging in the standpipe, choking in the riser or significant saltation in the eductor. There is a 'good operating region' for various nozzle flow rates and solids fractions. Three dimensional plots have been prepared for sand, limestone, and gypsum particles that can be used for predicting operating condition of the LFB with respect to nozzle combination, flow rate and void fraction. Good operating regions are shown in these plots.

(4) The data on sand and gypsum show that the pressure drop in the riser increases with solid density for the same particle size.

(5) The pressure drop in the riser section of a HVFAB can be expressed by the sum of the individual energy loss items:

$$\Delta P = \Delta P_{SPE} + \Delta P_{GPE} + \Delta P_{SF} + \Delta P_{GWF}$$

(6) The pressure drop due to the solids frictional losses can be modeled by a Fanning type of equation:

$$\Delta P_{SF} = \frac{2 \; f_s \; (1-\varepsilon) \; U_s^2 \; \Delta L}{d_t}$$

(7) The solids friction factor, f_s, can be expressed by the equation:

$$f_s = 12.2 \; (1-\varepsilon)/U_s \varepsilon^3$$

(8) The pressure profile model represented by the computer program HVFBPP.FOR correctly predicts the relation between the equipment geometry, solids mass flux, gas mass flux, solids fraction and pressure drop at each point in the LFB.

(9) The coal combustion model contained in the computer program HVFBCC.FOR provides good estimates of the carbon conversion for a wide range of processes from the BFBCC to the PCC.

(10) The sulfur removal model contained in the computer program HVFBCC.FOR predicts sulfur removal values comparable to experimental data from other circulating fluidized bed combustors.

(11) The LFB combustor has better carbon conversion than BFBCC and better sulfur removal than PCC with limestone injection.

(12) The LFB combustor is an acceptable alternate to the Lurgi and Battelle processes.

9.0 RECOMMENDATIONS

This study has been confined to the: (1) design, fabrication, installation of the bench scale cold flow LFB, (2) collection of experimental data with respect to solid flow characteristics and pressure drop in the loop, and (3) development of pressure drop, pressure profile, coal combustion and sulfur removal models. The data collected have been presented in tabular, graphical, and mathematical forms.

This study accomplished the objective as specified. However, during the course of this investigation the following subject areas have been found as being theoretically and experimentally deficient and further research work is recommended:

(1) The pressure drop due to solids frictional effects is considered to be the sum of solid-wall, solid-solids, and solid-gas frictional losses. Experiments should be directed towards obtaining a better understanding of these phenomena and to develop separate mathematical relationships. The experiments should make use of the Auburn solids fraction monitor used in this study and the wall shear stress measurement instrument as used by van Swaaig et al.

138

(2) The fundamental mechanism for cluster formation should be investigated. This may be accomplished by developing a force balance equation for a few particles in close proximity flowing with the gas. Lift theory may be used to demonstrate how a low pressure region could develop between the particles due to higher gas velocities, thus forcing the particles to form clusters. A high speed photographic technique similar to that used by Reddy and Pei [44] may provide experimental verification of the theory.

(3) The formation of clusters and the phenomena of choking are directly related. Experimental investigations have revealed that choking does not occur in large diameter lines. This leads one to infer that there is a maximum cluster size. A theory to predict the maximum cluster size should be developed. This may be approached in the same manner as discussed above and use similar photographic techniques to verify it.

(4) There are no data available for coal combustion in an LFB unit. Experimental work is highly recommended on a process research unit.

(5) Based on coal combustion experimental data the mathematical models developed to predict percent combustion and sulfur removal profiles in the riser section can be verified and modified if necessary.

(6) Models to predict the gas composition and local temperature in a LFB should be developed and incorporated into the coal conversion and sulfur removal computer code.

(7) Work on the development of scale-up procedures should be undertaken to design a commercial coal LFB combustor.

(8) Economic feasilbility of a commercial LFB unit for coal combustion should be investigated.

10.0 NOMENCLATURE

A	cross sectional area, m^2
B	empirical constant equation 49
C	concentration, $kg mol/m^3$
Cd	drag coefficient
C_D	orifice discharge coefficient
C_p	specific heat, $Kcal/kg °K$
d	diameter, m
dc	cluster diameter, m
D	diffusivity, m^2/s
E	dielectric constant
f	friction factor
Fr	Froud number
g	gravitational constant, $9.807 \ m/s^2$
G	mass flux, $kg/m^2/s$
k	chemical reaction rate constant
k_d	mass transfer coefficient, m/s
WL	transport length, m
m	sulfination reaction order
m·	mass flow rate, kg/s
M	molcular weight, $kg/kg mol$
n	Richard and Zaki index, devolatilization reaction order
N	cluster number
P	pressure , kg/ms^2

ΔP	pressure drop, k_g/ms^2
$p*$	poor plugging constant
q	soot reaction rate
r	radius
R_e	Reynolds number
s	solid devolatilization product, surface area, m^2
Sh	Sherwood number
Sc	Schmidt number
t	time, s
U	velocity, m/s
V	volatile matter
w	sample weight, k_g
Y	Volatile fraction

Greek Letters

ε	voidage
θ	angle of inclination
μ	gas viscosity, kg/ms
μ	apparent viscoity, kg/ms
ϕ	spherocity
ρ	density, kg/m^3
ρ	density of mixture, kg/m^3
τ_w	shear stress at wall, kg/ms^2

τ	time constant
β	empirical constant
η	efficiency, effectiveness factor

Subscripts

A	air
b	bend
B	bubble
c	chemical, cluster
CAL	calcination
f	friction
GKE	gas kinetic energy
GPE	gas potential energy
GWF	gas-wall friction
i	equation index
mf	minimum fluidization
o	superficial
p	particle, poor plugging
PE	potential energy
sl	slip
SF	solids friction, sulfination
SGF	solids-gas friction
SKE	solids kinetic energy
SPE	solids potential energy

SSF   solids-solids friction

SWF   solids-wall friction

t   terminal, tube

T   total

∞   infinite time

11.0 REFERENCES

1. Yerushalmi, J., M. J. Gluckman, R. A. Graff, S. Dobner, and A. M. Squires, "Production of Gaseous Fuels from Coal in the Fast Fluid Bed", Fluidization Technology. Vol. II, ed. D. L. Kearns, Hemisphere Publishing Corp., Washington, D. C., 1975, 437.

2. Yerushalmi, J. and N. T. Cankurt, "High Velocity Fluid Beds", Chemtech, Sept., 1978, 564.

3. Yerushalmi, J. and N. t. Cankurt, "Further Studies of the Regimes of Fluidization", Powder Technology, 24, (1979), 187.

4. Yerushalmi, J., "Circulating Fluidized Bed Boilers" Fluid Processing Technology, 5 (1/2), 1981, 25.

5. Yerushalmi, J., D. H. Turner, and A. M. Squires, "The Fast Fluid Bed", Ind. Eng. Chem. Pro. Des. Dev., Vol. 15, No. 1, 1976, 47.

6. Yerushalmi, J., A. M. Squires, and R. A. Graff, "Studies Toward Improved Techniques for Gasifying Coal", Final Report to National Science Foundation, Grant GI-34286A-1, 1976.

7. Yerushalmi, J., N. T. Cankurt, D. Geldart, and B. Liss, "Flow Regimes in Vertical Gas-solid Contact Systems", AIChE Symposium Series, No. 172, Vol. 74, 1976, 1.

8. Squires, A. M., "Application of Fluidization Beds in Coal Technolgy", Alternate Energy Sources, ed. J. P. Hartnett, Hemisphere Publishing Corp., Washington, D. C., 1976, 59.

9. Matsen, J. M., "Mechanism of Choking and Entrainment", Powder Technology, 32, 1982, 21.

10. Gidaspow, D., "Hyperbolic Compressible Two-Phase Flow Equations Based on Stationary Principles and Fick's Law", Proceedings of the Two-Phase Flow and Heat Transfer Symp. Workshop, Oct. 1976, Hemisphere Publishing Corp., Vol. 1, 1978, 133.

11. Gidaspow, D., and H. Arastoopour, "A Comparison of Four Unequal Velocity Models - Flow of a Slurry Through a Venturi Meter", Proceedings of the Two Phase Flow and Heat Transfer Symposium, Oct. 1976, Hemisphere Publishing Corp., Washington, D.C., 1978, 133.

12. Gidaspow, D., "Fluid-Particle Systems", Proceedings of NATO Advanced Study Institute, Hemisphere Publishing Corp., Vol. 1, 1975, 115.

13. Matsen, J. M., "Flow of Fluidized Solids and Bubbles in Standpipes and Risers", Powder Technology, 7, 1973, 93.

14. Arastoopour, H., and D. Gidaspow, "Analysis of IGT Pneumatic Conveying Data and Fast Fluidization Using a Thermohydrodynamic Model", Power Technology, 22, 1979, 77.

15. Leung, L. S., "The Ups and Downs of Gas-Solid Flow - A Review", Fluidization, ed. J. R. Grace and J. M. Matsen, Plenum Press, N. Y., 1980, 25.

16. Judd, M. R., and P. N. Rowe, "Dense Phase Flow of a Powder Down a Standpipe", Fluidization, ed. J. F. Davidson and D. L. Kearns, Cambridge University Press, 1978, 110.

17. Leung, L. S. and P. J. Jones, "Coexistance of Fluidized Solids and Packed Bed Flow in Standpipes", Fluidization of J. F. Davidson and D. L. Kearns, Cambridge University Press, 1978, 116.

18. Leung, L. S., P. J. Jones, and T. M. Knowlton, "Analysis of Moving-Bed Flow of Solids Down Standpipes and Slide Valves", Powder Technology, 19, 1978, 7.

19. Yoon, S. M., and D. Kunii, "Gas Flow and Pressure Drop Through Moving Beds", Ind. Eng. Chem. Pur. Des. Dev., Vol. 9, No. 4, 1970, 559.

20. Eleftheriades, C. M. and M. R. Judd, "The Design of Downcomers Joing Gas-Fluidized beds in Multistage Systems", Powder Technology, 21, 1978, 217.

21. Takahashi, H. and H. Yanai, "Flow Profile and Void Fraction of Granular Solids in a Moving Bed", Powder Technology, 7, (1973), 205.

22. Spink, C. D. and R. M. Neederman, "Gravity Discharge Rate of Fine Particles from Hoppers", Powder Technology, 21, 1978, 245.

23. Singh, B., "The Role of a Standpipe as a Feeding Device in Pneumatic Conveying", Pneumotransport 4, California, 1978, E1-1.

24. Breault, R. W., "Loop Fluidized Bed Flow Studies", Report submitted to Morgantown Energy Technology Center, U. .S. Department of Energy, Sept. 1983.

25. Knowlton, T. M. and I. Hirsan, "The Effect of System Parametes on the Operation of Dense Phase Vertical Lift Lines and J-Valves." Pneumotransport 5, London, April 1980, E3.

26. Knowlton, T. M. and I. Hirsan, and L. S. Leung, "The Effect of Aeration Tap Location on the Performance of a J-Valve", Fluidization, Cambridge University Press, 1978, 128.

27. Leung, L. S., "A Quantitative Flow Regime Diagram for Vertical Pneumatic Conveying of Granular Solids", Pneumotransport 5, London, 1980, A3, 35.

28. Leung, L. S., R. J. Wiles, D. J. Nicklin, "Correlation for Predicting Choking Flow Rates in Vertical Pneumatic Conveying", Ind. Eng. Chem. Pro. Des. Dev., Vol. 10, No. 2, 1971, 183.

29. Yousif, Y. and G. Gau, "Aerodynamique de L'Ecoulement Verticle de Suspensions Concentress Gas-Soliuds - I. Regimes d'Ecoulement et Stabilite Aerodynamique", Chem. Eng. Sci., Vol. 29, 1974, 1939.

30. Yousif, Y. and G. Gau, "Aerodynamique de L'Ecoulement Verticle Suspensions Concentress Gas-Solids - II. Chute de Pression et Vitesse Relative Gas-Solids", Chem. Eng. Sci., Vol. 29, 1974, 1947.

31. Yang, W. C., "Mathematical Definition of Choking Phenomenon and Mathematical Model for Predicting Choking Velocity and Choking Voidage", AIChE J., Vol. 21, No. 5, 1975, 1013.

32. Yang, W. C., "A Criterion for 'Fast Fluidization'", Pneumotransport 3, Bath, England, 1976, E5-4999.

33. Smith, T. N., "Limiting Volume Fractions in Vertical Pneumatic Transport", Chem. Eng. Sci., Vol. 33, 1978, 745.

34. Riethmuller, M. L., and L. Lourenco, "Particle Number Density Measurement in a Gas-Solid Partickle Flow", Pneumotransport 5, London, 1980, X10.

35. Lech, M., "Some Aspects of Radiosotopic Measurement of Concentration of Mass Flow of Powder", Pneumotransport 5, London, 1980, EY.

36. Tsuji, Y., Morikawa, Y., "LDV Measurements of an Air-Solid Two-Phase Flow in a Horizontal Pipe", J. Fluid Mech., Vol. 120, 1982, 385.

37. Moley, S. R., Mathur, M. P., Klinzing, G. E., "Analysis of Dense Phase Fine Coal Pneumatic Systems", DOE/PETC/TR-8216, 1982.

38. Operations manual for the Auburn Monitor (Model No. 1090) Instrument Auburn, International of Danvers, Mass. Co., 5th ed., 1982.

39. Mathur, M. P., and G. E. Klinzing, "Measurement of Pneumatic Transport of Pulverized Coal", presented at Symposium of Instrumentation and Control for Fossil Fuels, San Francisco, CA 1981.

40. de Jong, J. A. H. and Q. E. T. J. M. Hoelon, "Aerated Solids Flow Through a Vertical Standpipe Below a Pneumatically Discharged Bunker", Powder Technology, Vol. 7, 1975, 197.

41. de Jong, J. A. H. and Q. E. T. J. M. Hoelon, "Concurrent Gas and Particle Flow During Pneumatic Discharge from a Bunker Through an Orifice", Powder Technology, Vol. 12, 1975, 201.

42. Kunni, D. and O. Levenspiel, 'Fluidization Engineering', Krieger Publishing Co., Huntington, NY, 1977.

43. Stemerding, S., "The Pneumatic Transport of Cracking Catalyst in Vertical Risers", Chem. Eng. Sci., Vol. 17, 1962, 599.

44. Reddy, K. V. S. and D. C. T. Pei, "Particle Dynamics in Solids-Gas Flow in a Vertical Pipe", I&EC Fund., Vol. 8, No. 3, 1969, 490.

45. Yang, W. C., "A Correlation for Solid Friction Factor in Vertical Pneumatic Conveying Lines", AIChE Journal, Vol. 24, No. 3, 1978, 548.

46. Van Swaaij, W. P. M., C. Buurman, and J. W. von Breusel, "Shear Stresses on the Wall of a Dense Gas-Solid Riser", Chem. Eng. Sci., Vol. 25, 1970, 181.

47. Capes, C. E. and K. Nakamura, "Vertical Pneumatic Conveying: An Experimental Study with Particles in the Intermediate and Turbulent Flow Regimes", Can. J. Chem. Eng., Vol. 51, 1973, 31.

48. Singh, B., "Lean Phase Vertical Pneumatic Conveying of Particulate Material - An Analysis of the Pressure Drop in the Non-Accelerating Zone", Chemeca 77, 1977, 315.

49. Klinzing, G. E., "Vertical Pneumatic Transport of Solids in the Minimum Pressure Drop Region", Ind. Eng. Chem. Pro. Des. Dev., Vol. 18, No. 3, 1979, 404.

50. Elliot, M. A., ed. "Chemistry of Coal Utilization - Second Supplementary Volume", John Wiley, NY, 1981.

51. Smoot, L. D. and P. J. Smith, "Combustion and Gasification of Coal, Char and Coal/Water Mixtures" Course Notes, 1982.

52. Field, M. A., D. W. Gill, B. B. Morgan, and P. G. W. Hawksley, "Combustion of Pulverized Coal", British Coal Utilization Research Association, Cheney and Sons, Leatherhead, 1967.

53. Smoot, L. D. and D. T. Pratt, ed., "Pulverized-Coal Combustion and Gasification", Plenum Press, NY, 1979.

54. Gamble, R. L., "Operation of the Georgetwon University Fluidized Bed Steam Generator", The Proceedings of the Sixth International Conference on Fluidized Bed Combustion, 1980, 307.

55. Breault, R. W., "The Economic and Technical Feasibility of a Solar-Coal Hybrid Gasification System", M. S. Thesis, University of New Hampshire, 1980.

56. Mathur, V. K., "Coal Power - Its Promises and Problems", Energy Sources, ed. L. H. Klotz, University of New Hampshire, 1980.

57. Ruethur, J. A., "Direct Coal Liquifaction Processes", ASC Meeting, 1983.

58. Mathur, V. K., "Liquifaction of Bituminous Coals Using Dispoable Ore Catalyst and Hydrogen", Final Report, Contract DE-AC22-81PC41035, 1982.

59. Levenspiesl, O., "Chemical Reaction Engineering", John Wiley & Sons, NY, 1972.

60. Borgwardt, R. H., "Kinetics of the Reaction of SO_2 with Calcined Limestone", Environmental Science and Technology, Vol. 4, No. 2, 1970, 59.

61. Lee, D. C. and C. Georgakis, and J. L. Hodges, "Modeling SO_2 Emissions from Fluidized Bed Coal Combustors", Chem. Eng. Sci., Vol. 35, 1980, 302.

62. Lee, D. C. and C. Georgakis, "A Single, Particle Size Model for Sulfur Retention in Fluidized Bed Coal Combustors", AIChE Journal, Vol. 27, No. 3, 1981, 476.

63. Wen, C. Y. and M. Ishida, "Reaction Rate of Sulfur Dioxide with Particles Containing Calcium Oxide", Environmental Science and Technology, Vol. 7, No. 8, 1973, 703.

64. Hartman, M. and R. W. Coughlin, "Reaction of Sulfur Dioxide with Limestone and the Grain Model", AIChE Journal, Vol. 22, No. 3, 1976, 490.

65. Beisswenger, H., G. Daradimos, K. Janssen and V. Peterson, "Use of Circulating Fluidized Bed as High Temperature Reactor for Endothermic and Exothermic Processes", Ger. Chem. Eng., Vol. 4, 1981, 285.

66. Nack, H., R. D. Litt, and B. C. Kim, "Multisolid Fluidized-Bed Combustion", CEP, 1984, 41.

67. Battelle Memorial Institute, "Battelle's Multisolid Fluidized Bed Combustion Process", Summary Report on the Status of Development and Commercialization, 1982.

68. Goetz, G. M. Micolli, and D. Eskinazi, "Fireside Consequences of Furnace Limestone Injection for SO_2 Capture", ASME paper 84-JPGC-APC-10, Joint Power Generation Conference, 1984.

69. LaRue, A. and A. Liang, "Furnace Limestone Injection Technologies to Reduce SO_2", ASME paper 84-JPGC-FO-11, Joint Power Generation Conference, 1984.

70. Farag, I. H., fortran program DYSIM.FOR, Univeristy of New Hampshire

71. Farag, I. H., Fortran programs STPRL.LFOR and RGRID1.FOR, Univeristy of New Hampshire.

72. Farag, I. H., Fortran program HIMIF.FOR, Univeristy of New Hampshire.

APPENDICES

APPENDIX A

HYDRODYNAMIC DATA

Table A1

Void Fractions for Nozzle N_1 & N_3 and N_2 & N_3 Combinations

Nozzle and Flow Rates (x 10^3, m^3/s)		Voidage
N_1	N_3	
3.14	0	no flow
3.93	0	no flow
4.72	0	no flow
5.50	0	no flow
6.29	0	no flow
6.67	0	0.983
3.14	0.79	no flow
3.53	0.79	no flow
4.72	0.79	no flow
5.50	0.79	no flow
6.29	0.79	0.987
5.50	1.58	no flow
6.88	1.58	0.993
N_2	N_3	Voidage
3.14	0	no flow
3.93	0	no flow
4.32	0	0.992
4.87	0	0.994
5.50	0	0.987
6.37	0	~1
3.14	0.79	no flow
3.93	0.79	0.994
4.72	0.79	0.998
3.14	0.99	no flow
3.14	1.19	0.975
3.93	1.19	0.995
3.14	1.50	0.982
2.75	1.58	no flow
3.14	1.58	0.982
3.93	1.58	0.996
4.32	1.58	~1
4.80	1.58	~1

Table A2

Flow Rates Through N_2 & N_3 Combination vs. Voidage for Sand Particles

Orifice Plate: 0.025 m

Nozzle and Flow Rates (x 10^3 m^3/s)		Voidage
N_2	N_3	
3.14	0	no flow
4.17	0	no flow
4.56	0	0.992
5.19	0	0.994
5.50	0	0.997
6.45	0	∿1
4.17	0.39	0.997
4.56	0.38	0.879
5.19	0.39	0.990
3.73	0.59	no flow
3.14	0.79	no flow
3.77	0.79	0.975
4.17	0.79	0.981
3.14	1.18	0.975
3.14	1.18	0.974
3.77	1.18	0.981
4.17	1.18	0.986
3.14	1.57	0.980
3.14	1.57	0.982
3.77	1.57	0.987
4.17	1.57	0.990
2.75	2.36	0.988
3.14	2.36	0.992
4.17	2.36	0.994
5.19	2.36	0.996

Table A3

Flow Rates Through N_2 & N_3 Combination vs. Voidage for Limestone Particles

Orifice Plate: 0.025m

Nozzle and Flow Rates (x 10^3 m^3/s)		Voidage
N_2	N_3	
4.86	0.0	0.981
5.36	0.0	0.982
5.81	0.0	0.984
5.81	0.0	0.984
6.45	0.0	0.989
7.62	0.0	0.995
4.32	0.39	0.976
4.86	0.39	0.978
5.36	0.39	0.982
5.81	0.39	0.985
4.32	0.79	0.980
4.66	0.79	0.981
4.66	0.79	0.981
4.86	0.79	0.983
5.20	0.79	0.984
5.20	0.79	0.984
5.36	0.79	0.985
5.81	0.79	0.988
4.18	1.18	0.979
4.18	1.18	0.978
4.18	1.18	0.978
4.32	1.18	0.983
4.66	1.18	0.986
4.66	1.18	0.986
4.66	1.18	0.986
4.86	1.18	0.986
5.20	1.18	0.987
5.20	1.18	0.987
5.36	1.18	0.988
5.81	1.18	0.990
3.76	1.57	0.983
4.86	1.57	0.990
5.36	1.57	0.992
5.81	1.57	0.993

Table A4

Flow Rates Through N_2 & N_3 Combination vs. Voidage for Gypsum Particles

Orifice Plate: 0.025 m

Nozzle and Flow Rates (x 10^3 m^3/s)		Voidage
N_2	N_3	
3.77	0.00	0.978
4.19	0.00	0.987
4.66	0.00	0.991
5.20	0.0	0.993
3.77	0.39	0.980
4.19	0.39	0.989
4.66	0.39	0.990
5.20	0.39	0.993
3.32	0.79	0.980
3.77	0.79	0.982
3.77	0.79	0.977
4.19	0.79	0.990
4.19	0.79	0.988
4.66	0.79	0.992
4.66	0.79	0.990
5.20	0.79	0.993
5.20	0.79	0.994
2.49	1.18	0.979
2.49	1.18	0.975
2.90	1.18	0.977
2.90	1.18	0.980
3.32	1.18	0.983
3.32	1.18	0.981
3.32	1.18	0.980
3.32	1.18	0.995
3.77	1.18	0.990
3.77	1.18	0.989
3.77	1.18	0.989
3.77	1.18	0.990
4.19	1.18	0.994
4.19	1.18	0.995
4.19	1.18	0.994
4.19	1.18	0.991
4.66	1.18	0.992
5.20	1.18	0.994
2.49	1.58	0.978
2.90	1.58	0.981
2.90	1.58	0.980
3.32	1.58	0.991
3.32	1.58	0.985
3.77	1.58	0.990
4.19	1.58	0.994
4.66	1.58	0.993
5.20	1.58	0.995

Table A5

Solids Mass Flux vs. Nozzle, N_0 Flow Rate for Sand Particles

Orifice Plate: 0.025 m

$N_2 = 4.18 \times 10^{-3}$ m^3/s	$N_3 = 1.18 \times 10^{-3}$ m^3/s
Flow Rates, N_0 ($\times 10^4$ m^3/s)	Solids Mass Flux (kg/m^{2}s)
0.0	53.7
	54.7
3.2	67.7
	64.7
	71.0
	67.7
3.94	63.3
	61.9
	63.9
	63.9
	61.9
	61.7
	59.2
6.29	48.3
	48.5
	50.2
	51.2
	50.2
	50.2
	50.2

Table A6

Solids Mass Flux vs. Nozzle, N_0 Flow Rate for Sand Particles

Orifice Plate: 0.025 m

$N_2 = 3.15 \times 10^{-3}$ m^3/s $N_3 = 1.58 \times 10^{-3}$ m^3/s $N_0 + N_4 = 1.58 \times 10^{-3}$ m^3/s

Flow Rate, N_0 ($\times 10^4$ m^3/s)	Solids Mass Flux (kg/m^{2}s)
0.0	52.7
	50.9
3.94	76.6
	69.3
	72.5
	72.5
	79.4
6.29	58.2
	59.2
	58.2
	52.9

Table A.7

Solid Mass Flux vs. Nozzle, N_0 Flow Rate for Sand Particles

Orifice Plate: 0.025 m

$N_2 = 3.76 \times 10^{-3} \ m^3/s$ $\qquad\qquad$ $N_3 = 1.18 \times 10^{-3} \ m^3/s$

Flow Rates, N_0 ($\times 10^4 \ m^3/s$)	Solids Mass Flux ($kg/m^2 s$)
0.0	56.0
	51.1
	52.9
3.94	83.1
	83.1
	72.8
7.90	57.1
	56.0
	53.9
	48.5

Table A8

Solids Mass Flux vs. Nozzle, N_0 Flow Rate for Limestone Particles

Orifice Plate: 0.025 m

$N_2 = 4.19 \times 10^{-3}$ m^3/s $N_3 = 1.18 \times 10^{-3}$ m^3/s

Flow Rates, N_0 ($\times 10^4$ m^3/s)	Solids Mass Flux ($kg/m^3/s$)
0.0	63.4
	63.4
	60.6
	64.8
	60.6
	62.0
3.9	87.1
	89.9
	89.9
	89.9
	87.1
	87.1
6.3	62.0
	60.6
	62.0
	62.0
7.9	42.9
	42.9
	42.9
	42.9

Table A9

Solids Mass Flux vs. Nozzle, N_0 Flow Rate for Limestone Particles

Orifice Plate: 0.025 m

$$N_2 = 3.77 \times 10^{-3} \ m^3/s \qquad\qquad N_3 = 1.18 \times 10^{-3} \ m^3/s$$

Flow Rate, N_0 (1 $10^4 \ m^3$s)	Solids Mass Flux (kg/m^{2}s)
0.0	No Flow
3.9	69.7
	75.4
	75.4
	69.7
6.3	53.6
	52.6
	52.6
7.9	42.2
	42.9
	45.6

Table A.10

Solids Mass Flux vs. Nozzle, N_0 Flow Rate for Gypsum Particles

Orifice Plate: 0.025 m

$N_2 = 4.19 \times 10^{-3} \ m^3/s$ $\qquad\qquad$ $N_3 = 1.18 \times 10^{-3} \ m^3/s$

Flow Rates, N_0 ($\times 10^4 \ m^3/s$)	Solids Mass Flux ($kg/m^2 s$)
0.0	50.2
	49.1
	48.0
	49.1
3.9	66.9
	66.9
	64.9
6.3	49.1
	50.2
	50.2
	50.2
7.9	49.1
	49.1
	50.2
	49.1

Table A11

Solids Mass Flux vs. Nozzle, N_0 Flow Rate for Gypsum Particles

Orifice Plate: 0.025 m

$N_2 = 3.77 \times 10^{-3} \ m^3/s$ $N_3 = 1.18 \times 10^{-3} \ m^3 s$

Flow Rates, N_0 ($\times 10^4 \ m^3 s$)	Solids Mass Flux ($kg/m^2 s$)
0.0	45.1
	45.1
	45.1
	46.0
3.9	58.1
	60.1
	58.1
	56.6
6.3	48.0
	49.1
	47.0
	49.1
7.9	47.0
	46.0
	47.0
	44.2
	35.6

Table A12

Experimental Data for Pressure Drop in Riser for Sand Particles

Solid Fraction	Solid Flux (kg/m^{2}S)	Gas Flux (kg/m^{2}S)	$\Delta P/\Delta Lg$ (kg/m^3)
0.003	44.6	7.19	37.9
0.005	50.2	6.26	33.3
0.005	50.2	6.26	33.3
0.005	48.3	6.26	33.3
0.005	44.6	6.35	50.5
0.006	52.7	6.68	54.8
0.006	50.9	6.68	54.8
0.007	53.9	5.93	41.7
0.007	56.0	5.93	41.7
0.007	57.1	5.93	41.7
0.009	72.5	6.68	84.1
0.009	74.4	6.68	84.1
0.009	48.8	5.94	75.5
0.012	53.7	5.54	82.0
0.012	54.7	5.54	82.0
0.015	61.7	5.89	128.9
0.015	59.2	5.89	128.9
0.015	64.4	5.89	128.9
0.016	72.8	5.52	116.6
0.016	83.1	5.52	116.6
0.016	83.1	5.52	116.6
0.018	52.9	5.12	138.3
0.018	51.1	5.12	138.3
0.018	56.0	5.12	138.3

Table A13

Experimental Data for Pressure Drop in Riser for Limestone Particles

Solid Fraction	Solid Flux (kg/m^{2}S)	Gas Flux (kg/m^{2}S)	$\Delta P/\Delta L g$ (kg/m^3)
0.005	80.4	7.85	58.2
0.007	82.1	7.60	66.7
0.008	78.2	7.14	70.8
0.008	43.7	5.48	53.3
0.008	44.0	6.55	53.3
0.009	47.0	5.73	63.3
0.009	50.7	6.49	60.0
0.009	42.8	6.32	60.0
0.010	42.9	6.32	60.0
0.010	73.5	6.62	79.1
0.010	80.5	7.20	91.7
0.011	83.6	6.64	74.8
0.011	68.0	4.07	91.7
0.012	78.2	6.74	100.0
0.012	82.9	6.80	100.0
0.013	42.9	5.89	90.0
0.013	77.4	6.55	66.7
0.013	79.7	6.55	73.3
0.014	64.1	5.99	83:3
0.014	64.8	5.99	83.3
0.014	65.6	5.99	83.3
0.014	71.5	6.22	125.0
0.015	78.8	6.34	125.0
0.015	78.9	6.39	125.0
0.016	79.7	6.15	83.3
0.016	78.5	6.15	90.0
0.016	61.3	6.16	106.6
0.016	62.0	6.16	106.6
0.016	82.0	5.98	133.3
0.016	84.6	5.98	124.7
0.017	62.3	5.46	166.7
0.017	66.4	5.67	166.7
0.017	75.4	5.82	150.0
0.018	79.7	5.92	154.2
0.018	78.7	5.52	141.3
0.019	72.7	5.00	157.9
0.019	64.1	5.59	116.4
0.019	64.8	5.59	116.5
0.019	88.5	5.91	123.3
0.019	89.9	5.91	123.3
0.019	87.1	5.91	126.6
0.019	52.9	6.06	123.3
0.021	63.4	5.50	157.9
0.022	62.7	5.50	150.0
0.022	61.3	5.50	139.9
0.028	72.4	6.22	190.0

Table A14

Experimental Data for Pressure Drop in Riser for Gypsum Particles

Solid Fraction	Solid Flux (kg/m^{2}S)	Gas Flux (kg/m^{2}S)	ΔP/ΔLg (kg/m^3)
0.002	15.9	6.65	25.0
0.004	13.6	6.22	33.3
0.005	49.1	5.51	33.3
0.005	53.1	6.92	36.7
0.006	49.1	5.92	43.3
0.006	44.8	6.55	41.7
0.006	44.2	6.15	43.3
0.006	48.0	5.51	40.0
0.006	49.1	5.51	40.0
0.006	64.9	6.16	50.0
0.007	65.9	5.75	58.2
0.007	61.9	5.35	50.0
0.007	40.4	6.49	50.0
0.007	44.8	6.40	50.0
0.008	44.7	5.99	50.0
0.008	77.0	5.61	58.2
0.008	37.6	6.06	50.0
0.009	42.2	5.03	58.3
0.009	50.2	5.51	58.3
0.009	49.3	6.32	56.7
0.009	67.6	4.79	50.0
0.010	74.4	5.20	50.0
0.010	73.6	5.12	58.2
0.010	46.0	5.08	60.0
0.010	46.0	5.49	60.0
0.010	46.0	5.59	60.0
0.010	46.0	5.89	58.3
0.010	49.9	6.16	58.3
0.010	45.1	5.08	53.3
0.011	79.8	4.71	66.5
0.011	45.1	5.08	58.3
0.011	45.1	5.08	58.3
0.012	47.7	5.11	73.3
0.012	68.5	5.91	66.7
0.012	48.3	5.73	66.7
0.013	76.1	4.31	66.5
0.013	58.9	3.48	76.7
0.015	74.4	5.04	58.2
0.017	40.6	4.62	93.3
0.018	76.1	4.69	83.1
0.019	38.7	4.60	113.3
0.019	40.1	4.62	86.7
0.020	40.9	4.62	93.3
0.020	40.9	4.62	93.3
0.020	38.1	4.19	123.3
0.020	71.2	4.28	116.4
0.020	73.6	4.32	108.1
0.020	72.8	4.61	124.7
0.021	62.5	3.78	99.8

Continued

Solid Fraction	Solid Flux (kg/m^{2}S)	Gas Flux (kg/m^{2}S)	$\Delta P/\Delta Lg$ (kg/m^3)
0.022	76.1	3.88	129.7
0.022	62.5	4.19	124.7
0.023	66.9	4.20	133.3
0.023	49.1	4.68	126.7
0.075	34.2	3.77	133.3

Table A15

Experimental Data for Sand Particles

(Pressure Profile)

Run Number	Solids Mass Flux (kg/m^2)	Total Air Mass Flux (kg/m^2)	Nozzle, N_D Air Mass Flux (kg/m^2)	Solids Fraction in Riser	Standpipe Height (m)
S1	53.7	5.54	0	0.12	0.70
S2	54.7	5.54	0	0.12	0.70
S3	61.7	5.89	0.35	0.015	0.75
S4	59.2	5.89	0.35	0.015	0.50
S5	64.4	5.89	0.35	0.015	0.75
S6	48.3	6.26	0.72	0.005	0.75
S7	44.6	6.36	0.82	0.005	0.75
S8	44.6	7.19	0.82	0.003	0.75
S9	56.0	5.12	0	0.018	0.65
S10	51.1	5.12	0	0.018	0.50
S11	52.9	5.12	0	0.018	0.45
S12	83.1	5.52	0.46	0.016	0.80
S13	83.1	5.52	0.40	0.016	0.70
S14	71.8	5.52	0.40	0.016	0.65
S15	57.1	5.93	0.81	0.007	0.88
S16	56.0	5.93	0.81	0.007	0.88
S17	53.9	5.93	0.81	0.007	0.86
S18	48.5	6.26	1.14	0.005	0.88
S19	50.2	6.26	1.14	0.005	0.88
S20	50.2	6.26	1.14	0.005	0.87

Table · A↑6

Experimental Data for Limestone Particles

(Pressure Profile)

Run Number	Solids Mass Flux (kg/m^2)	Total Air Mass Flux $(kg/m^2.)$	Nozzle, N_0 Air Mass Flux $(kg/m^2.)$	Solids Fraction in Riser	Standpipe Height (m)
L1	64.1	5.99	0.0	0.019	0.90
L2	64.8	5.99	0.0	0.014	0.90
L3	65.6	5.99	0.0	0.014	0.90
L4	77.4	6.55	0.0	0.013	0.90
L5	79.7	6.55	0.0	0.013	0.90
L6	63.4	5.50	0.0	0.021	0.90
L7	62.7	5.50	0.0	0.021	0.90
L8	61.3	5.50	0.0	0.021	0.90
L9	79.7	6.15	0.0	0.016	0.90
L10	78.5	6.15	0.0	0.016	0.90
L11	64.1	5.59	0.0	0.019	0.90
L12	64.8	5.59	0.0	0.019	0.90
L13	88.5	5.91	0.39	0.019	0.94
L14	89.9	5.91	0.39	0.019	0.90
L15	87.1	5.91	0.39	0.019	0.90
L16	61.3	6.16	0.63	0.016	1.00
L17	62.0	6.16	0.63	0.016	1.00
L18	42.9	6.32	0.79	0.009	1.20
L19	42.9	6.32	0.79	0.010	0.95
L20	50.7	6.49	0.95	0.0`9	1.00

Table A17

Experimental Data for Gypsum Particles

(Pressure Profile)

Run Number	Solids Mass Flux $(kg/m^2 \cdot)$	Total Air Mass Flux $(kg/m^2 \cdot)$	Nozzle, N_0 Air Mass Flux $(kg/m^2 \cdot)$	Solids Fraction in Riser	Standpipe Height (m)
G1	49.1	5.51	0.0	0.005	0.90
G2	48.0	5.51	0.0	0.006	0.90
G3	49.1	5.51	0.0	0.006	0.90
G4	45.1	5.08	0.0	0.016	0.90
G5	45.1	5.08	0.0	0.011	0.90
G6	45.1	5.08	0.0	0.011	0.90
G7	40.1	4.62	0.0	0.019	0.90
G8	40.9	4.62	0.0	0.020	0.90
G9	40.9	4.62	0.0	0.020	0.90

Table A18

Height vs. Static Pressure for Sand Particles

Height, m	0	.26	.36	.61	1.46	2.10	2.05	.99	.32
Pressure Port No.	P_1	P_2	P_3	P_4	P_5	P_6	P_7	P_8	P_9
Run Number					Static Pressure kg/ms^2				
S1	5590	4707	4413	2256	981	–	1373	1965	2550
S2	5590	4904	4511	2059	1079	–	1275	2059	2556
S3	6767	6178	–	1863	785	–	1079	2059	2746
S4	6571	6080	–	883	785	–	1177	2039	2844
S5	6767	6473	4119	2354	785	–	1079	2059	2746
S6	5688	4805	3138	1961	883	–	1079	1667	2746
S7	3727	3727	–	1961	1079	–	1177	1373	1765
S8	2746	6963	–	3923	1079	–	1177	1275	1275
S9	5982	5198	2844	1373	981	981	1471	2550	3727
S10	6080	5100	2550	1177	833	833	1471	2550	3432
S11	6276	5198	2158	1177	981	981	1471	2940	3825
S12	7944	7944	5198	3825	1275	1275	1569	2648	3432
S13	7159	7144	4511	3138	1275	1373	1569	2548	3531
S14	7355	7061	4119	3040	1275	1373	1569	2844	3236
S15	4315	4119	3236	2746	1373	1471	1765	2158	3236
S16	4413	4021	3138	2746	1373	1373	1765	2158	2550
S17	4413	4021	3040	2648	1471	1471	1765	2256	2550
S18	3629	3236	2746	2648	1863	1765	1961	2354	2550
S19	3825	3334	2746	2354	1667	1765	1765	2158	2550
S20	3727	3334	2648	2452	1863	1863	1961	2250	2550

Table A.1.9

Height vs. Static Pressure for Limestone Particles

Height, m	0	.26	.61	.85	1.46	2.10	2.05	.99	.32
Pressure Port	P_1	P_2	P_3	P_4	P_5	P_6	P_7	P_8	P_9
Run Number					Static Pressure,	kg/mS^2			
L1	6767	5786	4315	3531	1569	1569	1863	2648	3334
L2	6767	5786	4217	3432	1569	1569	1863	2844	3334
L3	6571	5982	4315	3531	1569	1569	1961	2844	3334
L4	6275	5492	4119	3334	1765	1765	1863	2746	3825
L5	6275	5492	4119	3334	1765	1765	2059	2942	3727
L6	7453	6375	4707	3923	1569	1569	2059	3334	4315
L7	8041	6963	4707	3629	1569	1569	2059	4021	4707
L8	7944	6963	4511	3629	1569	1569	2158	3531	4707
L9	7061	6473	4511	3923	1765	1765	2059	3531	3923
L10	7061	6473	4707	3923	1765	1765	1961	3334	3923
L11	7846	6963	5100	4315	1667	1667	2059	3629	4707
L12	7944	7061	5394	4217	1765	1769	2158	3629	4707
L13	8336	8336	5786	4904	1667	1667	2059	3432	4413
L14	8434	8140	5786	4805	1569	1569	2059	3236	4119
L15	8434	8146	5786	4707	1667	1667	2158	3432	4413
L16	6571	6375	4805	4021	1765	1765	2158	3138	3431
L17	6571	6375	4805	4021	1765	1876	2059	3138	3629
L18	4904	4511	3629	3236	1961	1961	2354	3040	3531
L19	4904	4511	3727	3236	1863	1961	2354	2942	3629
L20	4707	4413	3531	2159	2059	2158	2432	3640	3727

Table A20

Height vs. Static Pressure for Gypsum Particles

Height, m	0	.26	.61	.85	1.46	2.10	2.05	.99	.32
Pressure Port	P_1	P_2	P_3	P_4	P_5	P_6	P_7	P_8	P_9
Run Number					Static Pressure, kg/ms^2				
G1	4707	4217	3432	3040	1961	1863	2256	2746	3040
G2	4904	4609	3531	3236	2059	2059	2256	2746	3040
G3	4904	4609	3629	3236	2059	2059	2256	2942	3236
G4	5394	5100	4119	3531	1961	1961	2354	2942	3432
G5	5492	5198	4119	3727	1961	1961	2452	3040	3432
G6	5492	5296	4217	3629	2059	1961	2452	3040	3531
G7	6473	6178	4904	4217	2156	2059	2550	3531	4119
G8	6973	6178	4904	4217	2059	2059	2550	3432	4119
G9	6571	6276	4904	4021	2059	2059	2550	3629	411;

173

APPENDIX B

COMPUTER CODE

APPENDIX B1

HIGH VELOCITY FLUIDIZED BED
PRESSURE PROFILE MODEL

```
00001  C-----PROGRAM TO CALCULATE PRESSURE DROP AND PRESSURE PROFILE
00002  C        IN A HIGH VELOCITY FLUIDIZED BED COLD FLOW REACTOR
00003  C
00004  C------VARIABLES USED IN THIS PROGRAM------
00005  C
00006  C        ABUSLP => ABSOLUTE VALUE OF THE SLIP VELOCITY, M/S
00007  C        ANG => POINT OF CALCULATIONS IN BENDS, DEGREES
00008  C        ANGLE => ANGLE OF TRANSPORT LINE , DEGREES
00009  C        ANGSTP => ANGLE OF STAND PIPE ,DEGREES
00010  C        BNDAGL => BEND ANGLE , DEGREES
00011  C        BNDL90 => BEND ANGLE LESS 90 , DEGREES
00012  C        DEPRES => PRESSURE DROP IN FLUIDIZED BED OF HEIGHT H, KG/MS2
00013  C        DP => PARTICLE DIAMETER, M
00014  C        DP2 => PARTICLE DIAMETER SQUARED, M2
00015  C        DPIN => PRESSURE DIFF IN CALC INLET PRESSURES, KG/M/S2
00016  C        DT => TUBE INSIDE DIAMETER, M
00017  C        FB => BEND FRICTION FACTOR
00018  C        FDNSTY => FLUID DENSITY, KG/M3
00019  C        FFXMN => MINIMUM FLUID FLUX EXPERIMENTAL, KG/M2S
00020  C        FG => FLUID FRICTION FACTOR
00021  C        FMFX => FLUID MASS FLUX, KG/M2S
00022  C        FMFX2 => FLUID MASS FLUX SQUARED, (KG/M2S)2
00023  C        FS => SOLIDS FRICTION FACTOR
00024  C        FVSCTY => FLUID VISCOSITY, KG/MS
00025  C        GFRFCT => FUNCTION FOR FLUID FRICTION FACTOR
00026  C        GG => GRAVITATIONAL CONSTANT =9.807 M2/S
00027  C        H => HEIGHT, M
00028  C        HO => INITIAL HEIGHT GIVEN TO SUBROUTINES, M
00029  C        IR => INPUT UNIT NUMBER
00030  C        IPLO => OUTPUT UNIT NUMBER FOR PLOTTING
00031  C        IW => OUTPUT UNIT NUMBER
00032  C        MUBAR => APPEARENT VISCOSITY FOR MIXTURE, KG/MS
00033  C        KPRINT => PRINT REGARDLESS OF AGREEMENT =1
00034  C        KH1HO => =1, HEIGHT INCREASES FROM HO
00035  C               =2, HEIGHT DECREASES FROM HO
00036  C        KHVFBC => =1 HIGH VELOCITY FLUIDIZATION
00037  C               =2 PNEUMATIC TRANSPORT
00038  C        KTPFS => TYPE OF SOLIDS FRICTION FACTOR CORRELATION
00039  C               = 1, STEMMERDING
00040  C               = 2, KONNO & SAITO
00041  C               = 3, VAN SWAAGI
00042  C               = 4, REDDY & PIE
00043  C        KTPTL => TYPE OF TRANSFER LINE
00044  C               = 1, STRAIGHT SECTION, MAY BE ANGLED
00045  C               = 2, BEND, XLNGHT=RADIUS, ANGLE=# DEGREES IN BEND
00046  C        NC => NUMBER OF CALCLULATIONS FOR EACH SECTION
00047  C        PO => PRESSURE AT EXIT TO SECTION, M OF H2O
00048  C        PXL => PRESSURE AT X IN SECTION, M OF H2O
00049  C        PINMX => PRESSURE AT FLUID ENTRANCE TO LOOP, M OF H2O
00050  C        PEXIT => PRESSURE AT FLUID EXIT FROM LOOP, M OF H2O
00051. C        PRSTOL => TOLERANCE IN CALC INLET PRESSURES, KG/MS2
00052  C        RBND => RADIUS OF BEND, M
00053  C        RBDT => RBND/DT
00054  C        SDNSTY => SOLIDS DENSITY,KG/M3
00055  C        SFRFCT => FUNCTION TO PREDICT SOLIDS FRICTION FACTOR
00056  C        SFXMX => MAXIMUM SOLIDS FLUX EXPERIMENTAL, KG/M2S
```

```
00057  C      SFXMN => MINIMUM SOLIDS FLUX EXPERIMENTAL, KG/M2S
00058  C      SMFX => SOLIDS MASS FLUX, KG/M2S
00059  C      SMFX2 => SOLIDS MASS FLUX SQUARED, (KG/M2S)2
00060  C      SFRCTN => SOLIDS FRACTION
00061  C      SFRMX => MAXIMUM SOLIDS FRACTION
00062  C      SNAGL => SINE OF ANGLE
00063  C      SPRCTY => PARTICLE SPHEROCITY
00064  C      SPRC2 => PARTICLE SPHEROCITY SQUARED
00065  C      USLIP => SLIP VELOCITY, M/S
00066  C      X => POINT OF CALCULATION
00067  C      XHVCT1 => = 1./0.7  FACTOR CORRECTING PNEUMATIC TRANSPORT
00068  C                     EQUATION FOR HIGH VELOCITY FLUIDIZATION REGIME
00069  C      XLNGTH => LENGTH OF EACH SECTION, M
00070  C      XSTEP => STEP SIZE FOR CALCULATION IN EACH SECTION, M
00071  C      XLBND => LENGTH OF BEND, M
00072  C      VOID => VOIDAGE
00073  C      VOIDPB => PACKED BED VOIDAGE
00074  C
00075  C
00076  C
00077  C      DIMENSION MAIN INPUT
00078         DIMENSION IDNT(15),DT(15),KTPTL(15),ANGLE(15),XLNGTH(15),VOID(15)
00079         DIMENSION SFRCTN(15),SP(75),XHIGHT(75)
00080  C
00081  C      DIMENSION VARIABLES FOR STRPL.FOR ***PLOTTING***
00082         DIMENSION LG(2),LGWR(4),NDEC(2),FDATA(3),XLBL(5),YLBL(2),
00083       1   DST(2),CRVLB(3)
00084         EXTERNAL DPINRS
00085         DOUBLE PRECISION FNAMI,FNAMO
00086         COMMON DT,DP,FDNSTY,ANGLE,FVSCTY,FDATA,GG,PINRSR,
00087        1HEXIT,IRO,IR1,IPLO,IW,PEXIT,SPRCTY,
00088        2SDNSTY,SMFX,XLNGTH,VOIDPB,SFRCTN,VOID
00089         DATA XLBL/'STATIC PRESSURE, KG/MS2 '/
00090         DATA YLBL/' HEIGHT, M'/
00091         DATA FDATA/'( 1P7E11.4)'/,NFDATA/3/
00092  C
00093  C      ASK USER TO INPUT FILE NAME
00094  C
00095  C
00096  C      SPECIFY UNIT NUMBER TO BE USED FOR PLOTTING FILE
00097  C
00098         IRO = 22
00099         IW = 5
00100         IPPM=20
00101         IPLO=21
00102         CALL FLOPCL(IRO,IW,3,FNAMI)
00103         CALL FLOPCL(IRO,IW,1,FNAMI)
00104  C
00105  C      OPEN FILE ON UNIT IR, AND PLOT FILE ON IPLO
00106  C
00107         CALL FLOPCL(IPLO,IW,3,FNAMO)
00108         CALL FLOPCL(IPLO,IW,1,FNAMO)
00109         CALL FLOPCL(IPPM,IW,1,'PPMO.I')
00110  C
00111         GG=9.807
00112  C
```

```
00113    C        READ VARIABLES FOR SIMULATION
00114             READ(IRO,*) NC,NSCTNS
00115             DO 100 I=1,NSCTNS
00116               READ(IRO,*) IDNT(I),DT(I),KTPTL(I),ANGLE(I),XLNGTH(I),VOID(I)
00117               SFRCTN(I)=1.-VOID(I)
00118    100      CONTINUE
00119    C        READ SOLIDS PROPERTIES
00120             READ(IRO,*) SMFX,SDNSTY,SPRCTY,TEMP.CPS,THCONS
00121             READ(IRO,*) VOIDPB,DP
00122    C        READ FLUID PROPERTIES AND FLOW RATE
00123    C             ***RISER***
00124             READ(IRO,*) FMFXR,FDNSTY,FVSCTY,CPF,THCONF,TEMP
00125    C           ***STANDPIPE***
00126             READ(IRO,*) FMFXSP,FDNSTY,FVSCTY,CPF,THCONF,TEMP
00127    C        READ PRESSURE OUTLET AND MAXIMUM PRESSURE AT INLET
00128             READ(IRO,*) PEXIT,PINMX,HEXIT,PRSTOL
00129    C        READ VALUES FOR HIMIF.FOR
00130             READ(IRO,*) EST1,EST2,MAXIT,ERR
00131    C
00132    C
00133    C
00134    C
00135             DPMX=PINMX-PEXIT
00136    C
00137    C
00138    C
00139    C
00140    C
00141    C        SET VALUES FOR PLOTTING
00142    C
00143             KSYMB=0
00144             XMIN=400000.
00145             XMAX=PINMX
00146             YMIN=-1.0
00147             YMAX=34.
00148             L10=0
00149             LG(1)=0
00150             LG(2)=0
00151             KSLG=-7
00152             CYCLX=-6.8
00153             CYCLY=-5.8
00154             NXLB=23
00155             NYLB= 10
00156             ROTA=0.0
00157             LIN=1
00158             NW=1
00159             SZLT=0.12
00160             SZPL=0.04
00161             DST(1)=0.06
00162             DST(2)=0.06
00163             LTK=0
00164             LPNT=1
00165             INTCH=0
00166             LRPT=2
00167             LFMI=0
00168             LWSL=0
```

```
00169         LDATA=0
00170         LGWR(1)=0
00171         LGWR(2)=1
00172         LGWR(3)=0
00173         LGWR(4)=1
00174         LF811=1
00175         NDEC(1)=-4
00176         NDEC(2)=-2
00177         KCOL=2
00178         JCON=1
00179         NDPNT=-7
00180         JCRVLB=0
00181   C
00182         CALL RISER(ANGLE,DT,FDNSTY,FMFXR,FVSCTY,FDATA,GG,
00183        1KH1HO,KHVFBC,H,HO,IRO,IR1,IPLO,IW,NC,PINRSR,PO,PXL,
00184        2PEXIT,HEXIT,SDNSTY,SMFX,SFRCTN,KTPFS,XLNGTH,VOID)
00185   C
00186   C
00187   C
00188   C
00189         CALL HIMIF(FMFXSP,IT,MAXIT,EST1,EST2,DPINRS,ERR,IER,IRO,IW,FRT)
00190         IF(IER.EQ.1) GO TO 400
00191         WRITE(IW,7500) IER
00192         GO TO 9999
00193   400   CONTINUE
00194   C
00195         REWIND IPLO
00196         REWIND IW
00197   C
00198   C
00199   C
00200         CALL STRPL(IPLO,IW,XMIN,XMAX,YMIN,YMAX,LIO,LG,KSLG,CYCLX,
00201        1 CYCLY,NXLB,NYLB,ROTA,LIN,NW,SZLT,SZPL,DST,LTK,LPNT,
00202        2 INTCH,LRPT,LFM1,LWSL,LDATA,LGWR,LF811,LWS1,LWS2,NDEC,KCOL,
00203        3 JCON,FDATA,XLBL,YLBL,NFDATA,NDPNT,JCRVLB,CRVLB)
00204   C
00205   C
00206   C     WRITE VALUES ON PLOT FILE
00207   C     CALCULATE PRESSURE PROFILE FOR GAS-SOLID CO-CURRENT FLOW SECTION
00208   C
00209   999   CONTINUE
00210         WRITE(IW,7900) PEXIT,HEXIT
00211         WRITE(IPLO,FDATA) PEXIT,HEXIT
00212   C
00213         CALL RISER(ANGLE,DT,FDNSTY,FMFXR,FVSCTY,FDATA,GG,
00214        1KH1HO,KHVFBC,H,HO,IRO,IR1,IPLO,IW,NC,PINRSR,PO,PXL,
00215        2PEXIT,HEXIT,SDNSTY,SMFX,SFRCTN,KTPFS,XLNGTH,VOID)
00216   C
00217   C
00218         DUM=-999.
00219         WRITE(IPLO,FDATA) DUM,DUM
00220   C
00221         DUM=-4.
00222         WRITE(IPLO,FDATA) DUM,DUM
00223   C
00224   C
```

```
00225    C       CALCULATION FOR STANDPIPE GAS-SOLID FLOW PRESSURE PROFILE
00226    C
00227    C
00228    C
00229    C
00230            CALL STRPL(IPLO,IW,XMIN,XMAX,YMIN,YMAX,L10,LG,KSLG,CYCLX,
00231         1  CYCLY,NXLB,NYLB,ROTA,LIN,NW,SZLT,SZPL,DST,LTK,LPNT,
00232         2  INTCH,LRPT,LFM1,LWSL,LDATA,LGWR,LF811,LWS1,LWS2,NDEC,KCOL,
00233         3  JCON,FDATA,XLBL,YLBL,NFDATA,NDPNT,JCRVLB,CRVLB)
00234    C
00235            WRITE(IW,7900) PEXIT,HEXIT
00236            WRITE(IPLO,FDATA) PEXIT,HEXIT
00237    C
00238    C
00239           CALL STNDPP(DT,DP,FDNSTY,FMFXSP,FVSCTY,FDATA,GG,
00240          1H,HO,IRO,IR1,IPLO,IW,NC,PO,PXL,SPRCTY,
00241          2PEXIT,HEXIT,SFRCTN,SDNSTY,SMFX,XLNGTH,VOIV,VOIDPB)
00242    C
00243            ADPIN=ABS(PXL-PXLCO)
00244            DPIN=(PXL-PXLCO)
00245    9999    CONTINUE
00246    C
00247    C
00248    C
00249    C       TERMINATE PLOT BY WRITING A -1 THEN CLOSE FILES
00250    C
00251    C
00252            DUM=-999.
00253            WRITE(IPLO,FDATA) DUM,DUM
00254            READ(IRO,*) EXNDTA
00255            IF(EXNDTA.EQ.-2.) GO TO 1150
00256            DUM=-4.
00257            WRITE(IPLO,FDATA) DUM,DUM
00258            GO TO 1160
00259    1150    CONTINUE
00260            DUM=-1.
00261            WRITE(IPLO,FDATA) DUM,DUM
00262            GO TO 8888
00263    1160    CONTINUE
00264            LIN=0
00265            LPNT=2
00266    1175    CONTINUE
00267            CALL STRPL(IPLO,IW,XMIN,XMAX,YMIN,YMAX,L10,LG,KSLG,CYCLX,
00268         1  CYCLY,NXLB,NYLB,ROTA,LIN,NW,SZLT,SZPL,DST,LTK,LPNT,
00269         2  INTCH,LRPT,LFM1,LWSL,LDATA,LGWR,LF811,LWS1,LWS2,NDEC,KCOL,
00270         3  JCON,FDATA,XLBL,YLBL,NFDATA,NDPNT,JCRVLB,CRVLB)
00271            KSYMB=KSYMB
00272            WRITE(IPLO,8700) KSYMB
00273    C
00274            DO 1200 I=1,75
00275            READ(IRO,*) SP(I),XHIGHT(I)
00276            NPTEXP=I-1
00277            IF(SP(I).EQ.-1) GO TO 1250
00278            IF(SP(I).EQ.-2) GO TO 1285
00279    1200    CONTINUE
00280    1250    CONTINUE
```

```
00281          DO 1300 I=1,NPTEXP
00282             WRITE(IPLO,FDATA) SP(I),XHIGHT(I)
00283   1300   CONTINUE
00284          DUM=-999.
00285          WRITE(IPLO,FDATA) DUM,DUM
00286          DUM=-4.
00287          WRITE(IPLO,FDATA) DUM,DUM
00288          KSYMB=KSYMB+1
00289          GO TO 1175
00290   1285   CONTINUE
00291          DO 1320 I=1,NPTEXP
00292             WRITE(IPLO,FDATA) SP(I),XHIGHT(I)
00293   1320   CONTINUE
00294          DUM=-999.
00295          WRITE(IPLO,FDATA) DUM,DUM
00296          DUM=-1.
00297          WRITE(IPLO,FDATA) DUM,DUM
00298   8888   CONTINUE
00299          WRITE(IPPM,*) SDNSTY,VOID(3),SMFX,DP,SFRCTN(3)
00300          WRITE(IPPM,*) FMFXR,FDNSTY,FVSCTY,CPF,THCONF
00301          WRITE(IPPM,*) XLNGTH(3),DT,XLNGTH(7),VOID(7),SFRCTN(7)
00302   C
00303          CALL FLOPCL(IPLO,IW,2,FNAM)
00304          CALL FLOPCL(IRO,IW,2,FNAM)
00305          CALL FLOPCL(IR1,IW,2,FNAM)
00306          STOP
00307   C      FORMAT STATEMENTS
00308   C
00309   7500   FORMAT(' ERROR, IER= ',I5)
00310   7900   FORMAT(1P7E11.4)
00311   8000   FORMAT(' PRESSURE DROP TOO LARGE,CHOOSE NEW SMFX & FMFXR')
00312   8100   FORMAT(' OLD SOLID & GAS FLUX ARE:',2F12.4,' ENTER NEW DATA',$)
00313   8200   FORMAT(2F12.4)
00314   8300   FORMAT(' PRESSURE DROP IN STANDPIPE TOO SMALL ',F12.4)
00315   8230   FORMAT(' GAS FLUX IN STAND PIPE TOO LARGE: ',F12.4)
00316   8250   FORMAT(' ENTER NEW GAS FLUX: F12.4 ',$)
00317   8270   FORMAT(F12.4)
00318   8400   FORMAT(' GAS FLUX IS: ',$)
00319   8500   FORMAT(F12.4)
00320   8700   FORMAT(I5)
00321   9000   FORMAT(2X,'NPNTS=',I3,' DPM=',F5.3,' FO=',F6.3,' F1=',
00322       1   F5.2,2X,'W=',F7.2,'  XK=',1PE10.3)
00323   9050   FORMAT(1X,'  I',3X,' DP',5X,' PO',8X,'EK',8X,'XI',
00324       1   7X,'P1',7X,' P2')
00325   9100   FORMAT(1X,I2,1P6E10.3)
00326   9150   FORMAT(2X,' W/FO=',F8.2,2X,' FO=',0PF6.3,2X,' W=',F8.2)
00327   9250   FORMAT(2X,'FO=',F6.3,2X,'F1=',F5.2,2X,'F2=',1PE9.2,
00328       1   2X,'W=',0PF7.2,2X,'FR.CONV=',F6.3)
00329   9300   FORMAT(2X,' FO=',F6.3,2X,' F1=',F5.2,2X,'F2 FROM P2 INTGRTN',
00330       1   '=',F7.4,2X,'FR.CONV.=',F6.3)
00331   9350   FORMAT(7A5,F5.3,F5.2,F5.2,F8.2)
00332   9400   FORMAT(20A5)
00333   9410   FORMAT(' IS DPIN SMALL ENOUGH, TYPE 1 IF YES,2 IF NO ',$)
00334   9450   FORMAT(I10)
00335          END
```

COMMON BLOCKS

/.COMM./(+135)

DT	+0	DP	+17	FDNSTY	+20	ANGLE	+21	FVSCTY	+40
FDATA	+41	GG	+44	PINRSR	+45	HEXIT	+46	IRO	+47
IR1	+50	IPLO	+51	IW	+52	PEXIT	+53	SPRCTY	+54
SDNSTY	+55	SMFX	+56	XLNGTH	+57	VOIDPB	+76	SFRCTN	+77
VOID	+116								

SUBPROGRAMS CALLED

HIMIF   STNDPP   STRPL   RISER   DPINRS   FLOPCL

SCALARS AND ARRAYS ["*" NO EXPLICIT DEFINITION - "%" NOT REFERENCED]

DST	1	*LFM1	3	*CYCLY	4	KTPTL	5	*FNAM	24
*DPMX	25	*EST1	26	*YMAX	27	*JCRVLB	30	*NYLB	31
*MAXIT	32	FNAMO	33	*EXNDTA	35	*XMIN	36	*H	37
XHIGHT	40	*IER	153	*LPNT	154	*CYCLX	155	*NDPNT	156
*INTCH	157	*LIO	160	*ERR	161	*VOIV	162	FNAMI	163
*NXLB	165	*KHVFBC	166	*HO	167	*THCONF	170	*KCOL	171
*LIN	172	YLBL	173	IDNT	175	*NW	214	*JCON	215
*LRPT	216	*XMAX	217	*KSLG	220	*NPTEXP	221	*LDATA	222
*DPIN	223	*FMFXR	224	*FRT	225	*SZLT	226	*THCONS	227
*PRSTOL	230	*PINMX	231	*PXLCO	232	*LWS2	233	.S0003	234
*LTK	235	.S0002	236	*LWSL	237	*CPS	240	.S0001	241
*ADPIN	242	*PO	243	.S0000	244	*IT	245	LGWR	246
*DUM	252	*LWS1	253	*KH1HO	254	*KSYMB	255	XLBL	256
NDEC	263	*TEMP	265	*PXL	266	*SZPL	267	*YMIN	270
*I	271	*KTPFS	272	*NSCTNS	273	*IPPM	274	*FMFXSP	275
*ROTA	276	LG	277	*EST2	301	SP	302	*NC	415
CRVLB	416	*LF811	421	*NFDATA	422	*CPF	423		

MAIN.   [No errors detected]

```
00001      C
00002      C
00003             SUBROUTINE FLOPCL(IUNIT,IW,KOPR,FNAM)
00004      C
00005      CFLOPCL.FOR
00006      C
00007      C       THIS SUBROUTINE IS TO OPEN AND CLOSE A FILE ON DISK
00008      C       AND TO ASK USER TO INPUT FILE NAME FROM TTY
00009      C
00010      C       IUNIT THE UNIT NUMBER USED FOR FILE I/O
00011      C       IW IS THE OUTPUT UNIT NUMBER
00012      C       KOPR THE OPERATION TYPE DESIRED.
00013      C        KOPR=1 TO OPEN FILE,
00014      C        KOPR = 2 TO CLOSE FILE
00015      C        KOPR = 3 TO ASK USER TO ENTER INPUT FILE NAME AND THEN
00016      C          ECHO IT BACK TO TERMINAL
00017      C       FNAM NAME OF FILE..NOT MORE THAN 8 CHARACTERS. THIS NAME
00018      C       IS NOT NEEDED IN CLOSING THE FILE
00019      C
00020             DOUBLE PRECISION FNAM
00021             DATA DSKZ/'DSK'/
00022             GO TO(50,100,150), KOPR
00023        50   CONTINUE
00024      C
00025      C       OPEN FILE AND WRITE A MESSAGE
00026      C
00027             OPEN(UNIT=IUNIT,DEVICE=DSKZ,FILE=FNAM)
00028             WRITE(IW,9000) IUNIT,FNAM
00029             GO TO 200
00030       100   CONTINUE
00031      C
00032      C       CLOSE FILE AND WRITE A MESSAGE
00033      C
00034             CLOSE(UNIT=IUNIT)
00035             WRITE(IW,9050) IUNIT
00036             GO TO 200
00037       150   CONTINUE
00038      C
00039      C       ASK USER TO INPUT FILE NAME
00040      C
00041             TYPE 9100
00042             ACCEPT 9150,FNAM
00043             TYPE 9200,FNAM
00044       200   CONTINUE
00045             RETURN
00046      9000   FORMAT(' UNIT NO.',I3,' IS USED TO OPEN FILE ',A10)
00047      9050   FORMAT('   FILE ON UNIT',I3, ' IS CLOSED')
00048      9100   FORMAT('  INPUT FILE NAME ',$)
00049      9150   FORMAT(A10)
00050      9200   FORMAT('  INPUT FILE IS ',A10)
00051             END
```

SCALARS AND ARRAYS ["*" NO EXPLICIT DEFINITION - "%" NOT REFERENCED]

FNAM   1   *IW   3   *IUNIT 4   *KOPR   5   *DSKZ   6

TEMPORARIES

.A0016 7

FLOPCL [No errors detected]

```
00001   C
00002           SUBROUTINE PDVPC(ANGLE,DT,FDNSTY,FMFX,FVSCTY,FDATA,GG,
00003          1KH1HO,KHVFBC,H,HO,IRO,IR1,IPLO,IW,NC,PO,PXL,
00004          2SDNSTY,SMFX,SFRCTN,KTPFS,XLNGTH,VOID)
00005           DIMENSION FDATA(3)
00006   C
00007   C       SUBROUTINE PDVPC PRESSURE DROP IN VERTICLE OR ANGLED PNEUMATIC
00008   C          TRANSPORT AND HIGH VELOCITY FLUIDIZATION
00009   C
00010   C
00011           SNANGL=SIND(ANGLE)
00012           SMFX2=SMFX**2
00013           FMFX2=FMFX**2
00014   C
00015           XLE=0.2
00016           XLR=XLNGTH
00017           XLRLE=XLR-XLE
00018           FG=0.001
00019           US=SMFX/SDNSTY/SFRCTN
00020           FS=12.2*SFRCTN/US/VOID**3
00021   C
00022           PXL=PO
00023           H=HO
00024   C
00025           XSTEP=XLNGTH/NC
00026   C
00027   C       HIGH VELOCITY FLUIDIZATION !!!!
00028           IF(KHVFBC.EQ.1) GO TO 100
00029           GO TO 200
00030   100     CONTINUE
00031           IF(ANGLE.NE.90.) GO TO 150
00032           HVCTI=1.
00033           GO TO 300
00034   150     WRITE(IW,9000)
00035           GO TO 9999
00036   200     CONTINUE
00037   C
00038   C       PNEUMATIC TRANSPORT THEN !!!!
00039           IF(ANGLE.GT.0.) GO TO 250
00040           WRITE(IW,9100)
00041   250     CONTINUE
00042           HVCTI=1.
00043   300     CONTINUE
00044           DPKE=SMFX/SDNSTY/SFRCTN
00045           DO 400 I=1,NC
00046           X=XSTEP*FLOAT(I)
00047           IF(X.LT.XLRLE) GO TO 420
00048           DPKE=(SMFX2/SDNSTY/SFRCTN)*(XSTEP/XLE)
00049           GO TO 440
00050   420     CONTINUE
00051           DPKE=0.0
00052   440     CONTINUE
00053           PXL=PXL+(DPKE+XSTEP*(2*FS*SMFX2/SDNSTY
00054          1     /SFRCTN/DT+2*FG*FMFX2/FDNSTY/DT
00055          2     +SDNSTY*SFRCTN*GG))*HVCTI
00056           IF(KH1HO.EQ.2) GO TO 350
```

```
00057           H=H+SNANGL*XSTEP
00058           GO TO 375
00059     350   CONTINUE
00060           H=H-SNANGL*XSTEP
00061     375   CONTINUE
00062           WRITE(IW,9200) PXL,H
00063           WRITE(IPLO,FDATA) PXL,H
00064     400 CONTINUE
00065         RETURN
00066    9999 CONTINUE
00067    9000 FORMAT(' ERROR, HVF,ANGLE MUST EQUAL 90.0 ')
00068    9100 FORMAT(' ERROR, VPC, ANGLE MUST EXCEED 0.0 ')
00069    9200 FORMAT(1P7E11.4)
00070         END
```

SUBPROGRAMS CALLED

SIND.

SCALARS AND ARRAYS ["*" NO EXPLICIT DEFINITION - "%" NOT REFERENCED]

*SFRCTN	1	*VOID	2	%FVSCTY		*IW	3	*SMFX2	4
*XLRLE	5	*H	6	*XLE	7	*HVCT1	10	*KHVFBC	11
*DT	12	*HO	13	*DPKE	14	*FDNSTY	15	*XSTEP	16
*XLNGTH	17	%IRO		*IPLO	20	FDATA	21	*SMFX	22
*FMFX2	23	*ANGLE	24	.S0000	25	*PO	26	*GG	27
*SNANGL	30	*KH1HO	31	*US	32	*X	33	%IR1	
*PXL	34	*FS	35	*I	36	*XLR	37	%KTPFS	
*NC	40	*FG	41	*SDNSTY	42	*FMFX	43		

TEMPORARIES

.A0016 44

PDVPC   [No errors detected]

```
00001          SUBROUTINE PDHPC(DT,FMFX,FDNSTY,FDATA,FVSCTY,IRO,IR1,IPLO,IW
00002        1,HO,H,KTPFS,NC,PO,PXL,SMFX,SDNSTY,SFRCTN,XLNGTH,VOID)
00003          DIMENSION FDATA(3)
00004    C
00005    C     SUBROUTINE PDHPC PRESSURE DROP HORIZONTAL PNEUMATIC
00006    C         CONVEYING
00007          SMFX2=SMFX**2
00008          FMFX2=FMFX**2
00009          FS=0.0203
00010          XLE=1.7
00011          XLED=XLNGTH
00012           XLEDLE=XLED-XLE
00013          FG=0.001
00014          PXL=PO
00015          XSTEP=XLNGTH/NC
00016          DPKE=SMFX2/SDNSTY/SFRCTN
00017          DO 100 I=1,NC
00018           X=XSTEP*FLOAT(I)
00019           IF(X.LT.XLEDLE) GO TO 75
00020           DPKEST=(X**2.-(X-XSTEP)**2.)*DPKE/XLE**2.
00021           GO TO 85
00022    75     CONTINUE
00023           DPKEST=0.
00024    85     CONTINUE
00025           PXL=PXL+DPKEST+
00026        1   XSTEP*(2*FS*SMFX2/SDNSTY/SFRCTN/DT+2*FG*FMFX2/FDNSTY/DT)
00027           WRITE(IPLO,FDATA) PXL,H
00028           WRITE(IW,9000) PXL,H
00029    100 CONTINUE
00030          RETURN
00031    9000 FORMAT(1P7E11.4)
00032          END
```

SCALARS AND ARRAYS ["*" NO EXPLICIT DEFINITION - "%" NOT REFERENCED]

*SFRCTN 1		%VOID		%FVSCTY		*IW 2		*SMFX2 3	
*H 4		*XLE 5		*DT 6		%HO		*DPKEST 7	
*DPKE 10		*FDNSTY 11		*XSTEP 12		*XLNGTH 13		%IRO	
*IPLO 14		FDATA 15		*SMFX 16		*FMFX2 17		*XLED 23	
*PO 21		*X 22		%IR1				*PXL 24	
*FS 25		*I 26		%KTPFS		*XLEDLE 27		*NC 30	
*FG 31		*SDNSTY 32		*FMFX 33					

TEMPORARIES

.A0016 34

PDHPC   [No errors detected]

```
00001          SUBROUTINE PDBEND(BNDAGL,DT,FMFX,FDNSTY,FDATA,HO,H,KH1HO,
00002         1IRO,IR1,IPLO,IW,NC,PO,PXL,RBND,SDNSTY,SMFX,SFRCTN,VOID)
00003          DIMENSION FDATA(3)
00004       C
00005       C  SUBROUTINE PDBEND PRESSURE DROP IN BENDS FOR GAS-SOLID FLOW
00006       C
00007       C     RBND=XLNGTH
00008          BNDL90=BNDAGL-90.
00009          ANGSTP=BNDAGL/NC
00010          RBDT=RBND/DT
00011          XLBND=(3.1415/2+(3.1415/180.)*BNDAGL)*RBND
00012          PXL=PO
00013          H=HO
00014       C
00015          XSTEP=XLBND/NC
00016          IF (RBDT.GT.2) GO TO 100
00017       C  BEND FRICTION FACTOR FITTED EQUAL 1.
00018          FB=1.
00019       C     FB=0.375
00020          GO TO 200
00021   100  CONTINUE
00022          IF (RBDT.GT.6) GO TO 150
00023          FB=1.
00024       C     FB=0.188
00025          GO TO 200
00026   150  CONTINUE
00027          FB=1.
00028       C     FB=0.125
00029   200  CONTINUE
00030          DO 300 I=1,NC
00031          X=XSTEP*FLOAT(I)
00032          ANG=ANGSTP*FLOAT(I)
00033          PXL=PXL+(2.*FB*(SDNSTY*SFRCTN+FDNSTY*VOID)*(FMFX/FDNSTY)**2)
00034         1 *XSTEP/XLBND
00035          IF (BNDAGL.GT.90.) GO TO 250
00036          IF (KH1HO.EQ.2) GO TO 350
00037          H=HO+RBND*SIND(ANG)
00038          GO TO 375
00039   350  CONTINUE
00040          H=HO-RBND*SIND(ANG)
00041   375  CONTINUE
00042          GO TO 275
00043   250  CONTINUE
00044          H=HO+(SIND(BNDAGL-ANG)-SIND(BNDAGL))*RBND
00045   275  CONTINUE
00046          WRITE(IPLO,FDATA) PXL,H
00047          WRITE(IW,9000) PXL,H
00048   300  CONTINUE
00049          RETURN
00050  9000  FORMAT(1P7E11.4)
00051          END
```

SUBPROGRAMS CALLED

SIND.

SCALARS AND ARRAYS ["*" NO EXPLICIT DEFINITION - "%" NOT REFERENCED]

*SFRCTN	1	*VOID	2	*RBND	3	*IW	4	*H	5
*BNDAGL	6	*ANGSTP	7	*ANG	10	*DT	11	*HO	12
*FDNSTY	13	*XSTEP	14	%IRO		*IPLO	15	FDATA	16
%SMFX		*XLBND	17	.S0000	20	*PO	21	*KH1HO	22
*X	23	%IR1		*PXL	24	*I	25	*FB	26
*RBDT	27	*BNDL90	30	*NC	31	*SDNSTY	32	*FMFX	33

TEMPORARIES

  .A0016 34   .Q0000 35

PDBEND   [No errors detected]

```
00001          SUBROUTINE PDAGUP (ANGLE,DT,FDNSTY,FMFX,FVSCTY,FDATA,GG,
00002         1H,HO,KH1HO,IRO,IR1,IPLO,IW,NC,PO,PXL,
00003         2SMFX,SDNSTY,SFRCTN,XLNGTH,VOID)
00004          DIMENSION FDATA (3)
00005   C
00006   C      SUBROUTINE PDAGUP PRESSURE DROP AERATED GAS FLOW UP
00007   C
00008          XMUBAR=2.5E-05*EXP (30.70*SFRCTN)
00009          PXL=PO
00010          H=HO
00011   C
00012          XSTEP=XLNGTH/NC
00013          SNAGL=SIND (ANGLE)
00014          DO 100 I=1,NC
00015             X=XSTEP*FLOAT (I)
00016             PXL=PXL+XSTEP* (SDNSTY*GG*SFRCTN*SNAGL
00017        1        +32.*XMUBAR*SMFX/SDNSTY/SFRCTN/DT**2)
00018             IF (KH1HO.EQ.2) GO TO 50
00019             H=H+SNAGL*XSTEP
00020             GO TO 75
00021   50       CONTINUE
00022             H=H-SNAGL*XSTEP
00023   75       CONTINUE
00024             WRITE(IPLO,FDATA) PXL,H
00025             WRITE(IW,9000) PXL,H
00026   100  CONTINUE
00027          RETURN
00028   9000 FORMAT (1P7E11.4)
00029          END


SUBPROGRAMS CALLED

EXP.    SIND.

SCALARS AND ARRAYS [ "*" NO EXPLICIT DEFINITION - "%" NOT REFERENCED ]

*SFRCTN 1      %VOID          %FVSCTY        *IW     2      *SNAGL  3
*H      4      *DT     5      *HO     6      %FDNSTY        *XSTEP  7
*XLNGTH 10     %IRO           *IPLO   11     FDATA   12     *SMFX   13
*ANGLE  14     .S0000 15      *PO     16     %GG     17     *KH1HO  20
*XMUBAR 21     *X      22     %IR1           *PXL    23     *I      24
%NC     25     *SDNSTY 26     %FMFX

TEMPORARIES

 .A0016 27      .Q0000 30

PDAGUP  [ No errors detected ]
```

```
00001          SUBROUTINE PDAGD (ANGLE,DT,FDNSTY,FMFX,FVSCTY,FDATA,GG,
00002         1H,HO,KH1HO,IRO,IR1,IPLO,IW,NC,PO,PXL,
00003         2SDNSTY,SMFX,SFRCTN,XLNGTH,VOID)
00004          DIMENSION FDATA(3)
00005    C
00006    C     SUBROUTINE PDAGD PRESSURE DROP AERATED GAS FLOW DOWN
00007    C
00008          XMUBAR=2.5E-05*EXP (30.70*SFRCTN)
00009          PXL=PO
00010          H=HO
00011    C
00012          XSTEP=XLNGTH/NC
00013          SNAGL=SIND (ANGLE)
00014          DO 100 I=1,NC
00015             X=XSTEP*FLOAT(I)
00016             PXL=PXL+XSTEP* (SDNSTY*GG*SFRCTN*SNAGL
00017         1       -32.*XMUBAR*SMFX*SDNSTY/SFRCTN/DT**2)
00018             IF (KH1HO.EQ.2) GO TO 50
00019             H=H+SNAGL*XSTEP
00020             GO TO 75
00021    50       CONTINUE
00022             H=H-SNAGL*XSTEP
00023    75       CONTINUE
00024             WRITE (IPLO,FDATA) PXL,H
00025             WRITE (IW,9000) PXL,H
00026    100  CONTINUE
00027          RETURN
00028    9000 FORMAT (1P7E11.4)
00029          END


SUBPROGRAMS CALLED

EXP.    SIND.

SCALARS AND ARRAYS [ "*" NO EXPLICIT DEFINITION - "%" NOT REFERENCED ]

*SFRCTN 1      %VOID          %FVSCTY        *IW     2      *SNAGL   3
*H      4      *DT     5      *HO     6      %FDNSTY        *XSTEP   7
*XLNGTH 10     *IRO           *IPLO   11     FDATA   12     *SMFX   13
*ANGLE  14     .SO000 15      *PO     16     *GG     17     *KH1HO  20
*XMUBAR 21     *X      22     %IR1           *PXL    23     *I      24
*NC     25     *SDNSTY 26     %FMFX

TEMPORARIES

 .A0016 27     .Q0000 30

PDAGD    [ No errors detected ]
```

```
00001          SUBROUTINE PDSTNP (DT,DP,FDNSTY,FMFXSP,FVSCTY,FDATA,GG,
00002         1H,HO,IRO,IR1,IPLO,IW,NC,PO,PXL,SPRCTY,
00003         2SDNSTY,SMFX,XLNGTH,VOIDPB)
00004          DIMENSION FDATA(3)
00005   C
00006   C      SUBROUTINE PDSTNP PRESSURE DROP IN STANDPIPES
00007   C
00008          PXL=PO
00009          H=HO
00010   C
00011          XSTEP=XLNGTH/NC
00012          SPRC2=SPRCTY**2
00013          DP2=DP**2
00014          USLIP=SMFX/SDNSTY/(1.-VOIDPB)-FMFXSP/FDNSTY/VOIDPB
00015          ABUS=ABS(USLIP)
00016          DEPPRS=SDNSTY*(1.-VOIDPB)*GG*XLNGTH
00017          VOID3=VOIDPB**3
00018          VOID1=1.-VOIDPB
00019          VOID12=VOID1**2
00020          DO 100 I=1,NC
00021             X=XSTEP*FLOAT(I)
00022             PXL=PXL+XSTEP*(150.*VOID12*FVSCTY*ABUS/VOID3/SPRC2/DP2
00023         1      +1.75*VOID1*FDNSTY*ABUS**2/VOID3/SPRCTY/DP)
00024             H=H-XSTEP
00025             WRITE (IPLO,FDATA) PXL,H
00026             WRITE (IW,9000) PXL,H
00027   100   CONTINUE
00028          IF ((PXL-PO).LT.DEPPRS) GO TO 500
00029          WRITE (IW,9100)
00030   500   CONTINUE
00031          RETURN
00032   9000  FORMAT (1P7E11.4)
00033   9100  FORMAT (' ERROR, FMFX TOO LARGE, DPSP>PDF ')
00034          END
```

SCALARS AND ARRAYS ["*" NO EXPLICIT DEFINITION - "%" NOT REFERENCED]

*VOID12	1	*FVSCTY	2	*DP	3	*DP2	4	*IW	5
*SPRC2	6	*H	7	*DEPPRS	10	*VOIDPB	11	%DT	
*HO	12	*SPRCTY	13	*FDNSTY	14	*VOID3	15	*XSTEP	16
*XLNGTH	17	%IRO		*IPLO	20	FDATA	21	*SMFX	22
*ABUS	23	.S0000	24	*USLIP	25	*PO	26	*GG	27
*X	30	%IR1		*PXL	31	*VOID1	32	*I	33
*FMFXSP	34	*NC	35	*SDNSTY	36				

TEMPORARIES

.A0016 37

PDSTNP [No errors detected]

```
00001          SUBROUTINE PDORFC(CD,DO,DT,DP,FDNSTY,FMFXSP,FVSCTY,FDATA,GG,
00002         1H,HO,IRO,IR1,IPLO,IW,NC,PO,PXL,SPRCTY,
00003         2SDNSTY,SMFX,XLNGTH,VOIDPB)
00004          DIMENSION FDATA(3)
00005     C
00006     C     SUBROUTINE PDORFC PRESSURE DROP IN ORIFACE
00007     C
00008          PXL=PO
00009          H=HO
00010     C
00011          CD=.7
00012          SFRCTN=1.-VOIDPB
00013          CD2=CD*CD
00014          DODT4=(DO/DT)**4
00015          DO2=DO*DO
00016          SMFX2=SMFX*SMFX
00017          PXL=PO+SMFX2/SDNSTY/SFRCTN/CD2
00018          WRITE(IPLO,FDATA) PXL,H
00019          WRITE(IW,9000) PXL,H
00020          RETURN
00021     9000 FORMAT(1P7E11.4)
00022          END
```

SCALARS AND ARRAYS ["*" NO EXPLICIT DEFINITION - "%" NOT REFERENCED]

*SFRCTN	1	%FVSCTY		%DP		*IW	2	*SMFX2	3
*H	4	*DO	5	*DO2	6	*VOIDPB	7	*DT	10
*HO	11	%SPRCTY		%FDNSTY		%XLNGTH		%IRO	
*IPLO	12	FDATA	13	*CD	14	*CD2	15	*SMFX	16
*DODT4	17	*PO	20	%GG		%IR1		*PXL	21
%FMFXSP		%NC		*SDNSTY	22				

TEMPORARIES

.A0016 23

PDORFC [No errors detected]

```
00001          FUNCTION DPINRS (FMFXSP)
00002          DIMENSION IDNT (15) ,DT (15) ,KTPTL (15) ,ANGLE (15) ,XLNGTH (15) ,VOID (15)
00003          DIMENSION SFRCTN (15) ,FDATA (3)
00004          COMMON DT,DP,FDNSTY,ANGLE,FVSCTY,FDATA,GG,PINRSR,
00005         1HEXIT,IRO,IR1,IPLO,IW,PEXIT,SPRCTY,
00006         2SDNSTY,SMFX,XLNGTH,VOIDPB,SFRCTN,VOID
00007          FMFX=FMFXSP
00008          NC=1
00009          IF (FMFXSP.LT.0.) GO TO 1000
00010          HO=HEXIT
00011          KH1HO=2
00012          PO=PEXIT
00013          CALL PDAGD (90.0,DT (6) ,FDNSTY,FMFX,FVSCTY,FDATA,GG,
00014         1H,HO,KH1HO,IRO,IR1,IPLO,IW,NC,PO,PXL,
00015         2SDNSTY,SMFX,SFRCTN (6) ,XLNGTH (6) ,VOID (6) )
00016          PO=PXL
00017          HO=H
00018          CALL PDSTNP (DT (7) ,DP,FDNSTY,FMFXSP,FVSCTY,FDATA,GG,
00019         1H,HO,IRO,IR1,IPLO,IW,NC,PO,PXL,SPRCTY,
00020         2SDNSTY,SMFX,XLNGTH (7) ,VOIDPB)
00021          II=8
00022          PO=PXL
00023          HO=H
00024          CD=2.
00025          DO=.0254
00026          CALL PDORFC (CD,DO,DT (II) ,DP,FDNSTY,FMFXSP,FVSCTY,FDATA,GG,
00027         1H,HO,IRO,IR1,IPLO,IW,NC,PO,PXL,SPRCTY,
00028         2SDNSTY,SMFX,XLNGTH (II) ,VOIDPB)
00029          KH1HO=2
00030          HO=H
00031          PO=PXL
00032          CALL PDAGD (90.0,DT (9) ,FDNSTY,FMFX,FVSCTY,FDATA,GG,
00033         1H,HO,KH1HO,IRO,IR1,IPLO,IW,NC,PO,PXL,
00034         2SDNSTY,SMFX,SFRCTN (9) ,XLNGTH (9) ,VOID (9) )
00035          DPINRS=PINRSR-PXL
00036          TYPE *,DPINRS
00037          GO TO 2000
00038     1000 CONTINUE
00039          HO=HEXIT
00040          KH1HO=2
00041          PO=PEXIT
00042          CALL PDAGUP (90.0,DT (6) ,FDNSTY,FMFX,FVSCTY,FDATA,GG,
00043         1H,HO,KH1HO,IRO,IR1,IPLO,IW,NC,PO,PXL,
00044         2SMFX,SDNSTY,SFRCTN (6) ,XLNGTH (6) ,VOID (6) )
00045          HO=H
00046          PO=PXL
00047          CALL PDSTNP (DT (7) ,DP,FDNSTY,FMFXSP,FVSCTY,FDATA,GG,
00048         1H,HO,IRO,IR1,IPLO,IW,NC,PO,PXL,SPRCTY,
00049         2SDNSTY,SMFX,XLNGTH (7) ,VOIDPB)
00050          II=8
00051          PO=PXL
00052          HO=H
00053          CD=2.
00054          DO=.0254
00055          CALL PDORFC (CD,DO,DT (II) ,DP,FDNSTY,FMFXSP,FVSCTY,FDATA,GG,
00056         1H,HO,IRO,IR1,IPLO,IW,NC,PO,PXL,SPRCTY,
```

```
00057           2SDNSTY,SMFX,XLNGTH(II),VOIDPB)
00058            HO=H
00059            KH1HO=2
00060            PO=PXL
00061            CALL PDAGUP(90.0,DT(9),FDNSTY,FMFX,FVSCTY,FDATA,GG,
00062           1H,HO,KH1HO,IRO,IR1,IPLO,IW,NC,PO,PXL,
00063           2SMFX,SDNSTY,SFRCTN(9),XLNGTH(9),VOID(9))
00064            DPINRS=PINRSR-PXL
00065             TYPE *,DPINRS
00066      2000 CONTINUE
00067            RETURN
00068            END

COMMON BLOCKS

/.COMM./(+135)
DT       +0     DP       +17    FDNSTY  +20    ANGLE   +21    FVSCTY  +40
FDATA    +41    GG       +44    PINRSR  +45    HEXIT   +46    IRO     +47
IR1      +50    IPLO     +51    IW      +52    PEXIT   +53    SPRCTY  +54
SDNSTY   +55    SMFX     +56    XLNGTH  +57    VOIDPB  +76    SFRCTN  +77
VOID     +116


SUBPROGRAMS CALLED

PDSTNP  PDAGD   PDORFC  PDAGUP

SCALARS AND ARRAYS [ "*" NO EXPLICIT DEFINITION - "%" NOT REFERENCED ]

%KTPTL         *H      1     *DO     2     *HO      3    %IDNT
*CD     4      *II     5     *PO     6     *DPINRS 7     *KH1HO  10
*PXL    11     *FMFXSP 12    *NC     13    *FMFX   14

TEMPORARIES

.AOO16 15      .AOO15 16     .AOO14 17    .AOO13 20    .AOO12 21
.AOO10 23      .AOO7  24     .AOO6  25    .AOO5  26    .AOO4  27
.AOO2  31      .QOOOO 32     .QOOO1 33

DPINRS  [ No errors detected ]
```

```
00001          SUBROUTINE RISER(ANGLE,DT,FDNSTY,FMFXR,FVSCTY,FDATA,GG,
00002         1KH1HO,KHVFBC,H,HO,IRO,IR1,IPLO,IW,NC,PINRSR,PO,PXL,
00003         2PEXIT,HEXIT,SDNSTY,SMFX,SFRCTN,KTPFS,XLNGTH,VOID)
00004   C
00005   C
00006   C          SUBROUTINE RISER TO CALCULATE THE P[_RESSURE PROFILE
00007   C          IN THE RISER SIDE OF THE HIGH VELOCITY FLUIDIZED BED
00008   C
00009   C       DIMENSION ALL VARIABLES FOR SUBROUTINES CALLED
00010   C
00011   C       DIMENSION MAIN INPUT
00012          DIMENSION IDNT(15),DT(15),KTPTL(15),ANGLE(15),XLNGTH(15),VOID(15)
00013          DIMENSION SFRCTN(15),SP(75),XHIGHT(75)
00014   C
00015   C       DIMENSION VARIABLES FOR STRPL.FOR ***PLOTTING***
00016          DIMENSION LG(2),LGWR(4),NDEC(2),FDATA(3),XLBL(5),YLBL(2),
00017         1   DST(2),CRVLB(3)
00018   C
00019          FMFX=FMFXR
00020   C
00021          PO=PEXIT
00022          HO=HEXIT
00023          KH1HO=1
00024          II=1
00025          CALL PDAGD(ANGLE(II),DT(II),FDNSTY,FMFX,FVSCTY,FDATA,GG,
00026         1H,HO,KH1HO,IRO,IR1,IPLO,IW,NC,PO,PXL,
00027         2SDNSTY,SMFX,SFRCTN(II),XLNGTH(II),VOID(II))
00028          KTPFS=1
00029          II=2
00030          RBND=XLNGTH(II)
00031          HO=H
00032          FMFX=FMFXR
00033          KH1HO=1
00034          PO=PXL
00035          CALL PDBEND(ANGLE(II),DT(II),FMFX,FDNSTY,FDATA,HO,H,KH1HO,
00036         1IRO,IR1,IPLO,IW,NC,PO,PXL,RBND,SDNSTY,SMFX,SFRCTN(II),VOID(II))
00037          KHVFBC=1
00038          KH1HO=2
00039          II=3
00040          KTPFS=1
00041          HO=H
00042          PO=PXL
00043          CALL PDVPC(ANGLE(II),DT(II),FDNSTY,FMFX,FVSCTY,FDATA,GG,
00044         1KH1HO,KHVFBC,H,HO,IRO,IR1,IPLO,IW,NC,PO,PXL,
00045         2SDNSTY,SMFX,SFRCTN(II),KTPFS,XLNGTH(II),VOID(II))
00046          II=4
00047          KH1HO=2
00048          HO=H
00049          PO=PXL
00050          CALL PDBEND(ANGLE(II),DT(II),FMFX,FDNSTY,FDATA,HO,H,KH1HO,
00051         1IRO,IR1,IPLO,IW,NC,PO,PXL,RBND,SDNSTY,SMFX,SFRCTN(II),VOID(II))
00052          KTPFS=1
00053          II=5
00054          HO=H
00055          PO=PXL
00056          CALL PDHPC(DT(II),FMFX,FDNSTY,FDATA,FVSCTY,IRO,IR1,IPLO,IW
```

```
00057        1,HO,H,KTPFS,NC,PO,PXL,SMFX,SDNSTY,SFRCTN(11),XLNGTH(11),VOID(11))
00058    C
00059        DPRSR=PXL-PEXIT
00060        PINRSR=PXL
00061    C
00062        RETURN
00063        END
```

SUBPROGRAMS CALLED

PDVPC   PDHPC   PDAGD   PDBEND

SCALARS AND ARRAYS ["*" NO EXPLICIT DEFINITION - "%" NOT REFERENCED]

%DST	SFRCTN 1	VOID 2	*FVSCTY 3	%KTPTL
*RBND 4	*IW 5	*HEXIT 6	%XHIGHT	*H 7
*KHVFBC 10	DT 11	*PINRSR 12	*HO 13	%YLBL
%IDNT	*PEXIT 14	*FDNSTY 15	XLNGTH 16	*IRO 17
*IPLO 20	*FMFXR 21	FDATA 22	*SMFX 23	*II 24
ANGLE 25	*PO 26	*GG 27	%LGWR	*KH1HO 30
%XLBL	*IR1 31	*DPRSR 32	%NDEC	*PXL 33
*KTPFS 34	%LG	%SP	%CRVLB	*NC 35
*SDNSTY 36	*FMFX 37			

TEMPORARIES

.A0016 40   .Q0000 41   .Q0001 42   .Q0002 43   .Q0003 44

RISER   [No errors detected]

```
00001    C
00002    C
00003          SUBROUTINE STNDPP (DT,DP,FDNSTY,FMFXSP,FVSCTY,FDATA,GG,
00004         1H,HO,IRO,IR1,IPLO,IW,NC,PO,PXL,SPRCTY,
00005         2PEXIT,HEXIT,SFRCTN,SDNSTY,SMFX,XLNGTH,VOIV,VOIDPB)
00006    C
00007    CC
00008    C         SUBROUTINE STNDPP TO CALCULATE THE PRESSURE PROFILE IN
00009    C         THE STANDPIPE SIDE OF THE HIGH VELOCITY FLUIDIZED BED SYSTEM
00010    C
00011    C
00012    C         DIMENSION ALL VARIABLES NEEDED FOR ALL SUBROUTINES CALLED
00013    C         DIMENSION MAIN INPUT
00014          DIMENSION IDNT (15),DT (15),KTPTL (15),ANGLE (15),XLNGTH (15),VOID (15)
00015          DIMENSION SFRCTN (15),SP (75),XHIGHT (75)
00016    C
00017    C         DIMENSION VARIABLES FOR STRPL.FOR ***PLOTTING***
00018          DIMENSION LG (2),LGWR (4),NDEC (2),FDATA (3),XLBL (5),YLBL (2),
00019         1   DST (2),CRVLB (3)
00020    C
00021          FMFX=FMFXSP
00022    C
00023    C
00024    C
00025          IF (FMFXSP.LT.O.) GO TO 1000
00026          II=6
00027          HO=HEXIT
00028
00029          KH1HO=2
00030          PO=PEXIT
00031          CALL PDAGD (90.0,DT (II),FDNSTY,FMFX,FVSCTY,FDATA,GG,
00032         1H,HO,KH1HO,IRO,IR1,IPLO,IW,NC,PO,PXL,
00033         2SDNSTY,SMFX,SFRCTN (II),XLNGTH (II),VOID (II))
00034          II=7
00035          PO=PXL
00036          HO=H
00037          CALL PDSTNP (DT (II),DP,FDNSTY,FMFXSP,FVSCTY,FDATA,GG,
00038         1H,HO,IRO,IR1,IPLO,IW,NC,PO,SPRCTY,
00039         2SDNSTY,SMFX,XLNGTH (II),VOIDPB)
00040          II=8
00041          PO=PXL
00042          HO=H
00043          CD=2.
00044          DO=.0254
00045          CALL PDORFC (CD,DO,DT (II),DP,FDNSTY,FMFXSP,FVSCTY,FDATA,GG,
00046         1H,HO,IRO,IR1,IPLO,IW,NC,PO,PXL,SPRCTY,
00047         2SDNSTY,SMFX,XLNGTH (II),VOIDPB) ·
00048          II=9
00049          KH1HO=2
00050          HO=H
00051          PO=PXL
00052          CALL PDAGD (90.0,DT (II),FDNSTY,FMFX,FVSCTY,FDATA,GG,
00053         1H,HO,KH1HO,IRO,IR1,IPLO,IW,NC,PO,PXL,
00054         2SDNSTY,SMFX,SFRCTN (II),XLNGTH (II),VOID (II))
00055          DPINRS=PINRSR-PXL
00056          GO TO 2000
```

```
00057    1000 CONTINUE
00058    C
00059          II=6
00060          HO=HEXIT
00061          KH1HO=2
00062          PO=PEXIT
00063          CALL PDAGUP(90.0,DT(II),FDNSTY,FMFXSP,FVSCTY,FDATA,GG,
00064         1H,HO,KH1HO,IRO,IR1,IPLO,IW,NC,PO,PXL,
00065         2SMFX,SDNSTY,SFRCTN(II),XLNGTH(II),VOID(II))
00066          II=7
00067          HO=H
00068          PO=PXL
00069          CALL PDSTNP(DT(II),DP,FDNSTY,FMFXSP,FVSCTY,FDATA,GG,
00070         1H,HO,IRO,IR1,IPLO,IW,NC,PO,PXL,SPRCTY,
00071         2SDNSTY,SMFX,XLNGTH(II),VOIDPB)
00072          PO=PXL
00073          HO=H
00074          CD=2.
00075          II=8
00076          DO=.0254
00077          CALL PDORFC(CD,DO,DT(II),DP,FDNSTY,FMFXSP,FVSCTY,FDATA,GG,
00078         1H,HO,IRO,IR1,IPLO,IW,NC,PO,PXL,SPRCTY,
00079         2SDNSTY,SMFX,XLNGTH(II),VOIDPB)
00080          II=9
00081          HO=H
00082          KH1HO=2
00083          PO=PXL
00084          CALL PDAGUP(90.0,DT(II),FDNSTY,FMFXSP,FVSCTY,FDATA,GG,
00085         1H,HO,KH1HO,IRO,IR1,IPLO,IW,NC,PO,PXL,
00086         2SMFX,SDNSTY,SFRCTN(II),XLNGTH(II),VOID(II))
00087          DPINRS=PINRSR-PXL
00088    2000 CONTINUE
00089          RETURN
00090          END
```

SUBPROGRAMS CALLED

PDSTNP   PDAGD   PDORFC   PDAGUP

SCALARS AND ARRAYS ["*" NO EXPLICIT DEFINITION - "%" NOT REFERENCED]

%DST		SFRCTN	1	VOID	2	*FVSCTY	21	*DP	22
%KTPTL		*IW	23	*HEXIT	24	%XHIGHT		*H	25
*DO	26	%VOIV		*VOIDPB	27	DT	30	*PINRSR	31
*HO	32	%YLBL		%IDNT		*SPRCTY	33	*PEXIT	34
*FDNSTY	35	XLNGTH	36	*IRO	37	*IPLO	40	*CD	41
FDATA	42	*SMFX	43	*II	44	%ANGLE		*PO	45
*GG	46	*DPINRS	47	%LGWR		*KH1HO	50	%XLBL	
*IR1	51	%NDEC		*PXL	52	*FMFXSP	53	%LG	
%SP		%CRVLB		*NC	54	*SDNSTY	55	*FMFX	56

TEMPORARIES

.A0016	57	.Q0000	60	.Q0001	61	.Q0002	62	.Q0003	63

STNDPP   [No errors detected]

APPENDIX B2

HIGH VELOCITY FLUIDIZED BED
COAL COMBUSTION MODEL

```
00001  C    PROGRAM TO FOLLOW THE COMBUSTION OF A COAL PARTICLE
00002  C      AS IT FLOWS THROUGH THE HIGH VELOCITY FLUIDIZED BED COMBUSTOR
00003  C
00004  C
00005  C    VARIABLE DEFINITION - UNITS
00006  C      A      => AREA OF CARBON PARTICLE
00007  C      A1     => FREQUENCY FACTOR FOR DEVOLATILIZATION
00008  C      A2     => FREQUENCY FACTOR FOR DEVOLATILIZATION
00009  C      AFC    => FREQUENCY FACTOR FOR CARBON RXN RATE
00010  C      AFS    => FREQUENCY FACTOR FOR SULFUR RXN RATE -
00011  C      AFH    => FREQUENCY FACTOR FOR HYDROGEN RXN RATE -
00012  C      CNO2   => CONC. OF O2 IN GAS - KGMOL/M3
00013  C      CDNSTY => COAL DENSITY - KG/M3
00014  C      DP1    => DIAMETER OF PARTICLE AT EACH TIME STEP - M
00015  C      DPC    => DIAMETER OF PARTICLE FOR CALCULATION - M
00016  C      DPSTN  => DIAMETER OF SORBENT - M
00017  C      DIFFO2 => DIFFUSION COEF. FOR O2 - M2/S
00018  C      DT     => DIAMETER OF COMBUSTOR - M
00019  C      DT2    => DT*DT - M2
00020  C      DPC3   => DPC*DPC*DPC - M3
00021  C      DPSTN3 => DPSTN*DPSTN*DPSTN - M3
00022  C      E1     => ACTIVATION ENERGY FOR DEVOLATILIZATION - KCAL/KGMOL
00023  C      E2     => ACTIVATION ENERGY FOR DEVOLATILIZATION - KCAL/KGMOL
00024  C      EPS    => VOID FRACTION IN COMBUSTOR
00025  C      EPS1   => SOLIDS FRACTION IN COMBUSTOR
00026  C      EPSC   => 1. - COAL FRACTION
00027  C      EPSC1  => COAL FRACTION
00028  C      EPSTN  => 1. - SORBENT FRACTION
00029  C      EPSTN1 => SORBENT FRACTION
00030  C      EAC    => ACTIVATION ENERGY FOR CARBON RXN - KCAL/KGMOL
00031  C      EAS    => ACTIVATION ENERGY FOR SULSUR RXN - KCAL/KGMOL
00032  C      EAH    => ACTIVATION ENERGY FOR HYDROGEN RXN - KCAL/KGMOL
00033  C      F( )   => VALUE OF DERIVATIVE AT EACH TIME STEP
00034  C                  1 => CARBON
00035  C                  2 => SULFUR
00036  C                  3 => HYDROGEN
00037  C      FMFX   => GAS MASS FLUX
00038  C      FDNSTY => FLUID DENSITY (GAS) - KG/M3
00039  C      FLOARA => FLOW AREA - M2
00040  C      GG     => ACCELERATION OF GRAVITY - 9.807 M/S2
00041  C      IR     => INPUT UNIT NUMBER  KINETIC DATA
00042  C      IPLO   => OUTPUT UNIT NUMBER PLOT MASS FRACTION
00043  C      IW     => OUTPUT UNIT NUMBER (WRITE)
00044  C      IPLOT  => OUTPUT UNIT NUMBER PLOT COAL CONVERSION
00045  C      IPLT   => OUTPUT UNIT NUMBER PLOT CONVERSION OF SO2 CASO4
00046  C      IPPM   => IN*RPUT UNIT NUMBER FLOW DATA
00047  C      H      => DYSIM CALCULATION STEP SIZE
00048  C      HPLOT  => DYSIM PRINT INTERVAL
00049  C      HPRNT  => DYSIM PLOT INTERVAL
00050  C      METH   => DYSIM CALCULATION METHOD
00051  C      N      => DYSIM NUMBER OF EQUATIONS
00052  C      NTASK  => DYSIM DIRECTOR
00053  C      PHIC   => STOIC COEFF. CARBON
00054  C      PHIS   => STOIC. COEFF. SULFUR
00055  C      PHIH   => STOIC. COEFF. HYDROGEN
00056  C      PI     => 3.141592
```

```
00057   C       RGV    => GAS CONSTANT VOLUME - M3ATM/KGMOLK
00058   C       RGE    => GAS CONSTANT ENERGY - KCAL/KGMOLK
00059   C       SMFX   => SOLID MASS FLUX KG/M2S
00060   C       SDNSTY => SOLID PARTICLE DENSITY - KG/M3
00061   C       STNMFX => SORBENT MASS FLUX - KG/M2S
00062   C       T      => TIME - S
00063   C       TG     => GAS TEMP. - K
00064   C       TS     => SOLIDS TEMP. - K
00065   C       TVOL   => DEVOLATILIZATION TIME - S
00066   C       TSF    => SULFURIZATION TIME - S
00067   C       TSFVOL => TSF/(0.001**3*PI/6.)  - S/M3
00068   C       TF     => FINIAL CALCULATION TIME - S
00069   C       UG     => GAS VELOCITY - M/S
00070   C       US     => SOLIDS VELOCITY -M/S
00071   C       USLIP  => SLIP VELOCTIY - M/S
00072   C       VISC   => VISCOSITY - KG/MS
00073   C       WFVM   => MASS FRACTION VOLATLIE MATTER PROXIMATE ANALYSIS
00074   C       WFFC   => MASS FRACTION FIXED CARBON PROXIMATE ANALYSIS
00075   C       WFM    => MASS FRACTION MOISTURE PROXIMATE ANALYSIS
00076   C       WFA    => MASS FRACTION ASH PROXIMATE ANALYSIS
00077   C       WFC    => MAF MASS FRACTION CARBON
00078   C       WFH    => MAF MASS FRACTION HYDROGEN
00079   C       WFS    => MAF MASS FRACTION SULSUR
00080   C       WFO    => MAF MASS FRACTION OXYGEN
00081   C       WFN    => MAF MASS FRACTION NITROGEN
00082   C       X1     => ADJUSTED MASS FRACTION CARBON
00083   C       X2     => ADJUSTED MASS FRACTION SULFUR
00084   C       X3     => ADJUSTED MASS FRACTION HYDROGEN
00085   C       XV     => MASS FRACTION VOLATILES
00086   C       X0     => ADJUSTED MASS FRACTION OXYGEN
00087   C       XN     => ADJUSTED MASS FRACTION NITROGEN
00088   C       XH2O   => MASS FRACTION WATER
00089   C       XVOL   => TOTAL VOLATILE MASS FRACTION
00090   C       XASH   => MASS FRACTION ASH
00091   C       XVOLHT => TOTAL VOLATILE MASS FRACTION FOR HIGH TEMPERATURE
00092   C       XMASH  => MASS OF ASH IN PARTICLE - KG
00093   C       XMVOL  => MASS OF TOTAL VOLATILES IN PARTICLE - KG
00094   C       X( )   => MASS OF PARTICLE - KG
00095   C       XI( )  => INITIAL X( )
00096   C                      1 => CARBON
00097   C                      2 => SULFUR
00098   C                      3 => HYDROGEN
00099   C       XMTOT  => TOTAL MASS OF PARTICLE - KG
00100   C       XMTOTI => INITIAL TOTAL MASS OF PARTICLE - KG
00101   C       XK1    => DEVOLATILIZATION RATE CONSTANT
00102   C       XK2    => DEVOLATILIZATION RATE CONSTANT
00103   C       XKDC   => MASS TRANSFER COEFF. O2 - M/S
00104   C       XKRC   => RXN RATE CONSTANT CARBON -
00105   C       XKRS   => RXN RATE CONSTANT SULFUR -
00106   C       XKRH   => RXN RATE CONSTANT HYDROGEN -
00107   C       XL     => CALCULATION HEIGHT - M
00108   C       XLF    => FINAL HEIGHT OF COMBUSTOR - M
00109   C       XMWTC  => MOLECULAR WEIGHT CARBON - KG/KGMOL
00110   C       XMWTS  => MOLECULAR WEIGHT SULFUR - KG/KGMOL
00111   C       XMWTO  => MOLECULAR WEIGHT OXYGEN - KG/KGMOL
00112   C       XMWTH  => MOLECULAR WEIGHT HYDROGEN - KG/KGMOL
```

```
00113   C       XMWTW  => MOLECULAR WEIGHT WATER - KG/KGMOL
00114   C       XMWSO2 => MOLECULAR WEIGHT SO2 - KG/KGMOL
00115   C       XMWCAO => MOLECULAR WEIGHT CAO - KG/KGMOL
00116   C       XMSO2G => MASS GENERATED SO2 - KG
00117   C       XMSO2R => MASS SO2 REMOVED FROM GAS - KG
00118   C       XMSO2  => MASS SO2 IN GAS - KG
00119   C       XNCP   => NUMBER OF COAL PARTICLES IN CALC. VOLUME
00120   C       XNSTN  => NUMBER OF SORBENT PARTICLES IN CALC. VOLUME
00121   C       XSOX   => EQUIVALENT MASS OF SO2 IN COAL - KG
00122   C       XSOXI  => INITIAL XSOX - KG
00123   C       Y1     => DEVOLATILIZATION FRACTION
00124   C       Y2     => DEVOLATILIZATION FRACTION
00125   C
00126   C
00127   C
00128   C
00129   C    DIMENSION ALL VARIABLES
00130   C
00131   C        USED FOR DYSIM
00132            DIMENSION XI(3),Y(3),X(3),F(3)
00133   C
00134   C        USED FOR STRPL.FOR
00135            DIMENSION LG(2),LGWR(4),NDEC(2),FDATA(3),XLBL(3),YLBL(3)
00136        1      ,YLBL3(4),YLBL2(3),DST(2),CRVLB(4)
00137   C
00138   C    LIST ALL COMMON VARIABLES
00139   C
00140   C        USED IN DYSIM
00141            COMMON N,METH,H,HPRNT,HPLOT,TF
00142   C
00143   C      INITIALIZATION SECTION
00144            DATA FDATA/'( 1P9E11.4)'/,NFDATA/3/
00145            DATA XLBL/' LENGTH,  M'/
00146            DATA YLBL/' MASS FRAC. '/
00147            DATA CRVLB/'TOT','CRBN','SLFR',
00148        1   'HDGN'/
00149            DATA YLBL2/' CONVERSION   '/
00150            DATA YLBL3/'CONVERSION OF SO2'/
00151            IR=18
00152            IPL0=19
00153            IPLOT=20
00154            IPLT=21
00155            IW=5
00156            IPPM=22
00157            NTASK=0
00158            GG=9.807
00159            PI=3.141592
00160            RGE=1.987
00161            RGV=0.08205
00162            N=3
00163            METH=3
00164            H=0.1
00165            HPRNT=0.5
00166            HPLOT=0.5
00167            XMSO2G=0.
00168   C
```

```
00169   C      OPEN INPUT AND OUTPUT FILES
00170              CALL OPCL(IR,IW,1,'HVFBC.IN')
00171              CALL OPCL(IPLO,IW,1,'HVFBC.PT')
00172              CALL OPCL(IPLT,IW,1,'HVFBC.SR')
00173              CALL OPCL(IPLOT,IW,1,'HVFBC.PL')
00174              CALL OPCL(IPPM,IW,1,'PPMO.I')
00175   C
00176   C
00177   C      READ HYDRODYNAMIC PARAMETERS AND EQUIPMENT SIZE
00178   C          DATA PROVIDED FOR HVFPPM.FOR
00179          READ(IPPM,*) SMFX,SDNSTY,EPS,DPSTN,EPS1
00180          READ(IPPM,*) FMFX,FDNSTY,VISC
00181          READ(IPPM,*) XLF,DT
00182   C
00183   C      READ PROXIMATE AND MAF ULTIMATE ANALYSIS
00184   C      AND PHISICAL PROPERTIES OF COAL
00185          READ(IR,*) WFVM,WFFC,WFM,WFA
00186          READ(IR,*) WFC,WFS,WFH,WFN,WFO
00187          READ(IR,*) CDNSTY
00188   C      READ KINETIC INFO
00189   C
00190   C          DEVOLATILIZATION RATE
00191          READ(IR,*) Y1,Y2,A1,A2,E1,E2,TVOL
00192   C
00193   C          COMBUSTION RATE
00194          READ(IR,*) PHIC,PHIH,PHIS,AFC,AFH,AFS,EAC,EAH,EAS
00195          READ(IR,*) TS,TG,CNO2,DPC,DIFFO2
00196   C
00197   C          DESULFURIZATION
00198          READ(IR,*) PSTR,TSF,XISO2G
00199   C
00200   C          MOLECULAR WEIGHT
00201          READ(IR,*) XMWTC,XMWTH,XMWTS,XMWTO,XMWTW,XMWSO2,XMWCAO
00202   C
00203   C          FLOW RATE OF COAL AND STONE
00204          READ(IR,*) CR,STNR
00205   CC
00206   C
00207   C      PRELIMINARY CALCULATIONS
00208   C
00209          DT2=DT*DT
00210          FLOARA=PI*DT2/4.
00211          US=SMFX*FLOARA/SDNSTY/EPS1
00212          UG=FMFX*FLOARA/FDNSTY/EPS
00213          USLIP=UG-US
00214          TF=XLF/US
00215          EPSC1=(CR/FLOARA/SMFX)*EPS1
00216          EPSC=1.-EPSC1
00217          EPSTN1=EPS1-EPSC1*CDNSTY/SDNSTY
00218          EPSTN=1.-EPSTN1
00219          STNMFX=SMFX*EPSTN1/EPS1
00220          X1=WFFC*WFC
00221          X2=WFFC*WFS
00222          X3=WFFC*WFH
00223          XV=WFVM
00224          XO=WFFC*WFO
```

```
00225      XN=H/FC*WFN
00226      XMASH=WFA
00227      XH2O=WFM
00228      XVOL=XV+XO+XN+XH2O
00229      DPSTN3=DPSTN3**3
00230      DPC3=DPC**3
00231      XNCP=3.*DT2*US*H*EPSC1/2./DPC3
00232      XNSTN=3.*DT2*US*H*EPSTN1/2./DPSTN3
00233    C
00234    C
00235      XK1=A1*EXP (-E1/RGE/TS)
00236      XK2=A2*EXP (-E2/RGE/TS)
00237    C
00238      X (1) =X1*CDNSTY*PI*DPC*#3./6.
00239      X (2) =X2*CDNSTY*PI*DPC*#3./6.
00240      X (3) =X3*CDNSTY*PI*DPC*#3./6.
00241      XHVOL=XVOL*CDNSTY*PI*DPC*#3./6.
00242      XASH=XMASH*CDNSTY*PI*DPC*#3./6.
00243      XSOX=X (2) *2.*XNCP
00244      DO 5 I=1,3
00245      XI (I) =X (I)
00246    5 CONTINUE
00247    C
00248      XSS=XI (2)
00249      XHTOTI=XI (1) +XI (2) +XI (3) +XHVOL+XASH
00250      TSFVOL=6.*TSF/P1/(0.001)*#3)
00251      SO2RGC=XNSTN/XMWCAO/TSFVOL/UG/H/FLORA
00252    C
00253    C  INITIALIZE AND CALL STRPL.FOR SUBROUTINE
00254    C  SET VALUES FOR PLOTTING
00255      XMIN=0.0
00256      XMAX=XLF
00257      YMIN=0.0
00258      YMAX=1.00
00259      L10=0
00260      LG (1) =0
00261      LG (2) =0
00262      KSLG=-7
00263      CYCLX=-6.8
00264      CYCLY=-5.8
00265      NXLB=1
00266      NXLB=12
00267      NYLB2=13
00268      NYLB3=17
00269      ROTA=0.0
00270      LIN=1
00271      NW=4
00272      SZLT=0.12
00273      SZPL=0.09
00274      DST (1) =0.06
00275      DST (2) =0.06
00276      LTK=0
00277      LPNT=1
00278      INTCH=0
00279      LRPT=2
00280      LFM1=0
```

```
00281          LWSL=0
00282          LDATA=0
00283          LGWR(1)=0
00284          LGWR(2)=1
00285          LGWR(3)=0
00286          LGWR(4)=1
00287          LF811=2
00288          NDEC(1)=-2
00289          NDEC(2)=-2
00290          KCOL=2
00291          JCON=1
00292          NDPNT=-7
00293          JCRVLB=2
00294  C
00295          CALL STRPL(IPLO,IW,XMIN,XMAX,YMIN,YMAX,L10,LG,KSLG,CYCLX,
00296        1  CYCLY,NXLB,NYLB,ROTA,LIN,NW,SZLT,SZPL,DST,LTK,LPNT,
00297        2  INTCH,LRPT,LFM1,LWSL,LDATA,LGWR,LF811,LWS1,LWS2,NDEC,KCOL,
00298        3  JCON,FDATA,XLBL,YLBL,NFDATA,NDPNT,JCRVLB,CRVLB)
00299          JCRVLB=1
00300          CALL STRPL(IPLOT,IW,XMIN,XMAX,YMIN,YMAX,L10,LG,KSLG,CYCLX,
00301        1  CYCLY,NXLB,NYLB2,ROTA,LIN,NW,SZLT,SZPL,DST,LTK,LPNT,
00302        2  INTCH,LRPT,LFM1,LWSL,LDATA,LGWR,LF811,LWS1,LWS2,NDEC,KCOL,
00303        3  JCON,FDATA,XLBL,YLBL2,NFDATA,NDPNT,JCRVLB,CRVLB)
00304          JCRVLB=0
00305          CALL STRPL(IPLT,IW,XMIN,XMAX,YMIN,YMAX,L10,LG,KSLG,CYCLX,
00306        1  CYCLY,NXLB,NYLB3,ROTA,LIN,NW,SZLT,SZPL,DST,LTK,LPNT,
00307        2  INTCH,LRPT,LFM1,LWSL,LDATA,LGWR,LF811,LWS1,LWS2,NDEC,KCOL,
00308        3  JCON,FDATA,XLBL,YLBL3,NFDATA,NDPNT,JCRVLB,CRVLB)
00309  C
00310  C
00311  C       START CALLING DYSIM TO SIMULATE COAL COMBUSTION
00312  C
00313  C
00314          IF(TS.LT.1350.) GO TO 7
00315          XVOLHT=(Y1*XK1+Y2*XK2)*(1.-EXP(-TVOL*(XK1+XK2)))/(XK1+XK2)
00316          X1=X1+XV-XVOLHT
00317          XV=XVOLHT
00318          XVOL=XV+X0+XN+XH2O
00319          XMVOL=XVOL*CDNSTY*PI*DPC3/6.
00320          X(1)= X1*CDNSTY*PI*PDC3/6.
00321          XI(1)=X(1)
00322          XMTOTI=XI(1)+XI(2)+XI(3)+XMVOL+XASH
00323      7   CONTINUE
00324  C
00325     10   CONTINUE
00326          CALL DYSIM(T,X,F,NTASK,IW)
00327          GO TO (50,100,150,200,250) NTASK
00328     50   CONTINUE
00329  C              NTASK=1
00330  C              MONITOR CALCULATIONS AT EACH TIME STEP
00331     55   CONTINUE
00332  C
00333          GO TO 10
00334  C
00335    100   CONTINUE
00336  C              NTASK=2
```

```
00337    C                   EVALUATE ALL DERIVATIVES
00338                XL=US*T
00339                IF (T.GT.O.) XMVOL=0.0
00340                XMTOT=X (1) +X (2) +X (3) +XMVOL+XASH
00341                DP1= (XMTOT*6./PI/CDNSTY) ** (1./3.)
00342                DPC=DP1
00343                RE=USLIP*DPC*FDNSTY/VISC
00344                SC=VISC/FDNSTY/DIFFO2
00345                XKDO2= (DIFFO2/DPC) * (2.+O.6*RE**0.5*SC**0.33)
00346                XKRC=TG*RGV*AFC*EXP (-EAC/RGE/TS) /XMWTO
00347                XKRS=TG*RGV*AFS*EXP (-EAS/RGE/TS) /XMWTO
00348                XKRH=TG*RGV*AFH*EXP (-EAH/RGE/TS) /XMWTO
00349                A=PI*DPC**2.
00350    C
00351                F (1) =-A*PHIC*XMWTC*CNO2* (X (1) /XMTOT) / (1./XKDO2+1./XKRC)
00352                F (2) =-A*PHIS*XMWTS*CNO2* (X (2) /XMTOT) / (1./XKDO2+1./XKRS)
00353                F (3) =-A*PHIH*XMWTH*CNO2* (X (3) /XMTOT) / (1./XKDO2+1./XKRH)
00354    C
00355                GO TO 10
00356    C
00357    150         CONTINUE
00358    C                   NTASK=3
00359    C                   PRINT AT INCREMENTS OF HPRNT
00360    C                   CALL PRNTA OR PRNTB
00361                XL=US*T
00362                XMSO2R=XISO2G*EXP (SO2RRC*T)
00363                XSOX=2.*XNCP* (XSS-X (2) )
00364                XMSO2G=XMSO2G+XSOX
00365                IF (T.GT.O.) GO TO 175
00366                XMSO2=XMSO2G-XMSO2R
00367                GO TO 180
00368    175         CONTINUE
00369                XMSO2=XMSO2-XMSO2R+XSOX
00370    180         CONTINUE
00371                XSS=X (2)
00372                IF (XMSO2.LT.O.O) XMSO2=0.0
00373                CALL PRNTA (7,XL,X (1) ,X (2) ,X (3) ,XSOX,XMSO2R,XMSO2,XMSO2G,0.,5)
00374                IF (T.GT.O.) GO TO 190
00375                XSO2=0.0
00376                GO TO 195
00377    190         CONTINUE
00378                XSO2=1.-XMSO2/XMSO2G
00379    195         CONTINUE
00380                WRITE (IPLT,FDATA) XL,XSO2
00381    C
00382    C
00383                GO TO 10
00384    C
00385    200         CONTINUE
00386    C                   NTASK=4
00387    C                   USED FOR PLOTTING AT INTERVALS HPLOT
00388                XL=US*T
00389                DO 225 I=1,3
00390    225             Y (I) =X (I) /XMTOTI
00391                CONTINUE
00392                YMTOT=XMTOT/XMTOTI
00393                WRITE (IPLO,FDATA) XL,YMTOT,Y (1) ,Y (2) ,Y (3)
```

```
00393                DO 226 I=1,3
00394                   Y(I)=1.-X(I)/XI(I)
00395        226    CONTINUE
00396                YMTOT=1.-(X(1)+X(2)+X(3))/(XI(1)+XI(2)+XI(3))
00397                WRITE(IPLOT,FDATA) XL,YMTOT,Y(1),Y(2),Y(3)
00398    C
00399                GO TO 10
00400    C
00401        250    CONTINUE
00402    C               NTASK=5
00403    C                  SIMULATION FINISHED
00404                DUM=-999.
00405                WRITE(IPLO,FDATA) DUM,DUM,DUM,DUM,DUM,DUM,DUM,DUM,DUM
00406                WRITE(IPLOT,FDATA) DUM,DUM,DUM,DUM,DUM,DUM,DUM,DUM,DUM
00407                WRITE(IPLT,FDATA) DUM,DUM,DUM,DUM,DUM,DUM,DUM,DUM,DUM
00408                DUM=-1.
00409                WRITE(IPLO,FDATA) DUM,DUM,DUM,DUM,DUM,DUM,DUM,DUM,DUM
00410                WRITE(IPLOT,FDATA) DUM,DUM,DUM,DUM,DUM,DUM,DUM,DUM,DUM
00411                WRITE(IPLT,FDATA) DUM,DUM,DUM,DUM,DUM,DUM,DUM,DUM,DUM
00412                 CALL OPCL(IPLO,IW,2,'HVFBC.PT')
00413                 CALL OPCL(IR,IW,2,'HVFBC.IN')
00414                 CALL OPCL(IPLOT,IW,2,'HVFBC.PL')
00415                 CALL OPCL(IPLO,IW,2,'HVFBC.SR')
00416                 CALL OPCL(IPLT,IW,2,'HVFBC.PT')
00417                 CALL OPCL(IPPM,IW,2,'PPMO.I')
00418        9999   CONTINUE
00419                 STOP
00420    C                  FORMAT STATEMENTS
00421    C
00422                END
```

COMMON BLOCKS

/.COMM./(+6)
| N | +0 | METH | +1 | H | +2 | HPRNT | +3 | HPLOT | +4 |
| TF | +5 | | | | | | | | |

SUBPROGRAMS CALLED

PRNTA   OPCL   STRPL   EXP.   DYSIM

SCALARS AND ARRAYS ["*" NO EXPLICIT DEFINITION - "%" NOT REFERENCED]

*XASH	1	DST	2	*XMSO2R	4	*XNCP	5	*E2	6
*VISC	7	*XSO2	10	*LFM1	11	*CYCLY	12	*CR	13
*PHIS	14	*TS	15	*AFS	16	*TSFVOL	17	*FLOARA	20
*XMWCAO	21	*WFC	22	*T	23	*YMAX	24	*JCRVLB	25
*CNO2	26	*IW	27	*XK2	30	*EAC	31	*NYLB	32
*XNSTN	33	*WFN	34	*XV	35	*RGE	36	*XMIN	37
*TG	40	*Y2	41	*PI	42	*E1	43	*NTASK	44
*RE	45	*XMTOT	46	*XH2O	47	*SC	50	*LPNT	51
*CYCLX	52	*XMWTO	53	*NDPNT	54	*INTCH	55	*L10	56
*XSOX	57	*XKRS	60	*EPSTN	61	*XMVOL	62	*NXLB	63
*PSTR	64	*EPS1	65	*DT	66	*X3	67	*DT2	70

*KCOL	71	*LIN	72	*EPSC1	73	*Y1	74	YLBL	75
Y	100	*XMSO2	103	*NW	104	*XO	105	*A2	106
*JCON	107	*DIFFO2	110	*FDNSTY	111	*WFO	112	*LRPT	113
*XMAX	114	*STNR	115	*CDNSTY	116	*KSLG	117	*IPLO	120
XI	121	*LDATA	124	*SO2RRC	125	*PHIC	126	*WFH	127
*XSOXI	130	*XMWTS	131	*EPSTN1	132	*SZLT	133	*XH2O	134
*EAH	135	*XLF	136	*NYLB3	137	*XMWTC	140	*WFA	141
FDATA	142	*X2	145	*WFS	146	*WFVM	147	*SMFX	150
*LWS2	151	*XVOL	152	*XKDO2	153	*XN	154	*XMWTH	155
*EAS	156	*A1	157	*A	160	*LTK	161	*IPLOT	162
.SOOO2	163	*LWSL	164	*XMASH	165	*EPSC	166	*XISO2G	167
*AFC	170	*WFFC	171	.SOOO1	172	*XVOLHT	173	.SOOOO	174
*USLIP	175	*XMWSO2	176	*DPSTN	177	*GG	200	*TSF	201
LGWR	202	*STNMFX	206	*DUM	207	*LWS1	210	*IPLT	211
*XKRC	212	*NYLB2	213	*X1	214	*US	215	*PHIH	216
XLBL	217	*XMWTW	222	X	223	*XMTOTI	226	NDEC	227
YLBL3	231	*DP1	235	*DPC	236	*SZPL	237	*YMIN	240
*XK1	241	*UG	242	*I	243	*DPSTN3	244	*WFM	245
*YMTOT	246	*IPPM	247	F	250	*XSS	253	*XMSO2G	254
*RGV	255	*ROTA	256	*DPC3	257	*EPS	260	LG	261
*XL	263	*TVOL	264	*POC3	265	CRVLB	266	*XKRH	272
YLBL2	273	*LF811	276	*SDNSTY	277	*NFDATA	300	*FMFX	301
*AFH	302	*IR	303						

TEMPORARIES

.QOOOO 304

MAIN. [No errors detected]

```
00001   C    THIS SUBROUTINE IS USED TO OPEN AND CLOSE FILES
00002   C
00003   C
00004   C
00005           SUBROUTINE FLOPCL(IUNIT,IW,KOPR,FNAM)
00006   C
00007   CFLOPCL.FOR
00008   C
00009   C       THIS SUBROUTINE IS TO OPEN AND CLOSE A FILE ON DISK
00010   C       AND TO ASK USER TO INPUT FILE NAME FROM TTY
00011   C
00012   C       IUNIT THE UNIT NUMBER USED FOR FILE I/O
00013   C       IW IS THE OUTPUT UNIT NUMBER
00014   C       KOPR THE OPERATION TYPE DESIRED.
00015   C        KOPR=1 TO OPEN FILE,
00016   C        KOPR = 2 TO CLOSE FILE
00017   C        KOPR = 3 TO ASK USER TO ENTER INPUT FILE NAME AND THEN
00018   C         ECHO IT BACK TO TERMINAL
00019   C       FNAM NAME OF FILE..NOT MORE THAN 8 CHARACTERS. THIS NAME
00020   C       IS NOT NEEDED IN CLOSING THE FILE
00021   C
00022           DOUBLE PRECISION FNAM
00023           DATA DSKZ/'DSK'/
00024           GO TO (50,100,150), KOPR
00025       50  CONTINUE
00026   C
00027   C       OPEN FILE AND WRITE A MESSAGE
00028   C
00029           OPEN(UNIT=IUNIT,DEVICE=DSKZ,FILE=FNAM)
00030           WRITE(IW,9000) IUNIT,FNAM
00031           GO TO 200
00032      100  CONTINUE
00033   C
00034   C       CLOSE FILE AND WRITE A MESSAGE
00035   C
00036           CLOSE(UNIT=IUNIT)
00037           WRITE(IW,9050) IUNIT
00038           GO TO 200
00039      150  CONTINUE
00040   C
00041   C       ASK USER TO INPUT FILE NAME
00042   C
00043           TYPE 9100
00044           ACCEPT 9150,FNAM
00045           TYPE 9200,FNAM
00046      200  CONTINUE
00047           RETURN
00048     9000  FORMAT(' UNIT NO.',I3,' IS USED TO OPEN FILE ',A10)
00049     9050  FORMAT('  FILE ON UNIT',I3, ' IS CLOSED')
00050     9100  FORMAT(' INPUT FILE NAME ',$)
00051     9150  FORMAT(A10)
00052     9200  FORMAT(' INPUT FILE IS ',A10)
00053           END
```

SCALARS AND ARRAYS ["*" NO EXPLICIT DEFINITION - "%" NOT REFERENCED]

  FNAM   1   *IW   3   *IUNIT 4   *KOPR   5   *DSKZ   6

TEMPORARIES

  .A0016 7

FLOPCL [No errors detected]

APPENDIX B3

OVERALL ENERGY BALANCE MODEL

```
00001   C        THIS PROGRAM IS USED TO OBTAIN THE GAS MASS FLUX
00002   C             AND SOLIDS MASS FLUX GIVEN THE DESIRED COAL FLOW RATE
00003   C             THE PHYSICAL PROPERTIES FOR ALL COMPONENTS,THE HEAT
00004   C             OF REACTION FOR COMBUSTION AND CALCINATION,THE SOLIDS TO
00005   C             GAS MASS FLUX RATIO, AND THE CALCIUM TO SULFUR MOLAR RATIO
00006   C
00007   C
00008   C        OPEN INPUT AND OUTPUT FILES
00009   C
00010            IR=19
00011            IW=5
00012            IO=20
00013            CALL OPCL(IR,IW,1,'OAEB.IN')
00014            CALL OPCL(IO,IW,1,'OAEB.OUT')
00015   C
00016   C        READ INPUT FROM OAEB.IN UNIT 19
00017   C
00018            READ(IR,*) CFR,DHCMB,CPC,TC,EFF
00019            READ(IR,*) WFVM,WFFC,WFM,WFA
00020            READ(IR,*) WFC,WFS,WFH,WFN,WFO
00021            READ(IR,*) XMWTC,XMWTH,XMWTS,XMWTO,XMWTW,XMWSO2,XMWCAO,XMWSO4
00022        1   ,XMWCA3
00023            READ(IR,*) CPSTN,CASRTO,DHCLCN
00024            READ(IR,*) CPA,FDNSTY,SFXGFX
00025            READ(IR,*) DT
00026   C
00027   C
00028          FLOARA=3.141592*DT*DT/4.
00029          HTGEN= CFR*DHCMB
00030          XMLFRS= CFR*(1.-WFA-WFM)*WFS/XMWTS
00031          STNMFR=CASRTO*XMLFRS
00032          STNFR=STNMFR*XMWCA3
00033   C
00034   C        CALCULATE THE NECESSARY AIR FLOW RATE TO CONDUCT
00035   C             COMBUSTION AT TEMPERATURE TC
00036   C
00037          XMFLOA=(EFF*HTGEN-CFR*CPC*(TC-300.)-STNFR*DHCLCN
00038        1   -STNFR*CPSTN*(TC-300.))/CPA/(TC-300.)
00039          FMFX=XMFLOA/FLOARA
00040          SMFX=SFXGFX*FMFX
00041   C
00042   C        WRITE OUTPUT
00043   C
00044            WRITE(IO,9000) SMFX,FMFX
00045            WRITE(IO,9050) CFR,STNFR
00046   C
00047   C
00048            STOP
00049   9000     FORMAT(5X,'SOLIDS MASS FLUX, KG/M2S = ',1PE12.4,
00050        1   /5X,'GAS MASS FLUX, KG/M2S = ',1PE12.4)
00051   9050     FORMAT(5X,'COAL FLOW RATE, KG/S = ',1PE12.4,
00052        1   /5X,'STONE FLOW RATE, KG/S = ',1PE12.4)
00053            END
```

SUBPROGRAMS CALLED

OPCL

SCALARS AND ARRAYS ["*" NO EXPLICIT DEFINITION - "%" NOT REFERENCED]

*EFF	1	*FLOARA	2	*XMWCAO	3	*WFC	4	*CFR	5
*IW	6	*XMFLOA	7	*WFN	10	*CPC	11	*XMWTO	12
*DT	13	*XMLFRS	14	*CASRTO	15	*FDNSTY	16	*WFO	17
*DHCLCN	20	*WFH	21	*HTGEN	22	*XMWTS	23	*XMWTC	24
*WFA	25	*IO	26	*SMFX	27	*WFS	30	*WFVM	31
*XMWTH	32	*CPA	33	*WFFC	34	*STNMFR	35	*XMWSO2	36
*XMWSO4	37	*XMWCA3	40	*XMWTW	41	*STNFR	42	*SFXGFX	43
*WFM	44	*TC	45	*DHCMB	46	*CPSTN	47	*FMFX	50
*IR	51								

MAIN. [No errors detected]

APPENDIX C

INPUT DATA FOR
CONCEPTUAL DESIGN

Table C1

INPUT DATA FOR OAEB.FOR

Variable	Variable Name	Value
Coal Flow Rate	CFT	0.28 kg/s
Heat of Combustion	DHCMB	24000 kJ/kg
Heat Capacity of Coal	CPA	1.13 kJ/kg °K
Coal Particle Temperature	TC	1200°K
Process Efficiency due to Radiation Losses	EFF	0.90
Volatile Matter in Coal	WFVM	0.352
Fixed Carbon in Coal	WFFC	0.515
Moisture in Coal	WFM	0.174
Ash in Coal	WFA	0.1156
Ultimate Carbon in Coal	WFC	0.824
Ultimate Sulfur in Coal	WFS	0.014
Ultimate Hydrogen in Coal	WFH	0.055
Ultimate Nitrogen in Coal	WFN	0.031
Ultimate Oxygen in Coal	WFO	0.076
Molecular Weight of Hydrogen	XMWTC	12.0 kg/kgmol
Atomic Weight of Hydrogen	XMWTH	1.0 kg/kgmol
Molecular Weight of Sulfur	XMWTS	32.0 kg/kgmol
Molecular Weight of Oxygen	XMWTO	32.0 kg/kgmol
Molecular Weight of Water	SMWTW	18.0 kg/kgmol
Molecular Weight of Sulfur Dioxide	$SMWSO_2$	64.0 kg/kgmol
Molecular Weight of Calcium Dioxide	SMWCAO	56.0 kg/kgmol

Table C1
INPUT DATA FOR OAEB.FOR
(Continued

Variable	Variable Name	Value
Molecular Weight of Calcium Sulfate	$XMWSO_4$	13.0 kg/kgmol
Molecular Weight of Calcium Carbonate	XMWCA3	100 kg/kgmol
Heat Capacity of Limestone	CPSTIV	1.13 kJ/kg°K
Calcium to Sulfur Molar Ratio	CASRTO	2.0
Heat of Calcination	DHCLCN	1795 kJ/kg
Heat Capacity of Air	CPA	1.004 kJ/kg°K
Density of Combustion Gases	FDNSTY	1.17 kg/m^3
Solids Loading	SEXGFX	8.0
Riser Diameter	DT	1.0m

Table C2

INPUT USED BY HVFPPM.FOR

Variable	Variable Name	Value
Number of Calculation per Section	NC	50
Number of Sections in Loop	NSCTTVS	9
Identification for Section 1	IDNT (1)	GSD
Diameter	DT (1)	1.0 m
Straight or Bent Section	KTPTL (1)	1
Angle of Section to Horizontal	ANGLE (1)	45.0°
Length of Section	XLNGTH (1)	7.07 m
Voidage in Section	VOID (1)	0.999
Identification for Section 2	IDNT (2)	TBEND
Diameter	DT (2)	1.0 m
Straight or Bent Section	KTPTL (2)	2
Angle of Section Bend	ANGLE (2)	135.0°F
Radius of Section Bend	SLNGTH (2)	0.75 m
Voidage in Section	VOID (2)	0.999
Identification for Section 3	IDNT (3)	RISER
Diameter	DT (3)	1.0 m
Straight or Bent Section	KTPTL (3)	1
Angle of Section to Horizontal	ANGLE (3)	90.0°
Length of Section	XLNGTH (3)	30.0 m
Voidage in Section	VOID (3)	0.97
Identification for Section 4	IDNT (4)	LBEND
Diameter	DT (4)	0.25 m

Table C2
INPUT USED BY HVFPPM.FOR
(Continued)

Variable	Variable Name	Value
Straight or Bent Section	KTPTL (4)	2
Angle of Section Bend	ANGLE (4)	45.0°
Radius of Section Bend	XLNGTH (4)	0.75 m
Voidage in Section	VOID (4)	0.999
Identification for Section 5	IDNT (5)	EDCT
Diameter	DT (5)	0.25 m
Straight or Bent Section	KTPTL (5)	1
Angle of Section to Horizontal	ANGLE (5)	0.0°
Length of Section	XLNGTH (5)	4.0 m
Voidage in Section	VOID (5)	0.999
Identification of Section 6	IDNT (6)	SPDL1
Diameter	DT (6)	1.0 m
Straight or Bent Section	KTPTL (6)	1
Angle of Section to Horizontal	ANGLE (6)	90.0°
Length of Section	XLNGTH (6)	5.2 m
Voidage of Section	VOID (6)	0.999
Identification for Section 7	IDNT (7)	SPDNS
Diameter	DT (7)	1.0 m
Straight or Bent Section	KTPTL (7)	1
Angle of Section to Horizontal	ANGLE (7)	90.0°
Length of Section	XLNGTH (7)	20.0 m
Voidage in Section	VOID (7)	0.5

Table C2
INPUT USED BY HVFPPM.FOR
(Continued)

Variable	Variable Name	Value
Identification for Section 8	IDNT (8)	ORFC
Diameter	DT (8)	1.0 m
Straight or Bent Section	KTPTL (8)	1
Angle of Section to Horizontal	ANGLE (8)	90.0°
Length of Section	XLNGTH (8)	0.0 m
Voidage in Section	VOID (8)	0.5
Identification for Section 9	IDNT (9)	SPDL2
Diameter	DT (9)	1.0 m
Straight or Bent Section	KTPTL (9)	1
Angle of Section to Horizontal	ANGLE (9)	90.0°
Length of Section	XLNGTH (9)	0.75 m
Voidage in Section	VOID (9)	0.999
Solids Mass Flux	SMFX	63.76 kg/ms^2
Spherocity	SPBCTY	1.0
Solids Temperature	TEMP	1200°K
Solids Heat Capacity	CPS	1.13 kJ/kg
Solids Thermal Conductivity	THCONS	0.104 w/m°K
Packed Bed Voidage	VOID PB	0.5
Particle Diameter	DP	300 μ
Riser Gas Mass Flux	FMFXR	7.97 kg/m^{2}S
Gas Density	FDNSTY	1.17 kg/m^3
Gas Viscosity	FVSCTY	20 x 10^{-5}/kg/ms
Gas Heat Capacity	CTF	1.13 kJ/kg°K

Table C2
INPUT USED BY HVFPPM.FOR
(Continued)

Variable	Variable Name	Value
Gas Thermal Conductivity	THCONF	0.026 w/m°K
Gas Temperature	TEMP	1200°K
Standpipe Gas Mass Flux	FMFXSP	$-.02472 kg/m^2 S$
Exit Pressure	PEXIT	405 kPa
Maximum Inlet Pressure	PINMX	450 kPa
Height of Exit	HEXIT	26.06 m
Tollerance in Calculated Inlet Pressures	PRSTOL	100 Pa
Standpipe Gas Mass Flux Lower Esitimate	EST1	$-0.20 kg/m^2 S$
Standpipe Gas Mass Flux Upper Estimate	EST2	$1.8 \times 10^{-2}/kg/m^2 S$
Maximum Number of Iterations	MAXIT	100
Acceptable ERROR in Standpipe Gass Mass Flux	ERR	0.001

Table C3

INPUT USED BY HVFBCC.FOR
PROVIDED BY HVFBPP.FOR

Variable	Variable Name	Value
Solids Mass Flux	SMFX	63764 kg/m^{2}s
Solids Density	SDNSTY	2500 kg/m^3
Voidage	EPS	0.97
Limestone Particulate Diameter	DPSTN	300 μm
Solids Fraction	EPSI	0.03
Gas Mass Flux	FMFX	7.97 kg/m^{2}s
Gas Density	FDNSTY	1.17 kg/m^3
Gas Viscosity	VISC	1.9 x 10^{-5}/mS
Riser Length	XLF	30.0 m
Riser Diameter	DT	1.0 m

Table C4
INPUT USED BY HVFBCC.FOR

Variable	Variable Name	Value
Volatile Motor Weight Fraction	WFVM	0.352
Fixed Carbon Weight Fraction	WFFC	0.515
Moisture Weight Fraction	WFM	0.174
Ash Weight Fraction	WFA	0.1156
Carbon Weight Fraction	WFC	0.824
Sulfur Weight Fraction	WFS	0.013
Hydrogen Weight Fraction	WFH	0.055
Nitrogen Weight Fraction	WFN	0.031
Oxygen Weight Fraction	WFO	0.076
Coal Density	CONSTY	1500 kg/m^3
Devolatilization Fraction 1	Y1	0.3
Devolatilization Fraction 2	Y2	1.0
Devolatilization Frequency Factor 1	A1	20000 s^{-1}
Devolatilization Frequency Factor 2	A1	1.7 x 10^7 s^{-1}
Devolatilization Activation Energy 1	E1	25000 kcol/gmmol°K
Devolatilization Activation Energy 2	E2	40000 kcol/gmmol°K
Devolitilization Time	TVOL	1.0 S
Carbon Stoichiometric Coefficient	PHIC	2
Hydrogen Stoichiometric Coefficient	PH1H	4
Sulfur Stoichiometric Coefficient	PHIS	1
Carbon Activation Energy	EAC	23900 kcol/gmmol°K
Hydrogen Activation Energy	EAH	23900 kcol/gmmol°K

Table C4
INPUT USED BY HVFBCC.FOR
(Continued)

Variable	Variable Name	Value
Sulfur Activation Factor	EAS	23900 kcol/gmmol°K
Carbon Frequency Factor	AFC	920 S^{-1}
Hydrogen Frequency Factor	AFH	920 S^{-1}
Sulfur Frequency Factor	AFS	920 S^{-1}
Solids Temperature	TS	1200°K
Gas Temperature	TG	1200°K
Oxygen Concentration	CNO2	2.13×10^{-3} kgmol/m^3
Coal Particle Size	DPC	70 μm
Oxygen Diffusivity	DIFFO2	2.6×10^{-5} m^2/S
Pore Plugging Constant	PSTR	0.209 S kgmol/m^3
Sulfination Time	TSF	0.019 S
Initial SO_2 in Gas	X1502G	8.0×10^{-8} kgmol/m^3
Carbon Molecular Weight	XMWTC	12.0 kg/kgmol
Hydrogen Atomic Weight	XMWTH	1.0 kg/kgmol
Sulfur Molecular Weight	XMWTS	32.0 kg/kgmol
Oxygen Molecular Weight	XMWTO	32.0 kg/kgmol
Water Molecular Weight	XMWTW	18.0 kg/kgmol
Sulfur Dioxide Molecular Weight	XMWSO2	64.0 kg/kgmol
Calcium Dioxide Molecular Weight	XMWCAO	56.0 kg/kgmol